ลักษณะเฉพาะของพลอยแซปไฟร์จากแหล่งคุยเชา ประเทศเวียดนาม

นายชิตชน ชิตพยัคฆ์

รหัสนิสิต 5532711723

รายงานนี้เป็นส่วนหนึ่งของการศึกษาตามหลักสูตรปริญญาวิทยาศาสตร์บัณฑิต

ภาควิชาธรณีวิทยา คณะวิทยาศาสตร์ จุฬาลงกรณ์มหาวิทยาลัย

ปีการศึกษา 2558

CHARACTERISTICS OF SAPPHIRE FROM QUY CHAU DEPOSIT, VIETNAM

Mr. CHITTCHON CHITTPAYAK

ID. 5532711723

A REPORT SUBMITTED IN PARTIAL FULFILLMENT OF THE REQUIREMENTS FOR THE BACHELOR DEGREE OF SCIENCE

DEPARTMENT OF GEOLOGY, FACULTY OF SCIENCE

CHULALONGKORN UNIVERSITY

2015

Date of Submit

__/__/__

Date of Approval

__/__/__

Sign_____

(_____)

Advisor

หัวข้องานวิจัย : ลักษณะเฉพาะของพลอยแซปไฟร์จากแหล่งคุยเชา ประเทศเวียดนาม

ผู้ทำการวิจัย : นายชิตชน ชิตพยัคฆ์

อาจารย์ที่ปรึกษา : รศ.ดร. จักรพันธ์ สุทธิรัตน์

ภาควิชา : ธรณีวิทยา

ปีการศึกษา : 2558

บทคัดย่อ

เวียดนามนั้นเป็นหนึ่งในประเทศที่มีการผลิตพลอยแซปไฟร์ที่มีคุณภาพของโลก การสะสมตัวของอัญมณีดังกล่าวเกิดจากกระบวนการแปรสภาพและกระบวนการทางหินอัคนีจำพวกบะซอลต์ ซึ่งจากการศึกษาพบว่าการเกิดแหล่งพลอยจากการแปรสภาพนั้นมีความสัมพันธ์กับกระบวนการเกิดภูเขาหิมาลัย ซึ่งเป็นการชนกันของแผ่นทวีปอินเดียกับยูเรเซีย ทำให้การสะสมตัวหลักกระจายตัวบริเวณรอบๆแนวเทือกเขา และยาวต่อเนื่องมาจนถึงบริเวณรอยเลื่อนแม่น้ำแดงในประเทศเวียดนาม ซึ่งการเคลื่อนตัวอีกครั้งของรอยเลื่อนในแม่น้ำแดงทำให้เกิดบริเวณแนวการแปรสภาพและได้แหล่งสะสมตัวของคอรัมดัมที่มีคุณภาพหลายแหล่ง ซึ่งก็รวมถึงแหล่งคุยเชาในพื้นที่ศึกษานี้

แหล่งคุยเชาตั้งอยู่บริเวณทางตอนใต้ของแม่น้ำแดง เป็นแหล่งที่มีการผลิตแซปไฟร์และทับทิมที่มีคุณภาพสูง โดยเฉพาะในแหล่งสะสมตัวแบบลานแร่ แต่เนื่องด้วยความจำกัดทางด้านฐานข้อมูล จึงทำให้การจำแนกลักษณะจำเพาะของอัญมณีจากการสะสมตัวนี้เป็นเรื่องที่ทำได้ยาก

กลุ่มตัวอย่างพลอยแซปไฟร์จากแหล่งดังกล่าวสามกลุ่ม ได้แก่ กลุ่มสีน้ำเงิน กลุ่มสีชมพูอมส้ม และ กลุ่มสีชมพูอมแดง ได้ถูกนำมาวิเคราะห์สมบัติพื้นฐาน พบว่า ตัวอย่างไม่เกิดการเรืองแสงภายใต้แสงอัลตร้าไวโอเลต พบลักษณะ แร่มลทินสีดำภายในเนื้อพลอย ทั้งเป็นแท่งและเป็นก้อน ซึ่งอาจเป็นแร่สปิเนลหรือแอมฟิโบลต์ นอกจากนี้ยังมีการพบลักษณะแถบสี รอยแตก มลทินรอยนิ้วมือ

เมื่อนำไปวิเคราะห์ด้วยเครื่องมือขั้นสูงพบว่าพลอยทั้งสามกลุ่มแสดงลักษณะแถบสเปคตรัมการดูดกลืนช่วงแสง UV-Vis-NIR ที่แตกต่างกันชัดเจนโดยกลุ่มที่น้ำเงินมีการดูดกลืนช่วงของเหล็กสูง ในทางตรงข้าม กลุ่มสีชมพูอมแดงมีการดูดกลืนช่วงของโครเมี่ยมสูง ส่วนกลุ่มสีชมพูส้มนั้นมีการดูดกลืนของเหล็กและโครเมี่ยม นอกจากนี้การวิเคราะห์อัตราส่วนระหว่างปริมาณโครเมี่ยมและเหล็กยังแสดงถึงแนวโน้มที่บ่งชี้แหล่งกำเนิดจากกระบวนการแปรสภาพ การวิเคราะห์แร่มลทินพบแคลไซต์ ซึ่งแสดงถึงหินต้นกำเนิดแปรสภาพจำพวกหินอ่อน

คำสำคัญ : การแปรสภาพ, แซปไฟร์, คุยเชา, ลักษณะจำเพาะ, หินอ่อน

TITLE : CHARACTERISTICS OF SAPPHIRE FROM QUY CHAU DEPOSIT, VIETNAM

BY : Chittchon Chittpayak

ADVISOR : Associate Professor Dr. Chakkaphan Sutthirat

DEPARTMENT : Geology

ACADEMIC YEAR : 2015

ABSTRACT

Vietnam is one of the high quality sapphire production supplying to the global market. Gem depositions appear to have occurred in both metamorphic and basaltic environments. The significant metamorphism was related to Himalayan orogeny which has been related to the collision between India and Eurasia plates. Consequently, sapphire deposits occurred extensively along the mountain range and extended to the Red River in Vietnam. The Red River Fault Zone was reactivated and influenced metamorphism and led to large deposition of sapphire in this country including Quy Chau, this study area.

Quy Chau mine is located in the south of Red River Fault Zone. High quality sapphire and ruby are being produced mostly from the secondary placer deposit. However, due to lacking of database, origin determination of sapphire from this deposit is rather difficult.

Sapphire samples collected from the Quy Chau mine can be categorized into 3 groups, blue samples, orangey pink samples and reddish pink samples. Samples of all groups are inert under ultraviolet light. Tubular- and irregular -shaped black inclusions are observed inside these samples. They may be spinel or amphibole. In addition, various types of inclusions such as color zone, fracture and fingerprint are also found.

Based on advanced analyses, 3 distinctive spectra are discovered. Blue samples show strong absorption caused by iron whereas reddish pink sapphires display high chromium absorption. Orangey pink samples contain combination between iron and chromium absorptions.

Proportional plotting between chromium and iron reveals that these samples are related to metamorphic origin. Mineral inclusions identified by Raman spectroscopy is calcite which appears to be associated with carbonate protolith. The carbonate rocks might be metamorphosed into marble which has hosted these sapphires before weathering and transportation were taken place leading to alluvial deposits.

Keywords: metamorphism, sapphire, Quy Chau, characteristics, marble

ACKNOWLEDGEMENT

This senior project is aimed for academic practicing. It is a part of the Senior Project Subject 2301499. The working process has been completed under the supervision of Associate Professor Dr. Chakkaphan Sutthirat who has been well providing advices and supports throughout the project. My appreciation is also given to Mr. Tasnara Sripoonjan and Ms. Nataya Nilhud, gemologists of the Gem and Jewelry Institute of Thailand (GIT), for instruction and guidance on the topic of analytical equipments, techniques and knowledges. Moreover, it is my honor to have all the supports from every staff of the Geology Department as well as all the geology students who showed their kindness assisting throughout the project until receiving in this achievement.

INDEX

INDEX (Continue)

TOPIC **Page**

FIGURE INDEX

FIGURE INDEX

FIGURE INDEX (Continue)

FIGURE INDEX (Continue)

FIGURE INDEX (Continue)

TABLE INDEX

CHAPTER 1

INTRODUCTION

1.1 Background

Corundum, sapphire and ruby, is crucially recognized by the gem society as one of the most economic gems. Corundum is globally accepted as the precious gemstone, due to its beauty and durability. Sapphire varieties have wide ranges of color except red color which is characterized by ruby. In Thailand, specific ruby, called ***Siamese Ruby***, is very famous for its purplish red. Although, corundum mining activity in Thailand has been decreasing dramatically, production is still taking place in many countries including, Burma, Cambodia, China, Vietnam, Madagascar, Tanzania, Kenya, etc.

Vietnam is one the countries mentioned above. Various varieties of sapphire are domestically produced and exported to the international gem markets. These produced gemstones are known for their beauty; hence, it leads to the high value in the market. Quy Chau Deposit is one of the most popular mines known to produce various gem varieties as well as metamorphic corundum in the northern part of Vietnam. However, the major production is dark red ruby.

Nonetheless, information and research study in this deposit is rarely observable and unclearly represent all the occurrences. Quy Chau sapphires, for instance, have never been reported. Hence the characteristics of Quy Chau sapphire are appropriate for the recent research. Different gem occurrences should be recognized by some gem properties such as color and other optical phenomena. Moreover, chemical fingerprint, particularly trace elements, and some specific inclusions may be recognized as indicator of its origin.

More information gathered from this study may lead to identification of Quy Chau sapphire with more precision and accuracy. These results may be used as database for routinely origin determination and further experiment. Consequently, this will support gem certification and trading.

1.2 Objectives

To study physical, optical along with chemical characteristics of sapphires from Quy Chau Deposit in order to understand the occurrence of these sapphires.

1.3 Hypotheses

Characteristics of Quy Chau sapphire from Vietnam should be unique, and can be used to trace back to its original occurrence.

1.4 Scope of Work

Three groups of samples, orangey pink sapphire, reddish pink sapphire and blue sapphire, are collected for this research. The qualities of the samples are considered as low quality sapphires which might lead to the difficulty of experiment and data gathering. Both basic and advanced techniques are applied to examine these sapphire samples in order to collection of physical, optical and chemical properties.

1.5 Study Area

Vietnam is located in South East Asia Region at the coordinate of $8^{o}35'$- 23^{o} 17' North and $102^{o}10'$- $109^{o}21'$East. The country is bounded by Cambodia and Laos in the west and China is the north. The eastern boundary is connected to South China Sea as seen in Figure 1.1.

Figure 1.1 Map of Vietnam

Source: http://www.mapsofworld.com/vietnam/maps/vietnam-

The topography of Vietnam diverges from mountain in the north western part to coastal area in the south eastern part which have been resulted by the geological processes, particularly collision between micro-tectonic plates, Indochinna Plate, Sibumasu Plateand South China Plate

Quy Chau District, as shown in the rectangular in Figure 1.2, is located in the north central coast region of Vietnam, approximately 500 km south of the Red River Fault Zone in which the center of metamorphism is focused. The area has been intensively mined for limestone, marbles and corundum. The gem-graded sapphire was deposited in placers styles where gem-bearing metamorphic rocks (marble and its associate rocks) of Oligocene to Miocene have been weathered and transported to accumulate.

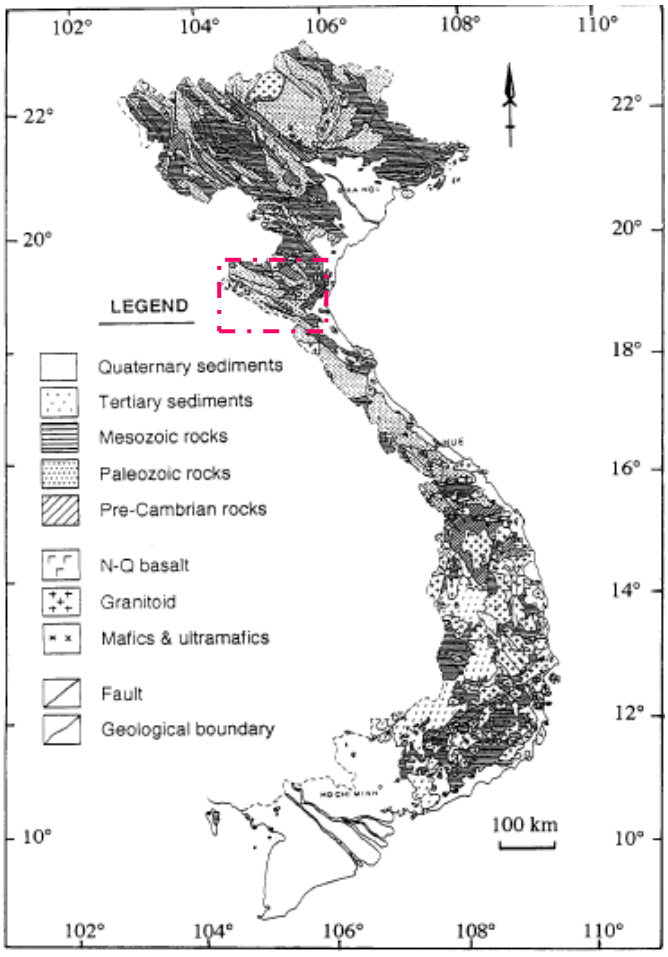

Figure 1.2 Geological Map of Quy Chau District (Tran & Ngyuyen, 1991)

1.6 Expected Results

1. Characteristics of sapphires from Quy Chau deposit
2. Relationship between these gem characteristics and origin of these sapphires
3. Criteria for origin determination of Quy Chau sapphires

CHAPTER 2

LITERATURE REVIEWS

2.1 Tectonic Events

Vietnam has suffered 2 tectonic events-Indosinian Orogeny and Himalayan Orogeny- which influenced the crystallization of sapphire and ruby.

The first orogeny (Indosinian) occurred during Early Triassic which is defined as an oblique collision of Sibumasu, Indochina and South China micro plate. The events formed Vietnam northern topography and Indosinian Mountain along with wide range of metamorphism (Liepvrier, 2004).

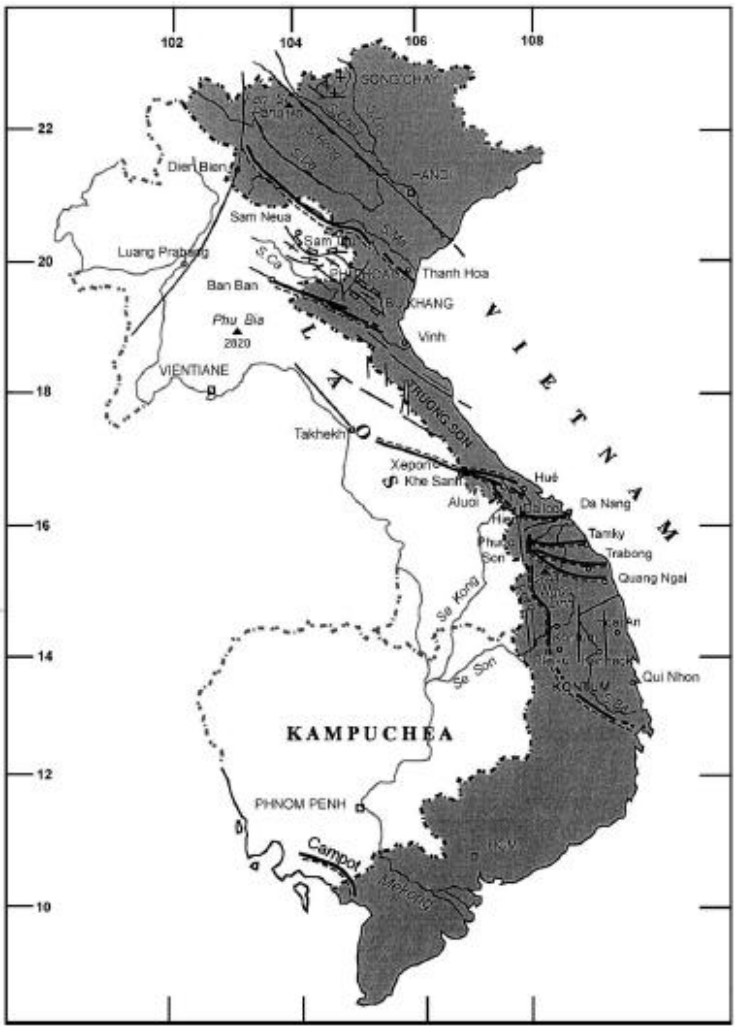

Figure 2.1 Indosinian Shear Zone and Trungson (Liepvrier, 2004)

Trungson (Figure 2.1) at which Quy Chau mine is located underwent ductile metamorphism from mylonitic to amphibolites facies. Metamorphic rocks from such process are restricted in the NW to SE trending, apparently between Song Da, Song Ma and Song Ca Shear Zone.

Song Da (Figure 2.2) consists of sedimentary and volcanic strata of Permo-Triassic which was later covered with carbonate sedimentation-protolith for corundum formation. The series of rocks are folde and foliated due to the low grade metamorphism. They are unconformably lying under the red bed of Cretaceous (Lacassin et al., 1998). In addition, the events can be divided into two stages, pre-Norian Indonisian Phase and post-Cretaceous shortening respectively.

Song Ma (Figure 2.2) is a metamorphic belt ranging from greenschist to amphibolites (Tran Van Tri et al., 1979). The rock assemblages found in the area are phyllite, pelitic schist, metaquartzite and garnet mica schist associated with marble; indicates a low-high grade metamorphism. Song Ma Zone rocks are North Western trending folded-Song Ma anticlinorium. Ophiolite sequence can be found as lenses and are intensively folded within the suture zone.

Song Ca Fault Zone is a seaward extensional fault area in a north western direction. The main trending of faults is in north western direction which is later reactivated and formed half-graben structures for Neogene detrital sediment supply.the rock in this area were mostly metamorphosed. The original rocks are mostly Carboniferous limestone with karstification. In Quy Chau district, north dipping ductile normal faults are found.

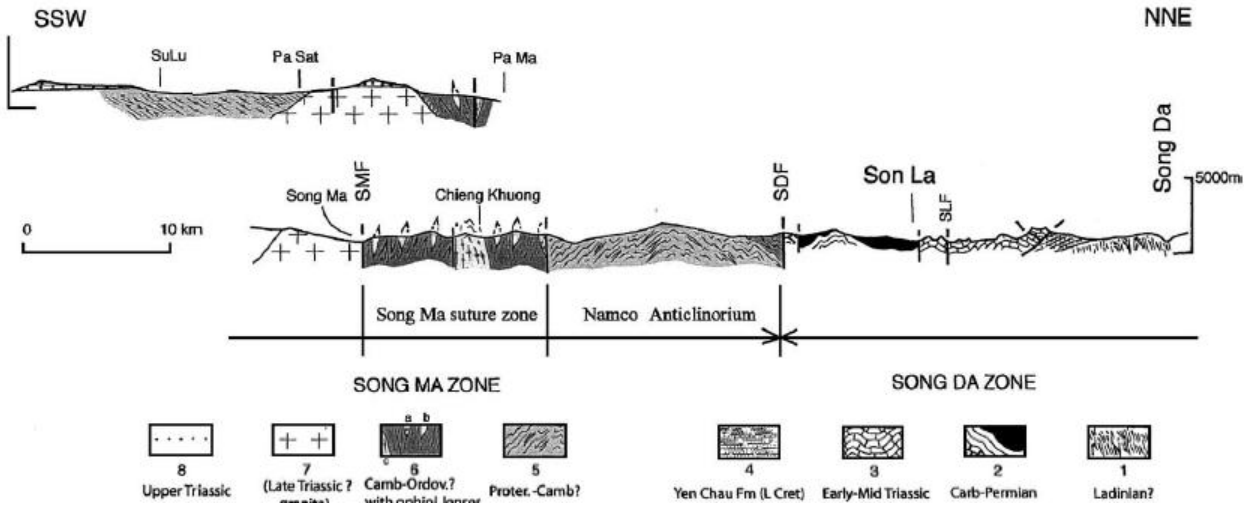

Figure 2.2 Synthetic Cross Section of Songma and Song Da
(Lacassin et al., 1998)

The second event took place in Cenozoic Era or as known as Himalaya Orogeny, the event was a collision of India and Eurasia Plate forming a Himalayan Mountain range. This influenced metamorphism and reactivations along the mountain range extending to Red River Fault Zone in Vietnam. Consequently, the ruby and sapphire marble-hosted deposit can be found along the range in the many countries in Central and South East Asia such as Afghanistan, Azad-Kashmir, Tajikistan, Nepal, Myanmar, southern China and Vietnam (Hughes, 1997). The distributions of each deposit can be seen in the figure 2.3.

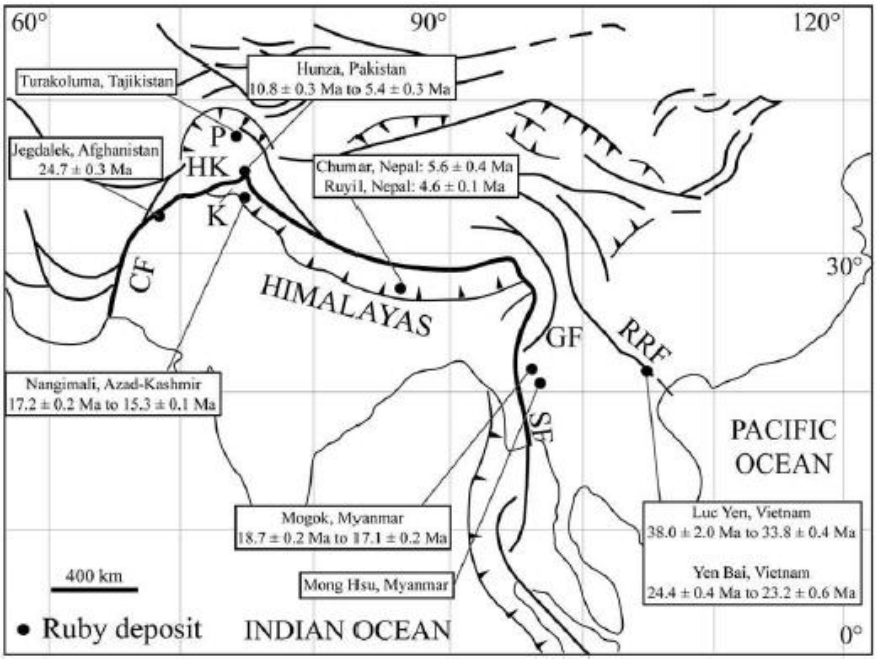

Figure 2.3 Marble Hosted Sapphire Deposit Distribution (Hughes, 1997)

Despite of a wide range of distribution, these corundum occurrences share some similarity in geological background:

1. They formed within the metamorphic region resulted from the tectonic event of Himalaya orogeny. For northern part of Vietnam such as Yen Bai or Quy Chau, the corundum depositions are focused around the Red River Fault Zone which is activated during the event.
2. The occurrence associated with marble which was metamorphosed from Permo-Triassic Carbonate Platform along with garnet-biotite-silimanite gneiss. The distribution of marble is along the shear and fault zone related to the orogeny. Conventionally, Ruby and sapphire crystallization is stratiformally bound with the marble bed (up to 300m). In Vietnam, the occurrence of marble presents in 3 styles

which are dissemination, veinlets, and pockets within marble associated with phlogopite, graphite, pyrite, spinel and some micas.

3. The age gathered after the $^{40}Ar - ^{39}Ar$ dating of phlogopite reviews approximately Cenozoic. With $^{206}U - ^{238}Pb$ dating method performed on zircon, It indicated that Vietnam sapphire crystallization occurred during the highest peak of metamorphism resulted from ductile deformation along Red River Fault and Shear Zone

2.2 Geological Setting in Vietnam

Complex geological features have been reported for Vietnam; extensive periods of rock exposures should indicate several tectonic events. The area is affected crucially by Shan Thai-Indochina collision and Himalayan Orogeny (Nam, 1995). These events were mainly focused on the northwestern boundary of the country, particularly along the Red River Fault Zone. The consequences are major metamorphism and volcanism throughout the country. In spite of such complicated features, Vietnam is classified into 5 regions (Nam, 1995), including Northeastern Block, Northwestern Block, Truongson Block, Kontum Block and Nambo Block, based on their distinctive structural features, as shown in Figure 2.1

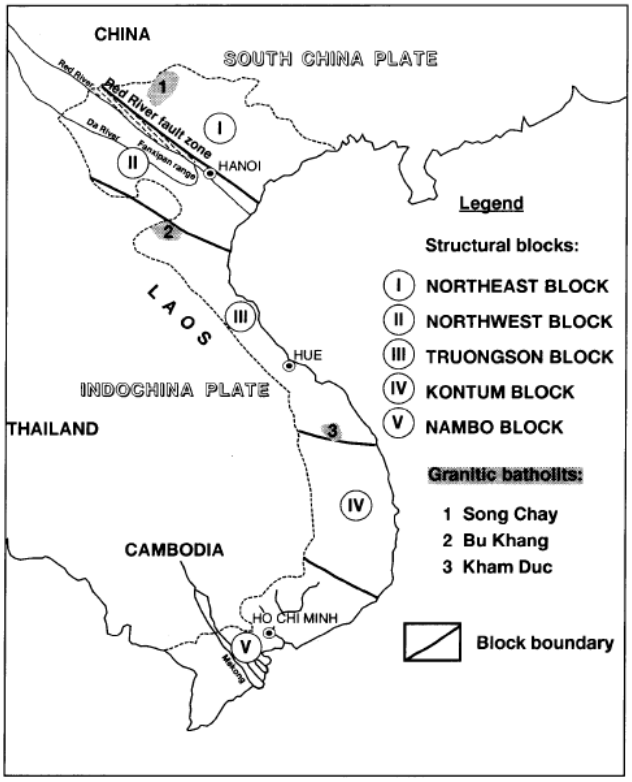

Figure 2.4 Division of Vietnam Region (Nam, 1995)

Rock formations in Vietnam consist of strata ranging from Archean to Cenozoic; some formations are highly metamorphosed and intensively folded in the Northwestern-Southeastern trend.

Precambrian rocks are found mainly in the Kontum Blocks lying in the central and northern regions. Some exposures of magmatic rocks and metamorphic rocks can also be found, especially near the Red River Zone.

Northern part mostly consists of series of Paleozoic rocks. These rocks are metamorphosed and interrupted by igneous activities ranging from granitoid intrusion to basaltic eruption during early to late Paleozoic. However, most strata from Devonian to Carboniferous are dominated by limestone.

Widespread Mesozoic rocks are found across Vietnam; they are characterized by marine sedimentary rocks ranging from Triassic to Jurassic. Some areas are covered by pyroclastic rocks due to the excessive volcanism during this period.

The latest rock strata belong to Cenozoic which is still unconsolidated. They have been mainly deposited in the graben basin resulted from the ancient tectonics. Some sediments are reworked and transported by the Red River and Kong River and deposited where the river mouth is located, Southern Vietnam plains in particular.

Long et al. (2004) reported that Vietnam is a potential area for gem mining due to the extensive proper geological activities. Various styles of deposition have been found throughout the country and can be roughly defined into 2 regions. The northern part of Vietnam is controlled by metamorphism which some popular mines, such as Luc Yen, Yen bai and Quy Chau, are located. The most popular gem variety produced in the area is pinkish ruby (Figure 2.2). On the other hand, all the gem mines in the south of the country are mostly associated with basaltic origin.

Figure 2.5 Quy Chau Rough Ruby (Long et al., 2004)

Quy Chau Mining distirct is located on the Trungson Block, about 200 km south of the Red River shear zone. This territory has complex geological features such as Bu Khang dome which dominates in the area (Figure 2.3) and is also controlled by extensional shear zone (Garnier, 2002). In addition, rock formations are highly metamorphosed due to the presence of gigantic antiform. Corundum mineralization process in this district can be categorized into 3 processes including association with graphitic pyrite-rich marble, within phlogopite-bearing skarn resulted from the pegmatitic fluid alteration and within gneisses contacting with intrusive pegmatite. However, the main gem grade sapphires are mostly mined from the secondary placer deposit. After performing $^{40}Ar/^{39}Ar$ dating of mineral inclusions (i.e., Phlogopite, Muscovite and Biotite) in the Marble, the results yielded a varying age range from 33 to 23 Ma falling between Oligocene and Miocene.

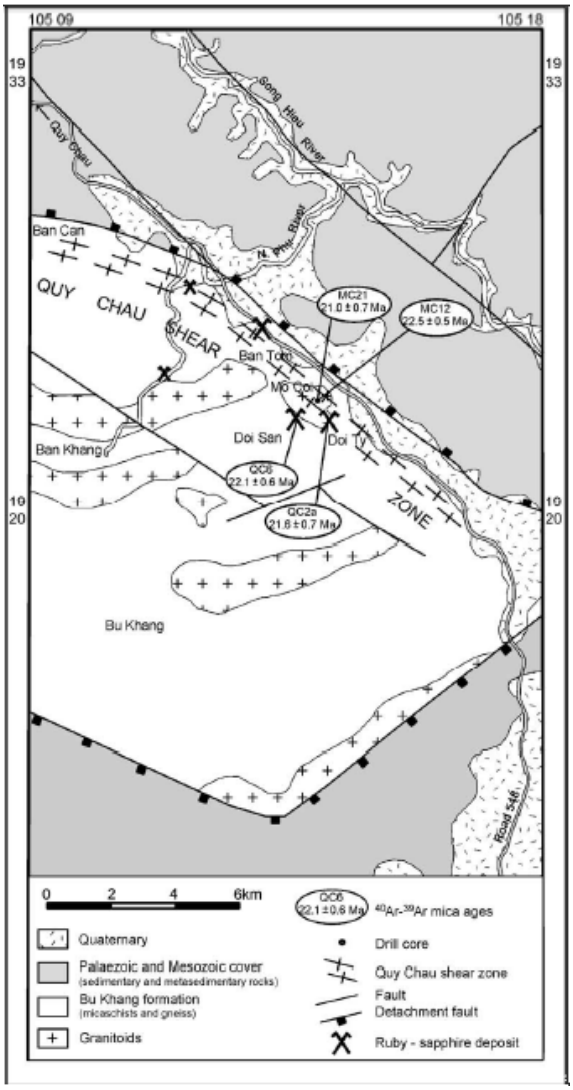

Figure 2.6 Geological Map of Quy Chau District (Garnier, 2002)

2.3 Corundum Formation

A study of marble-hosted corundum formation from Central to South East Asia has shown that the depositional zones lies along the Himalayan mountain range and is controlled by fault and shear zones (Garnier et al, 2008). The mountain range accounted for this mineralization was formed in Cenozoic by the collision between Indian Plate and Eurasian Plate. The events affected the red river fault zone in the northern part of Vietnam causing the carbonate series to undergo a metamorphism. Dating data of Ar-Ar and U-Pb methods also confirmed that the age of the orogeny and gem are isochronously matched (Garnier et al, 2008).

Many researchers (e.g., Dmitriev (1982), Kissin (1994), Okrusch et al. (1976)) have also proposed 4 possible conventional genetic models for corundum occurrence:

1. High grade regional metamorphism such as amphibolites facie can result in an enrichment of aluminum into carbonate rocks. Under such condition, oxic weathered impure limestone may experience high pressure and temperature condition forcing the prograde sequences from Hydragillite to bohemite, diaspore and finally corundum. An alternative is that sapphires alter from spinel with aluminum supplement from the contact metamorphism of clay mineral inside marble.
2. Presence of felsic intrusion may influence the occurrence of ruby and sapphire. Since the granitic intrusion usually carries aluminum mineral within its chamber; it may cause contact metamorphism with the country rock bounded around the chamber. Metamorphic zone may enrich aluminum and then form corundum.
3. With a presence of chromium and a scarceness of silica, potassium, sodium and high level of CO_2, sapphire crystallization may take place during high grade metamorphism of impure limestone coexisting with evaporites.During the metamorphism, at the temperature range between 620^oC and 660^oC with the pressure of approximately 2.5 kbar, Spinel will be destabilized forming both dolomite and corundum. The process can be summarized into a crucial reaction:

   $$MgAl_2O_4 \text{ (Spinel)} + CO_2 \rightarrow Al_2O_3 + Ca(Mg)CO_3$$

4. Another necessity situation is a high saturation environment. The ion exchange between limestone and evaporitic lens acting as molten salt can form ruby crystals and release CO_2 as byproduct-decarbonation.

Moreover, a new genetic model for corundum formation is described as a retrograde metamorphic process. The suitable condition under this model is a temperature range between 620 to 670 C^o with pressure varying from 2.6 to 3.3 kbar. Such condition, Si is believed to be the result of Himalayan Orogeny in Ceonozic. During the process, the

marbles acted as a closed fluid system without contamination from country rocks (Garnier, 2008). The evaporites also influence the movement of aluminum iron inside the system causing break down of spinel and muscovite.

The figure 2.4 illustrates the process of the new genetic model. Firstly, a deposition of Precambrian to Permo-Triassic protoliths formed a carbonate platform inside a lagoon environment. With an arid climate at the time, the platform is associated with evaporites and dolomites. The detrital supply from continent finally enriched clastic sediment such as clay. Secondly, a period of metamorphism of Cenozoic is influenced by the Himalayan orogeny characterized by a collision of India and Eurasia plate. At this stage, the platform underwent a high grade metamorphism forming marble and also causing an interaction among mineral such as clays, carbonate, micas and pyrite. Corundum is formed during both the prograde stage of the reaction with an increase in temperature and pressure and the retrograde stage. During the prograde stage, the main reaction of corundum formation is the breakdown of margarite which can be described as:

$$\text{Margarite} \rightarrow \text{Anorthite} + \text{Cordundum} + H_2O$$

However, the corundum from this stage will soon be unstabilized and change into others mineral. Meanwhile, the main process occurred during the retrograde stage from the destabilization of assemblage minerals (i.e., Muscovite, Spinel) as mentioned above. The main reaction of the two breakdowns is:

$$\text{Spinel} + \text{Calcite} + CO_2 \rightarrow \text{Corundum} + \text{Dolomite}$$

$$\text{Muscovite} \leftrightarrow \text{K-feldspar} + \text{Corundum} + H_2O$$

Anyhow, the main reaction in overall is the Spinel Destabilization.

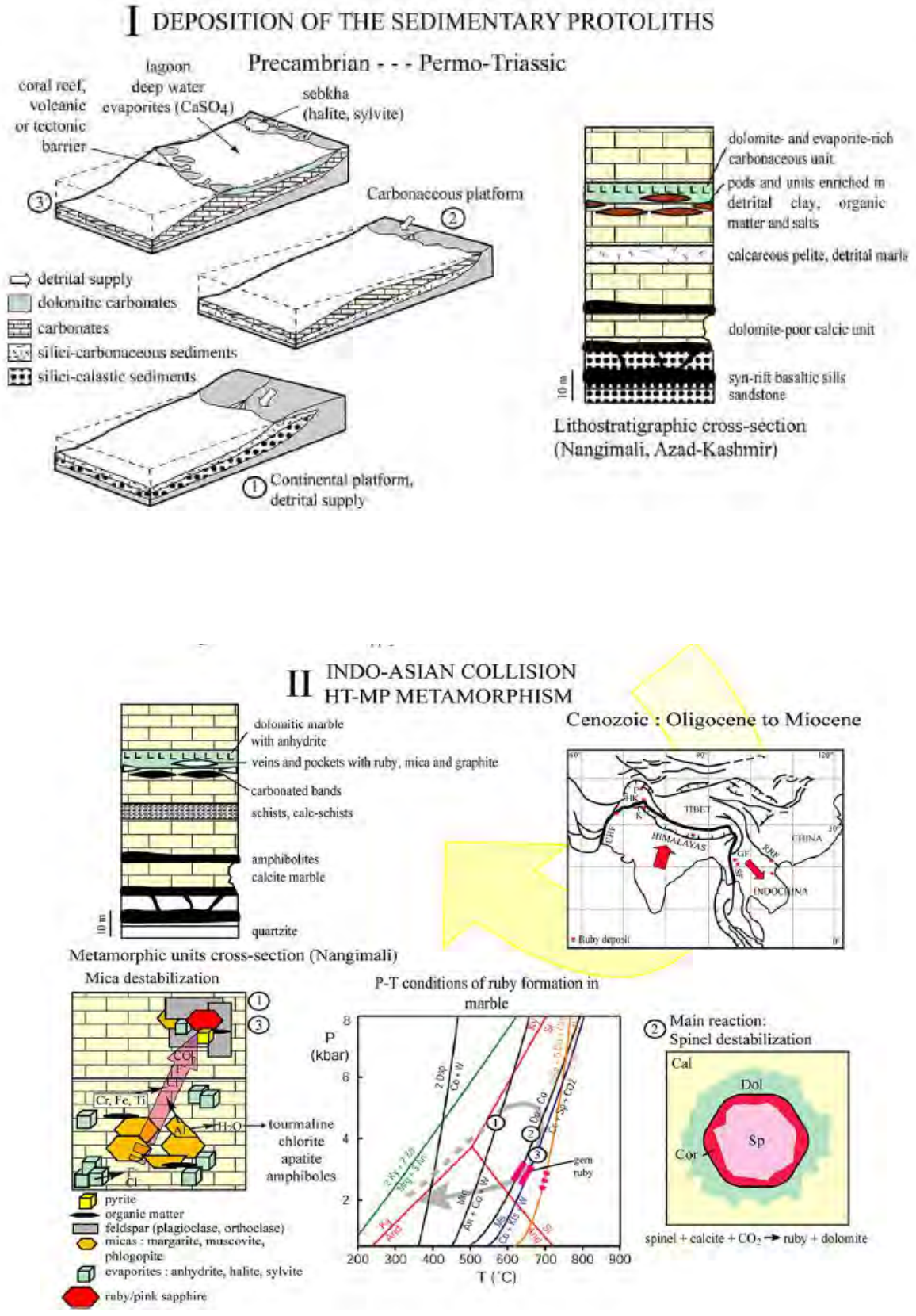

Figure 2.7 New Genetic Model of Corundum (Garnier el at., 2008)

2.4 Advanced Analytical Techniques for Corundum Analysis

Many techniques have been performed to analyze sapphire in order to collect properties and characteristics which are aimed for origin determination. Research done by Diep (2015) was used UV-Vis-NIR spectrometry to detect absorption of trace elements to identify the spectrum patterns that cause color and pleochroism. Fourier Transform Infrared (FTIR) spectrometry can be performed to observe the vibration mode of OH functional group and simultaneously determination whether the treatment has been done on gemstone, based on the presence of AlOOH and its polymers. Moreover, Laser Raman Spectrometry can be used to identify the inclusion in gemstone. Finally, Electron Probe Micro Analyzer (EPMA) is applied to quantitatively analysis elements with high accuracy and precision.

Sutherland et al. (1998b) , Sutherland and Schwarz (2001) and Long et al. (2004) used the principle of geological characteristic and chemical composition to differentiate origin of corundum. As the results, plots between Cr_2O_3/Ga_2O_3 and Fe_2O_3 contents analyzed by EPMA technique can distinguish origins of sapphire. Metamorphic-originated sapphires contain Cr_2O_3/Ga_2O_3 higher than 1 whereas its basaltic counterpart shows lower than one

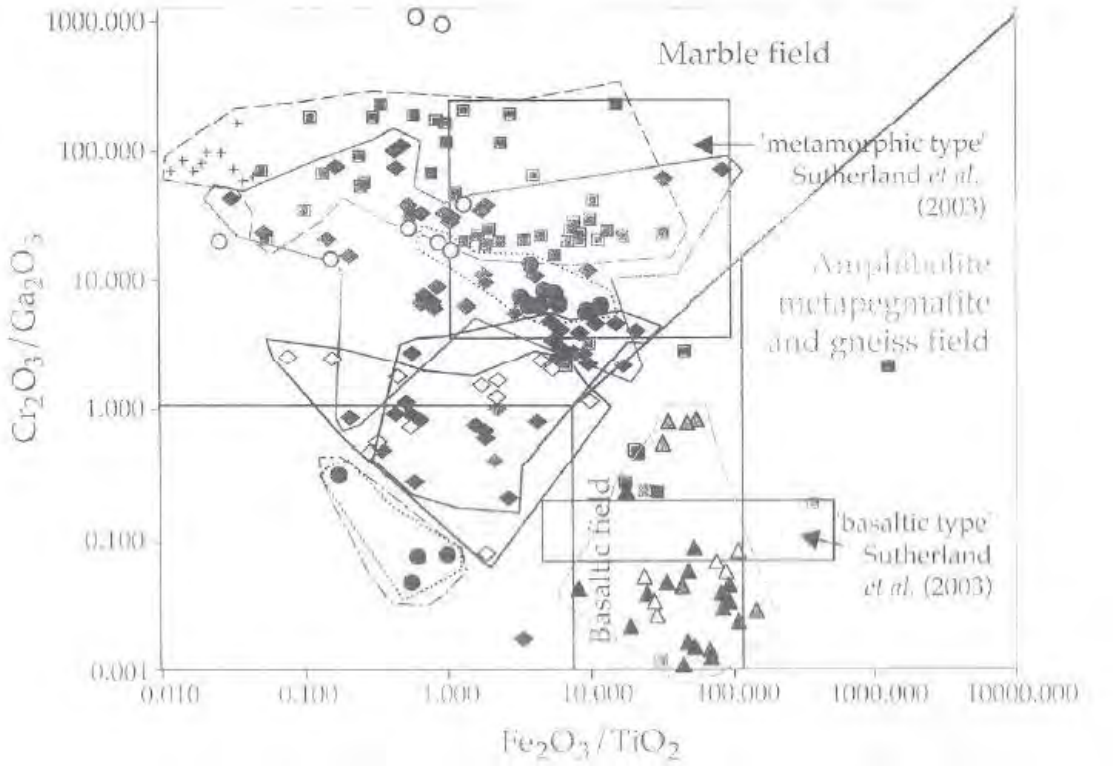

Figure 2.5 Plots of Cr_2O_3/Ga_2O_3 vs. Fe_2O_3 of sapphire samples from different deposits (Sutherland et al., 1998).

CHAPTER 3

METHODOLOGY AND ANALYTICAL TECHNIQUE

3.1 Methodology

Methodology of this research project consists of 5 main steps, including literature review, sample preparation, basic analyses, advanced analyses and Discussion/Conclusion. These processes are reported below and illustrated in figure 3.1

3.1.1 Literature Review

Previous researches are reviewed in order to understand research concept and geologic setting in Vietnam. This information includes Quy Chau sapphire deposit. In addition, a review on properties and characteristics of sapphire is also needed. The information obtained from this stage can be used to verify the study results and may lead to reconstruction of initial geological origin.

3.1.2 Sample Preparation

Thirty one rough sapphire samples from Quy Chau deposit provided by the Gem and Jewelry Institute of Thailand (GIT) are categorized into 3 main groups, including 13 orangey pink sapphires, 13 pinkish red sapphires and 5 blue sapphires. However, qualities of these samples are low gem quality. High content of impurity and fractures are usually observed and leading to low transparency. In order to perform further examination, surface polishing is required for all samples. The polished samples are then observed under the dichroscope. The principle behind this step is to find the plane cutting parallel to the C-axis in order the display both O ray and E ray at their maximum values. Once located, the samples will be marked and sent to polish at the proper direction.

3.1.3 Basic Analysis

- Samples are measured weights and specific gravity using the hydrostatic balance from GIT.
- Refractometer is used to determine the refractive indices of the stones.
- All samples are exposed to the UV lambs to observe the fluorescence habit.
- Dark field microscope is used to investigate the internal features inside the stone which will be used for further analyses.

3.1.4 **Advanced Analysis**

1. Fourier Transform Infrared Spectrometry (FTIR), which is highly sensitive to polar bond of oxygen and hydrogen, is used to identify CH- and OH-bonding and stretching caused by its structure and inclusion. This technique is also capable to determine some gem treatments. The FTIR model Nicolet 6700 with the wavelength range of 400 to 4000 nanometers is engaged for this study with analytical condition of 2 nanometers sampling interval under room temperature. A spectral resolution is estimated at about 4 cm^{-1}.
2. Ultraviolet-Visible Light-Near Infrared Spectrometry (UV-VIS-NIR) is used to examine the cause of color in gemstones by detecting absorption capacity on each wavelength region. This may also detect trace elements causing color in sapphire. Detection is specified within wavelength ranging from 250 to 1500 nanometers with the sampling interval of 3 nanometers. This step is done by Lambda 950 Perkin Elmer.
3. Laser Raman Spectrometry is performed for mineral inclusions located close to the samples' surface. This technique is capable to individually analyze mineral inclusion set in the gem sample. Renishaw T00A01-003 is used for this step.
4. Energy Dispersive X-Ray Fluorescence Spectrometry (EDXRF) is applied to detect chemical composition of the gemstones and report as oxide percent. This method is not time consuming and has considerable accuracy. Al_2O_3, TiO_2, V_2O_5, Cr_2O_3, Fe_2O_3 and Ga_2O_3 are designed for analyses which are carried out using EGLE III machine.
5. Electron Probe Micro-Analysis (EPMA) is finally used to analyze the polished samples mounted with soluble resin and coated by carbon vaporization. EPMA, model JEOL JXA-8100, provides more accurate chemical results with lower detection limit. It can be used to detect major and minor elements. The operation is taken place under the following conditions.
   Acceration Voltage – 15kV
   Current – 2.50 x 10^8 A
   Probe Diameter – 1 μm (Approximately)
   Probe Scan – Off
   Standard
   Al – Corundum
   Mg – Periclase
   Ca – Wollastonite
   Mn – Manganese Ferite
   Fe – Fayalite
   Si – Quartz

Ti – Potassium Titanium Phosonate
Ga – Gadolinium Ga Garnet
K – Potassium Titanium Phosonate
Cr – Eskolaite
V – Lead Vanadium Germanium Oxide

3.1.5 **Discussion/Conclusion**s

Results gathered from each technique are used to determine the characteristics of Quy Chau sapphires and to differentiate from other deposits. Chromium/Gallium vs Iron/Titanium plot is created from compositions of sapphire, analyzed by EPMA to point out the origin of sapphire (basaltic or metamorphic related). They should indicate the geological genesis.

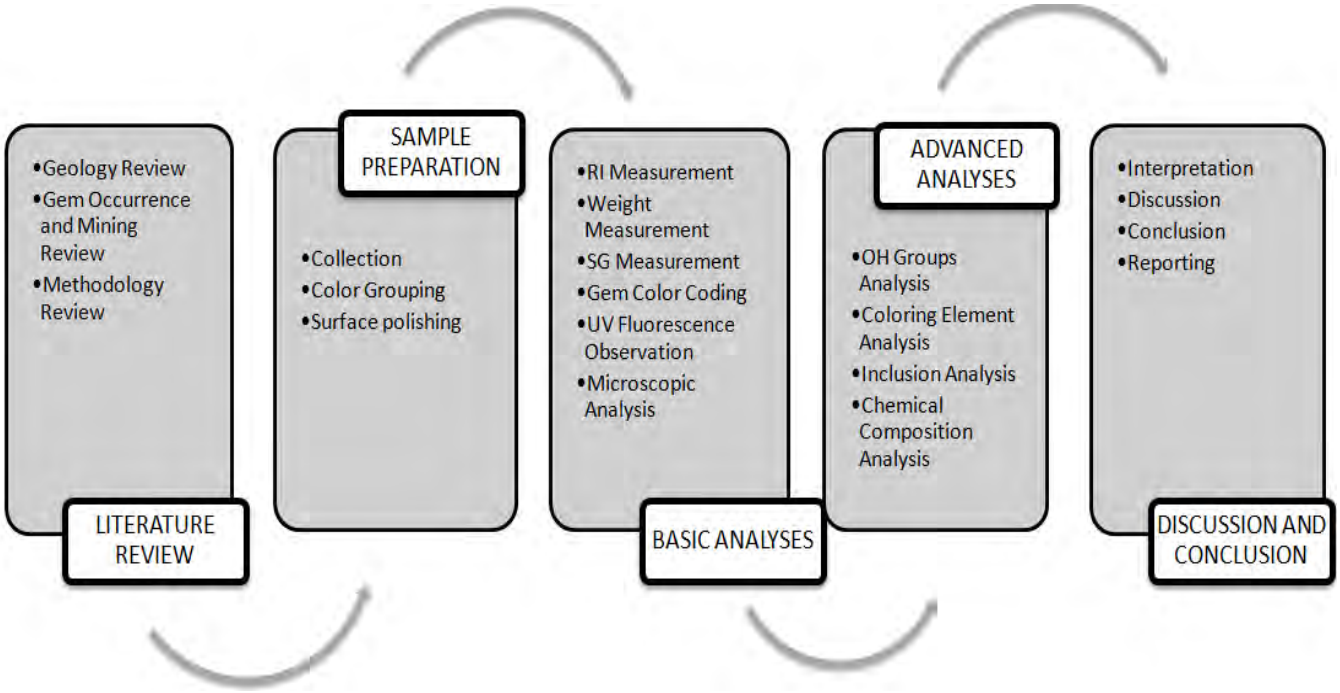

Figure 3.1 Methodology Flow Chart

3.2 Analytical Techniques

1. **Hydrostatic Balance**: is used to measure weight and specific gravity of samples (Figure 3.2).
2. **Refractometer**: is used to measure the refractive indices of sample (Figure 3.3).

3. **Dichroscope**: is used to observe the pleochroic color of gemstone. The tool (Figure 3.4) is equipped with 2 polarized lenses perpendicularly aligned inside the lens where we can observe both colors influenced by each ray.
4. **Gemological Microscope**: A microscope is used to observe and examine features and internal structures of gemstone. The tool (Figure 3.5) consists of 2 light sources-one on the base of the tool and the other on the stage. It can be used to study surface and interior of gemstone. Background field can be adjusted in order to detect light and dark inclusion inside.
5. **UV Lamp**: An ultraviolet light bulb is used to influence the fluorescence of gemstone if exist.
6. **Fourier Transform Infrared Spectrometer (FTIR)**: A spectrometer (Figure 3.8) is used to analyze the presence of organic material, resin and some specifics polymers due to the fact that it is highly sensitive to CH and OH bonding. The principle, that FTIR is relied on, is the relationship between the infrared region absorption and the chemical bonding inside the material. In gemstone experiment, it is performed on any gem to determine whether the gem has been undergone treatment process such as fracture filling or heat treating.
7. **Ultraviolet – Visible Light – Near Infrared Spectrometer (UV-VIS-NIR):** A spectrometer (Figure 3.9) is used to observe the absorption of material due to the presence of particular elements and crystalline defect. The UV-VIS-NIR covers a spectrum region beyond infrared including the visible lights, which makes this machine, is suitable to identify coloring elements of the gemstone. The colors are reflected light paths partially absorbed by hue elements inside the gemstone and are subsequently emitted in the form of visible light; an observation of visible light region can detect such absorption. The study on both E ray and O ray gathered from this machine can be furthered discussed on pleochroism.
8. **Laser Raman Spectrometer:** A spectrometer (Figure 3.6) is used to diagnose the material. It is based on the theory of Raman scattering. The phenomenon is caused after the laser light interacts with molecules and excites them. After which, the molecule will vibrate in a particular mode which changes the frequency of the original incident light. This change is also material-depended. This method is useful for identifying gemstones and inclusions due to the capability of laser to penetrate at considerable depth.
9. **Energy Dispersive X-Ray Fluorescence Spectrometer (EDXRF):** A spectrometer (Figure 3.7) is used to quantitatively analyze the chemical composition of material. X-ray is used as an energy source to bounce the inner electron out of the orbit. The process of electron substitution will emit characteristic light energy in the form of fluorescence which will be use to determine the element. The detection ranges from sodium to uranium.

10. **Electron Probe Micro Analyzer (EPMA):** A machine (Figure 3.10) is used to quantitatively measure the chemical composition of material. The technique is to launch electron to the polished surface of material then gather emitted X-ray and the secondary electron to process. Each standard element will be detected separately in different channels giving EPMA high accuracy and low detection limit.

Figure 3.2 Hydrostatic Balance based at the Gem and Jewelry Institute of Thailand (GIT)

Figure 3.3 Refractometer based at the Gem and Jewelry Institute of Thailand (GIT)

Figure 3.4 London Dichroscope based at the Gem and Jewelry Institute of Thailand (GIT)

Figure 3.5 Gemological Microscope based at the Gem and Jewelry Institute of Thailand (GIT)

Figure 3.6 Laser Raman Spectrometer model Renishaw T00A01-003 based at the Gem and Jewelry Institute of Thailand (GIT)

Figure 3.7 Energy Dispersive X-Ray Fluorescence Spectrometer (EDXRF) model EGLE III based at the Gem and Jewelry Institute of Thailand (GIT)

Figure 3.8 Fourier Transform Infrared Spectrometer (FTIR) model Nicolet 6700 based at the Gem and Jewelry Institute of Thailand (GIT)

Figure 3.9 Ultra Violet-Visible Light-Near Infrared Spectrometer (UV-Vis-NIR) model Lambda 950 Perkin Elmer based at the Gem and Jewelry Institute of Thailand (GIT)

Figure 3.10 Electron Probe Micro Analyzer (EPMA) model JEOL JXA-8100 based at Geology Department, Faculty of Science, Chulalongkorn University.

CHAPTER 4

RESULTS

4.1 General characteristics

Thirty one rough Quy Chau sapphire samples provided by the Gem and Jewelry Institute of Thailand (GIT) are classified into 3 groups including 5 blue samples, 13 orangey pink samples and 13 reddish pink samples. All the samples are considered as low to medium gem quality (see Appendix A).

Blue samples display a dark blue color with a glimpse of violet. The samples are highly fractured and almost opaque. There is heterogeneity of color inside with black inclusions. This group shows inert fluorescence under short wave and long wave ultraviolet light.

Orangey pink samples contain a large number of inclusions leading to the cloudy interior. Fractures and fluid fingerprints are normally found inside the crystal along with negative crystal arranging along the plane. Some samples are observed to have blue color zone. The samples are inert under ultraviolet region.

Reddish pinks samples have good transparent texture. They consist of crystal inclusions such as platelet and black inclusions. Fractures are moderately observed under the microscope. Fluorescence under short wave ultraviolet is very low.

Blue Samples:

Five untreated rough blue samples (Figure 4.1) from Quy Chau deposit are highly fractured interior. The transparencies of the crystals are almost opaque in some samples.

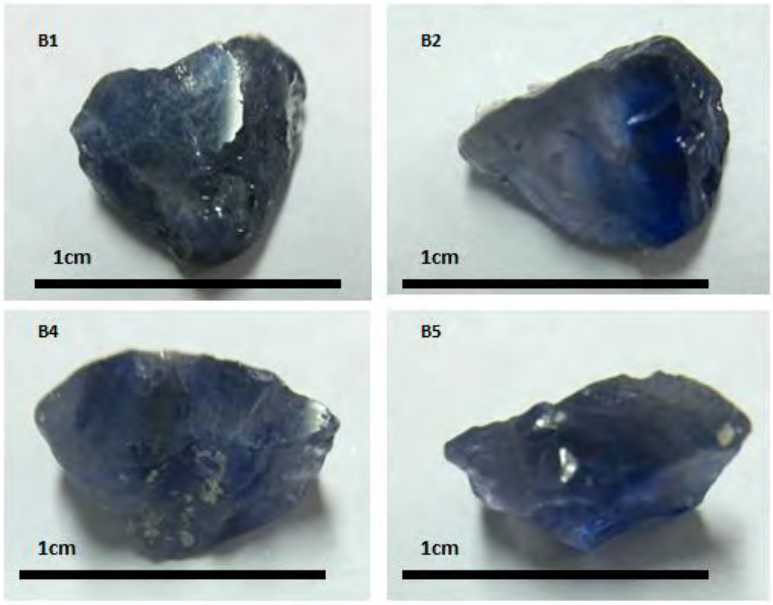

Figure 4.1 Representatives of blue sapphire sample

B1: 4.96 ct, B2: 1.50 ct, B4: 2.67 ct, B5: 2.49 ct

Orangey Pink Samples:

Thirteen untreated rough orangey pink samples (Figure 4.2) display cloudy texture due to minute inclusions. The samples consist of fractures and fluid fingerprints along with blue color zone. Black tubular samples are observed inside some samples.

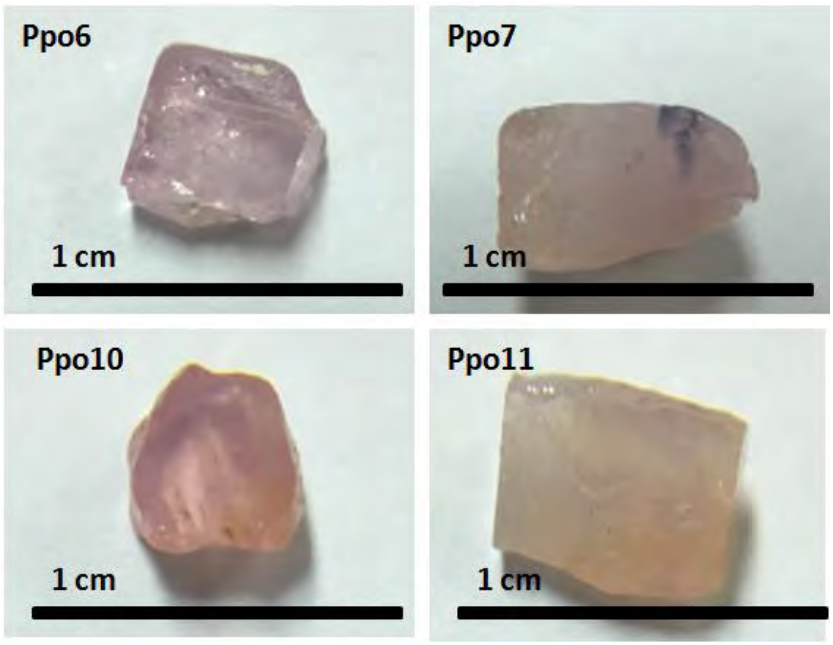

Figure 4.2 Representatives of orangey pink sapphire sample

Ppo6: 0.89 ct, Ppo7: 1.28 ct, Ppo10: 1.00 ct, Ppo11: 1.03 ct

Reddish Pink Samples:

Thirteen untreated rough reddish pink samples (Figure 4.3) appear to be transparent. Crystal inclusions are found ranging from low to intense. Crystal inclusions are found such as black inclusion, tubular inclusion and minute inclusion. The samples react weakly with the shortwave ultraviolet region.

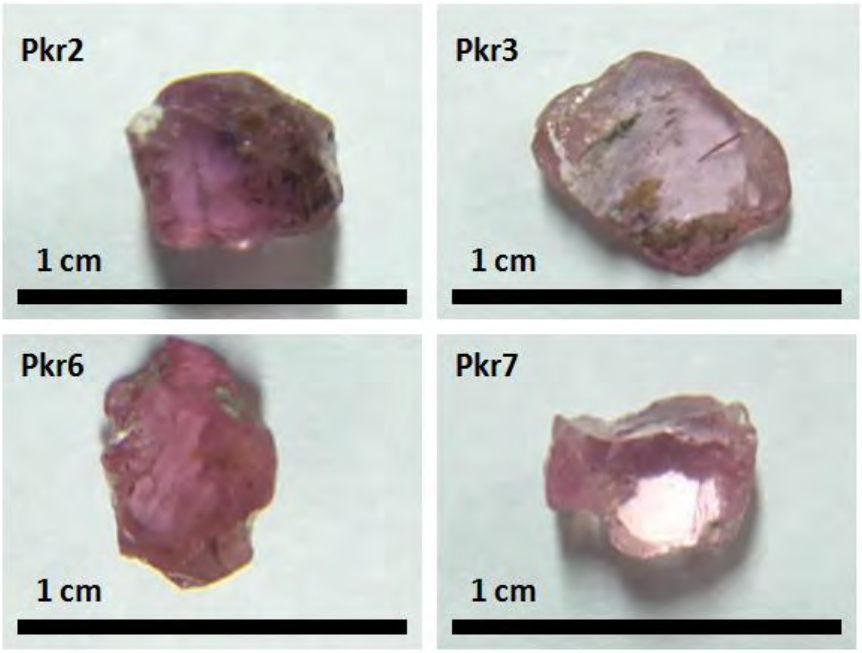

Figure 4.3 Representatives of reddish pink sapphire sample

Pkr2: 0.97 ct, Pkr3: 0.79 ct, Pkr6: 0.49 ct, Pkr7: 0.62 ct

All the samples are analyzed using basic equipment to determine their physical characteristics including weight, specific gravity, refractive index, birefringence, etc which are summarized in the Table 4.1

Table 4.1 Physical properties of sapphire samples

SAMPLE GROUP	Transparency	Weight (ct)	SG	RI		Birefringence	Fluorescence	
				NO	Ne		LW	SW
Blue	Opaque - Transparent	1.5-4.96 (2.90)	3.93-3.99 (3.95)	1.77	1.76-1.768	0.002-0.01	INNERT	INNERT
Orangey Pink	Semi Transparent - Transparent	0.61-1.63 (1.13)	3.9-3.98 (3.93)	1.76-1.77	1.75-1.762	0.005-0.015	INNERT	INNERT
Reddish Pink	Transparent	0.36-0.97 (0.61)	3.89-3.98 (3.93)	1.76-1.77	1.769-1.75	0.001-0.012	INNERT	W.Red - INNERT

4.2 Inclusions

A study under gemological microscope of Quy Chau sapphires has determined several types of inclusion inside the samples of all groups, for example, fingerprint, color zoning, crystal inclusions, cloud inclusion and minute inclusion.

Analytical results are illustrated in Table 4.2 showing that the blue samples are mostly fractured and the orangey pink samples have the highest number of cloud inclusion but shares approximately the same amount of crystal inclusions.

Table 4.2 Types of inclusion observed inside the samples

-None, *Low, **Considerable, ***High

Types of inclusion	Blue	Orangey Pink	Reddish Pink
Crystal Inclusion	**	***	***
Fingerprint	*	**	*
Minute Inclusion	*	*	***
Cloud Inclusion	*	***	*
Color Zoning	***	*	*
Cavity	*	**	*
Fracture	***	**	**

However, crystal inclusions located near the polished surface were analyzed using the Laser Raman Spectrometer.

Crystal Inclusion:

Due to low gem quality, most of the samples are highly accumulated with several types of crystal inclusions. Shapes of these inclusions vary from tubular to irregular. Some crystal are found associated with fingerprint or arrange along a plane. The examples of these crystal inclusions are shown in the following figures (Figures 4.4-4.7)

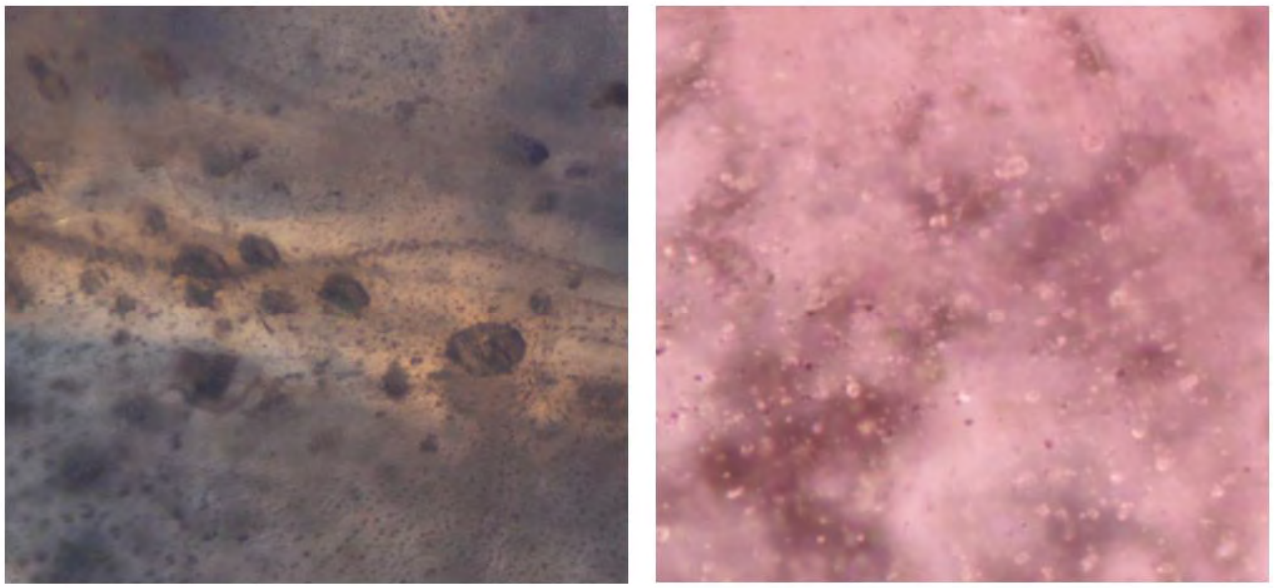

Figure 4.4 Several types of crystal inclusions found in sapphires from Quy Chau deposit, Vietnam

Left: Black inclusion from B1 with 2.5x magnification

Right: Group of irregular colorless inclusions from Pkr1 with 5.0x magnification

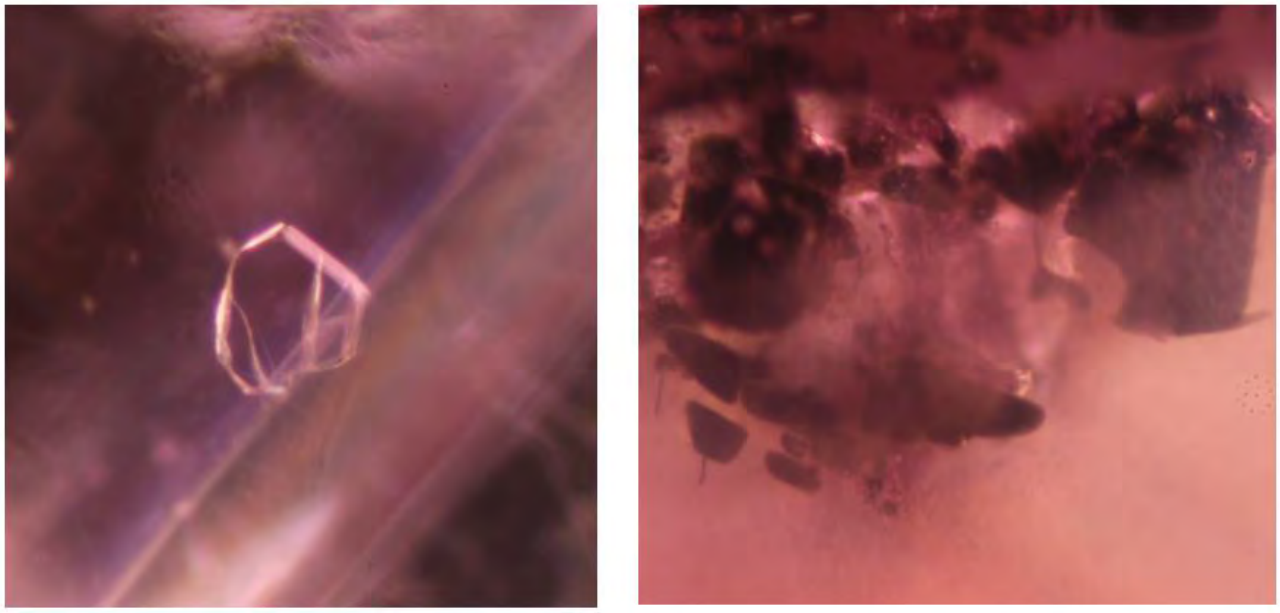

Figure 4.5 Several types of crystal inclusions found in sapphires from Quy Chau deposit, Vietnam

Left: Subhedral colorless crystal inclusion from Pkr8 with 5.0x magnification

Right: Group of irregular black inclusions from Pkr11 with 5.0x magnification

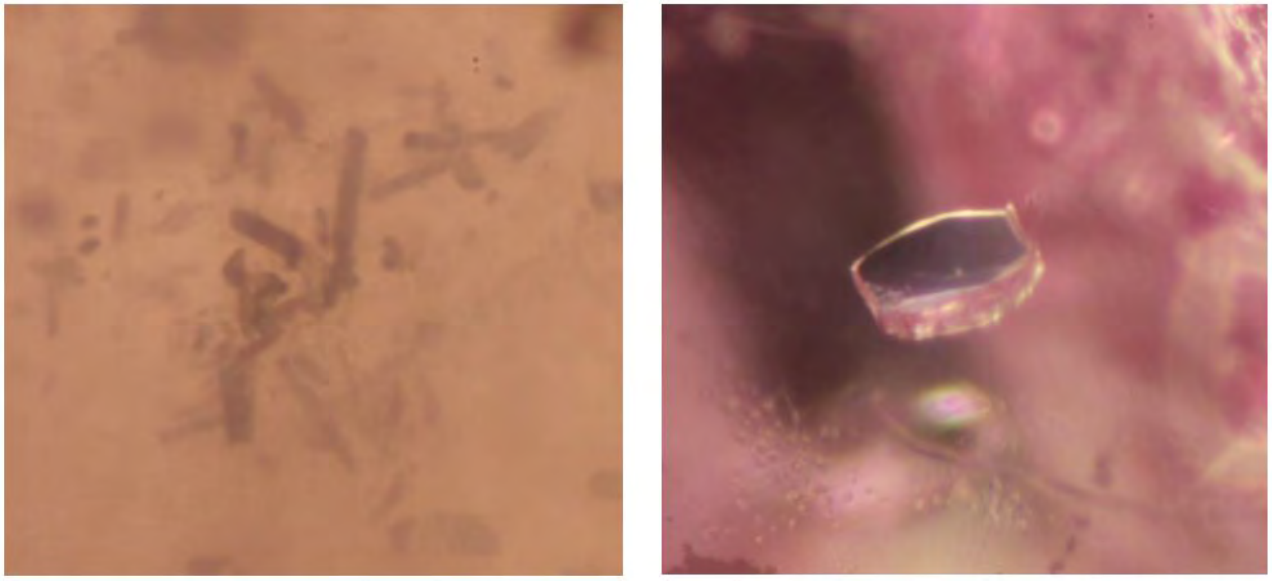

Figure 4.6 Several types of crystal inclusions found in sapphire from Quy Chau deposit, Vietnam

Left: Black tubular crystal inclusion from Ppo7 with 5.0x magnification

Right: Platelet inclusions from Pkr8 with 5.0x magnification

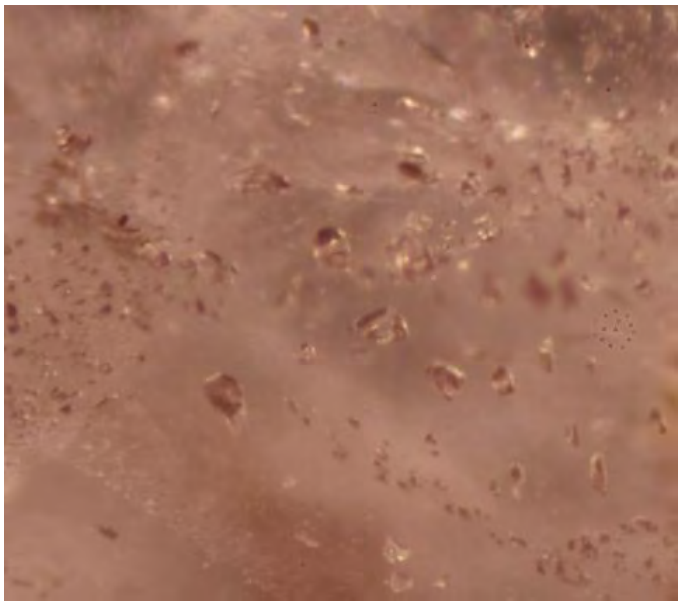

Figure 4.7 Group of colorless irregular crystal inclusion

Fingerprint:

Fingerprint inclusion (Figures 4.8 and 4.9) is a feature occasionally observed inside gemstones. It indicates the healing of fractures with remained substances in the fracture plane.

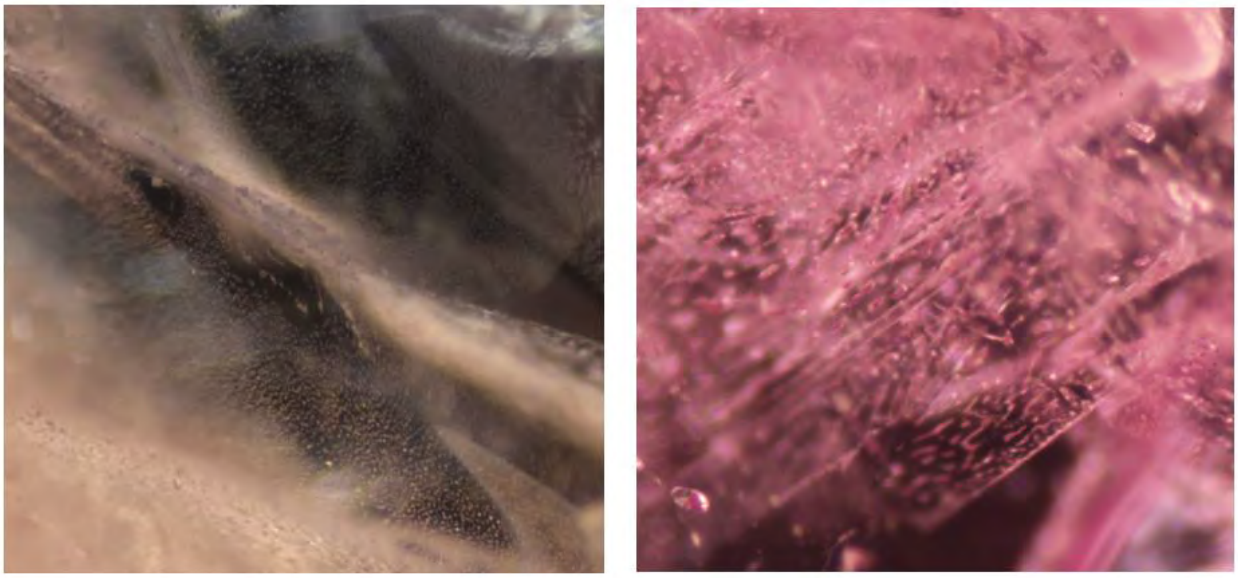

Figure 4.8 Several types of fingerprint inclusions found in sapphires from Quy Chau deposit, Vietnam

Left: Fingerprint inclusion from B5 with 2.0x magnification

Right: fingerprint inclusion from Pkr4 with 4.0x magnification

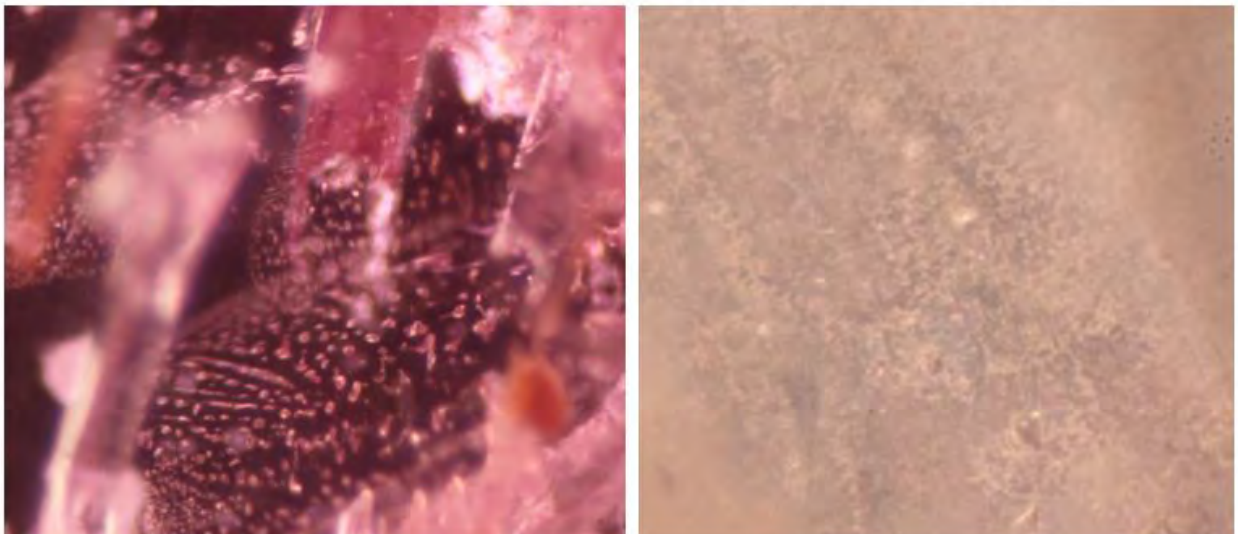

Figure 4.9 Several types of fingerprint inclusions found in sapphires from Quy Chau deposit, Vietnam

Left: Fingerprint inclusion from Pkr6 with 3.2x magnification

Right: fingerprint inclusion from Ppo12 with 5.0x magnification

Minute inclusion is a small crystal inclusion which resembles to bubble-like feature inside the gemstone. It is the most common form of inclusion present inside the crystal.

Figure 4.10 Minute inclusions from Pkr11 with 3.2x magnification

Cloud Inclusion:

Cloud inclusion usually causes the interior of gemstone appearing unclear (Figure 4.11). It can be found in several samples.

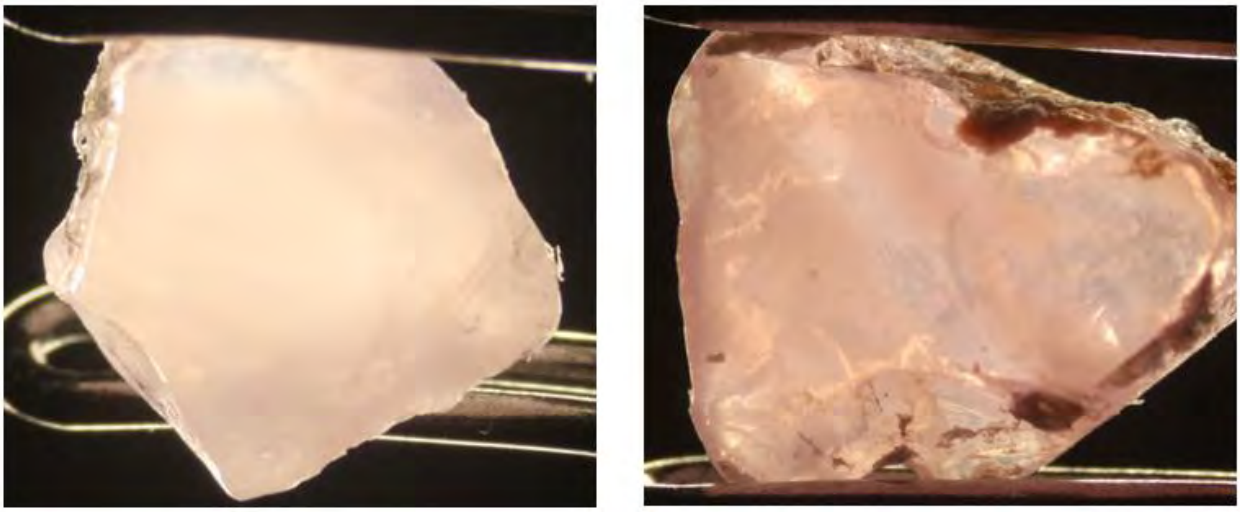

Figure 4.11 Cloud inclusion found in samples from Quy Chau deposit, Vietnam

Left: Cloud inclusion from Ppo5 with 0.8x magnification

Right: Cloud inclusion from Ppo12 with 1.0x magnification

Color Zoning:

Color zoning is a feature caused by heterogeneity of gem texture. It can be described as the uneven of color resulted from the rapid crystallization of gemstone

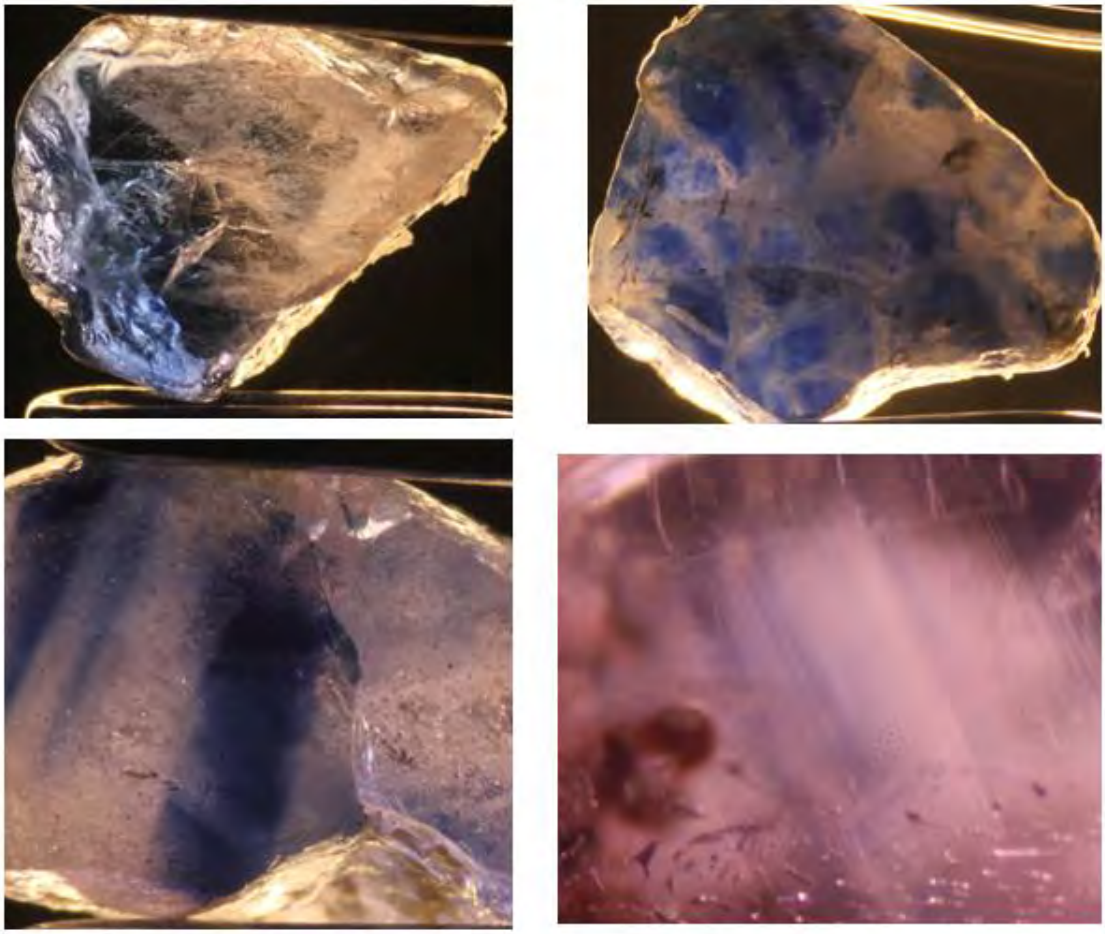

Figure 4.12 Color Zone in samples from Quy Chau Deposit, Vietnam

Upper Left: Blue color zoning from B2 with 0.8x magnification

Upper Right: Colorless color zoning along the fractures from B1 with 0.65x magnification

Lower Left: Blue straight color zoning from B4 with 0.8x magnifications

Lower Right: Blue color zoning inside pink sapphire from Pkr2 with 5.0x magnification

Cavity:

Cavity (Figures 4.13 and 4.14) is an internal feature which occurs during the crystallization process. It can be mistakenly identified as crystal but usually appears to be anhedral or connected as a tubular-like shape.

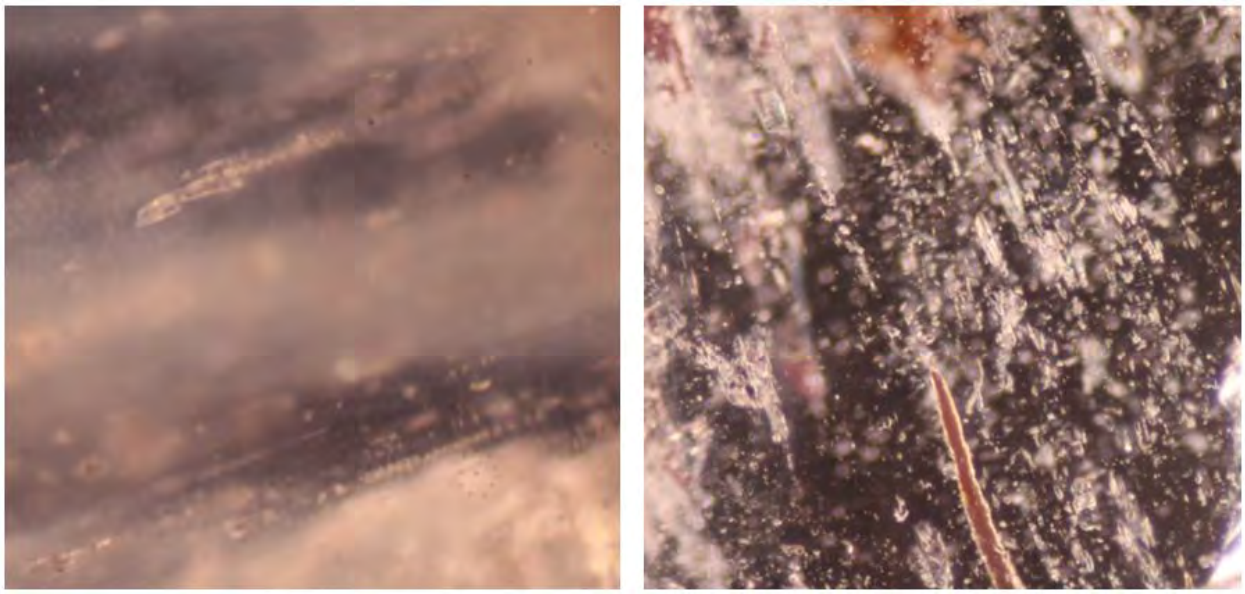

Figure 4.13 Cavities in sapphires from Quy Chau deposit, Vietnam

Left: Tubular cavities from Ppo10 with 2.5x magnification

Right: Tubular cavities associated with crystal from Pkr3 with 2.0x magnification

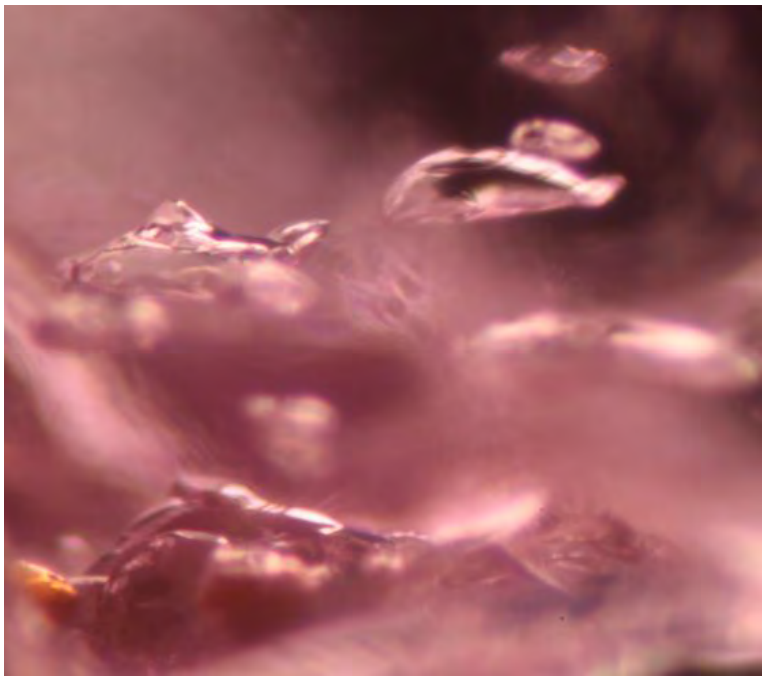

Figure 4.14 Irregular shaped cavities with fluid inclusion from Pkr8 with 5.0x magnification

Fracture:

Fracture (Figure 4.15) is formed due to the shortening of crystallization time in which the temperature decreases so fast that the contraction of molecule results in fracture.

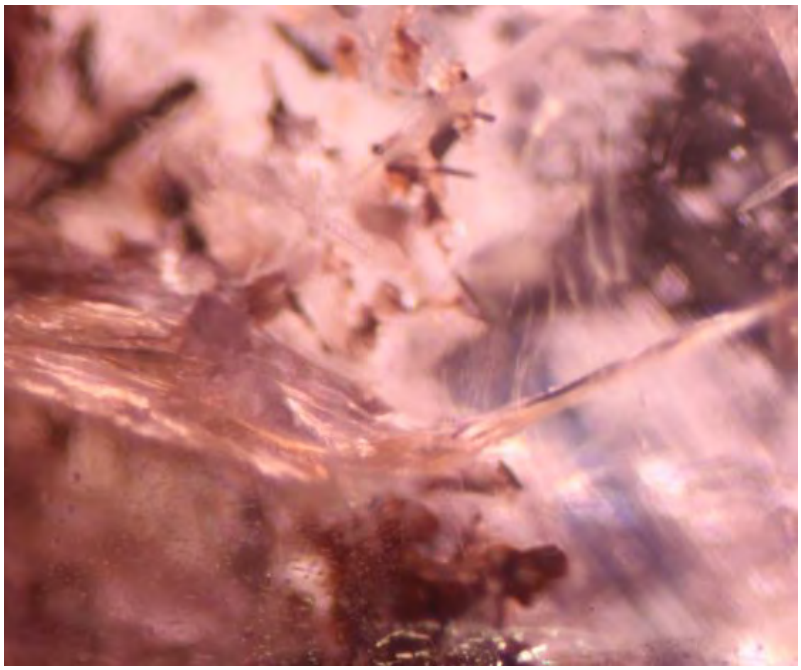

Figure 4.15 Fracture in sample Pkr2 with 5.0 magnification

4.3 Laser Raman Spectrometry Results

Raman spectrometry method was performed in order to analyze the mineral inclusion located near the polished surface of samples. In spite of a number of inclusions presenting within the crystal, only 2 crystals were found appropriate for the technique.

The first mineral inclusion was spotted under the microscope inside Pkr11 sample. The crystals are colorless, small and vary in shape. Some appear to be platelet. The spectrum of the crystal matched that of calcite as seen in Figure 4.16

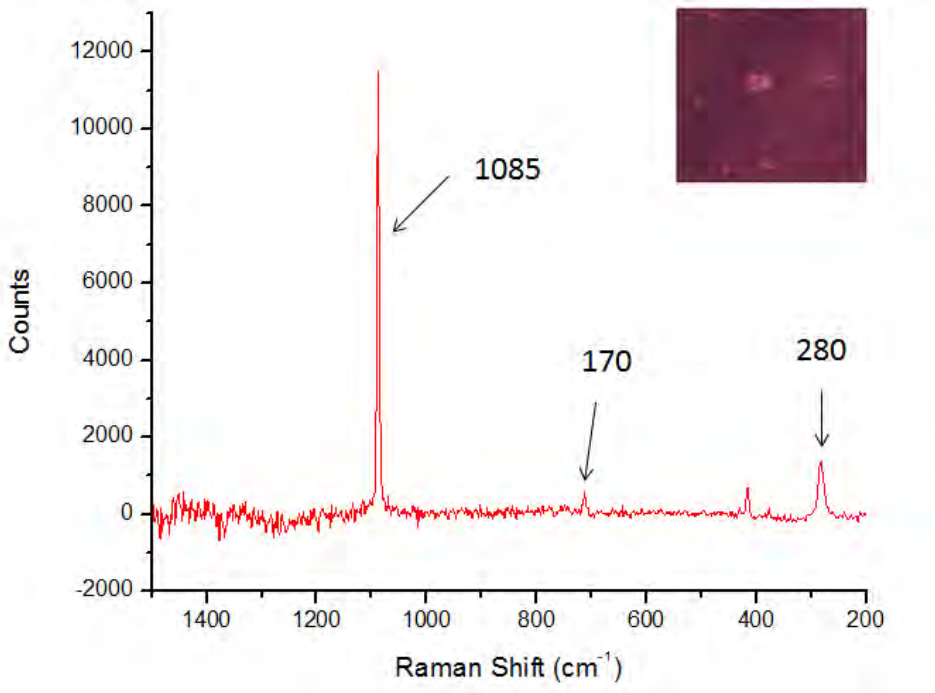

Figure 4.16 Laser Raman analytical results (Calcite) from inclusion in

Therefore, it can be assumed that sapphire from Quy Chau deposit was formed associated with carbonate rock such as impure limestone.

The second crystal inclusion found in Ppo7 was also colorless and appeared to be hexagonal platelet. It was identified by Laser Raman as apatite (Figure 4.17).

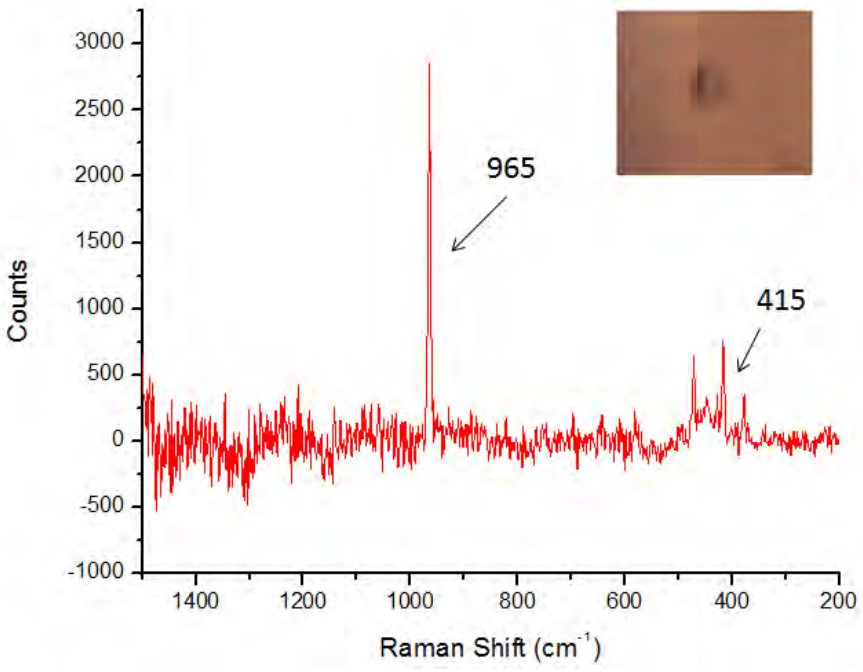

Figure 4.17 Laser Raman analytical results (Apatite) from inclusion in sample Ppo7.

Apatite can be found in a wide geological setting range from igneous condition to metamorphic condition. However, the most general condition is sedimentary condition of marine and lagoonal environment providing chlorine and sulfur from evaporite.

Nonetheless, there are more crystal inclusions such as black tubular mineral, black mineral and other colorless mineral that cannot be identified. Due to the exceeding of depth penetration capability of the machine

4.4 FTIR Spectrometry Results

FTIR analysis performed on 31 samples from Quy Chau deposit within the wavelength between 4000-400 cm^{-1}. The results show 3 distinctive trends from 3 groups (Appendix B).

Blue samples display a range of H_2O absorption from 3960-3520 cm^{-1} with a strong CO_2 absorption trough at 2361 cm^{-1}. The presence of H_2O is a result from an oxidation reaction of bohemite inside the corundum system. The amount of AlOOH (bohemite) in this group varies due to the incomplete of the reaction. The abosorption of such substances is determined at 3314, 2125 and 1997 cm^{-1}. It indicates a metamorphic origin of sapphire and implies that the gemstone has not been heat treated. C-H stretching absorption is found at 2915 and 2844 cm-1 which fall in the range of alkane group. The alkane group can occur in a small quantity during the metamorphism (Figure 4.18).

Orangey pink samples show 3950-3550 cm^{-1} absorption of H_2O which is a byproduct of the oxidation reaction of corundum. A strong CO_2 trough is also appeared at 2368 cm^{-1}. This group shows the strongest AlOOH absorption at approximately 2125 and 1984 cm^{-1}. The position of such mineral is sometimes incomplete due to the absence at about 3300 cm^{-1} in particular samples. The strong C-H stretching of alkane group is greatly found at 2922 and 2844 cm^{-1}. The results point out a metamorphic condition with no artificial treatment such as polymer filling and heat treatment (Figure 4.19).

Reddish pink samples mark H_2O absorption from 3980 to 3560 cm^{-1} resulted from the transformation of bohemite into corundum. CO_2, repeatedly, shows a strong trough of transmittance at 2346 cm^{-1} where the 3 groups share in common. Yet, this group possesses the lowest AlOOH content and even absent in some samples. This assumes that this group experienced the longest metamorphic period; therefore the reaction of the AlOOH had sufficient time to complete the reaction. A noticeable absorption of C-H stretching occurs at 2922 and 2851 cm^{-1} (Figure 4.20).

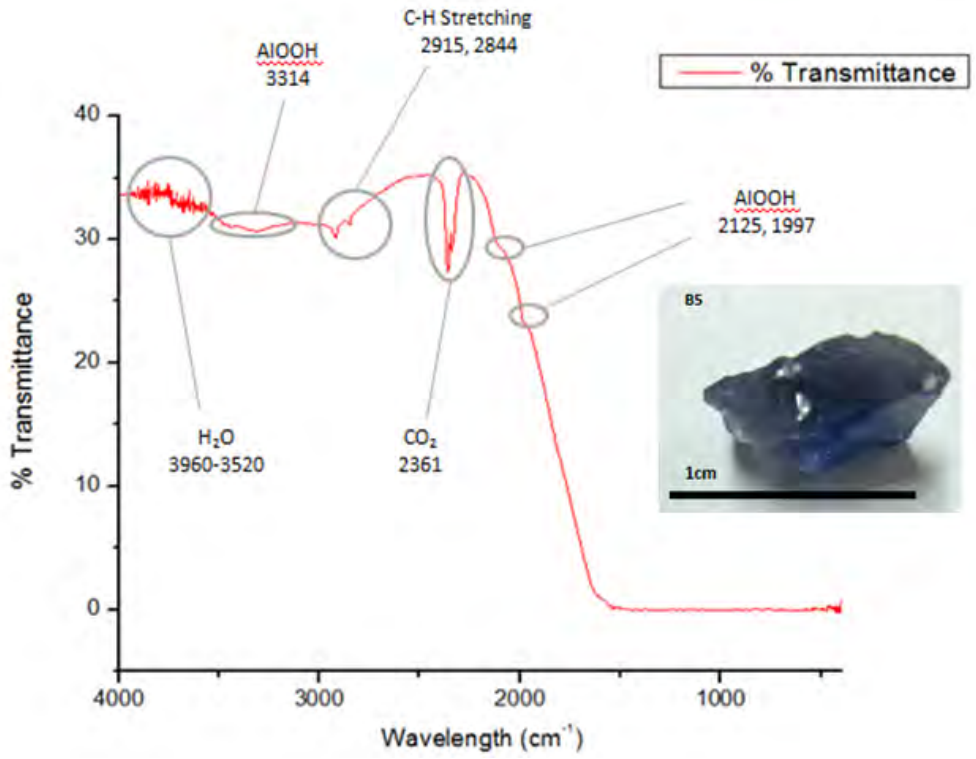

Figure 4.18 FTIR results from sample B5 showing an absorption of H_2O, C-H Stretching, CO_2 and AlOOH

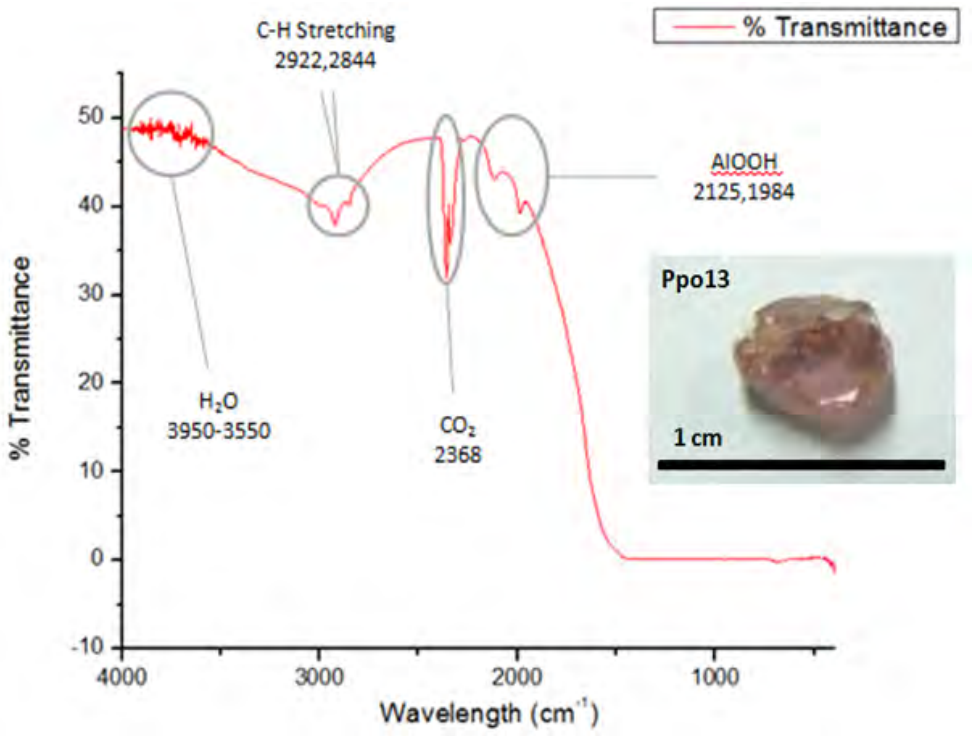

Figure 4.19 FTIR results from sample Ppo13 showing an absorption of H_2O, C-H Stretching, CO_2 and AlOOH

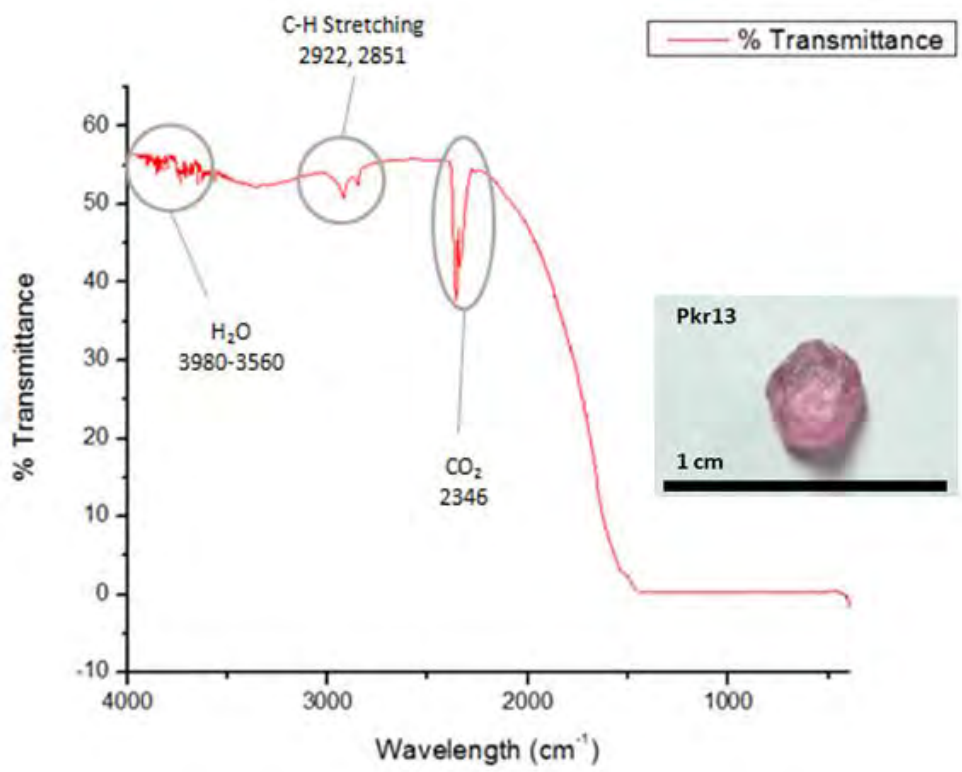

Figure 4.20 FTIR results from sample Pkr13 showing an absorption of H_2O, C-H Stretching and CO_2

4.5 UV-Vis-NIR Spectrometry Results

Based on UV-Vis-NIR absorption, the 3 groups illustrate 3 distinctive spectrum patterns which can be used as an explanation of the samples' colors (Appendix C).

Spectra of blue samples show absorption of Fe^{3+} at 324 and 390 nm. Individually, Fe^{3+} gives sapphire a yellowish tone. With a presence of Fe^{2+}/Ti^{4+} at 576 nm, the color can appear to be a greener. Fe^{3+}/Fe^{3+} are found between the range of 800-1000 nm which is out of visible light region. Yet, titanium content usually produces a colorless sapphire. Combine with iron, they transfer molecular charge and produce deep blue color of the samples (Figure 4.20).

Orangey pink samples reveal a color resulted from the content of both iron and chromium. Fe^{3+} absorption found at 340 and 375 nm result in an emission of yellow tone. Meanwhile, Cr^{3+} observed at 410 and 552 nm falls into green color absorption which contributes to red color reflection. Together, yellow and red, they form a orangey tone of the samples in this group (Figure 4.21).

Reddish pink samples only show a strong Cr^{3+} absorption at 401 and 555 nm. The element gives pinkish tone to the sapphires which characterizes the group (Figure 4.22).

Results also represent the differences of spectrum between O ray and E ray, which differentiates the colors given by each ray. It results in the effect called pleochroism which can be used as criteria for determining the facet of the gemstone.

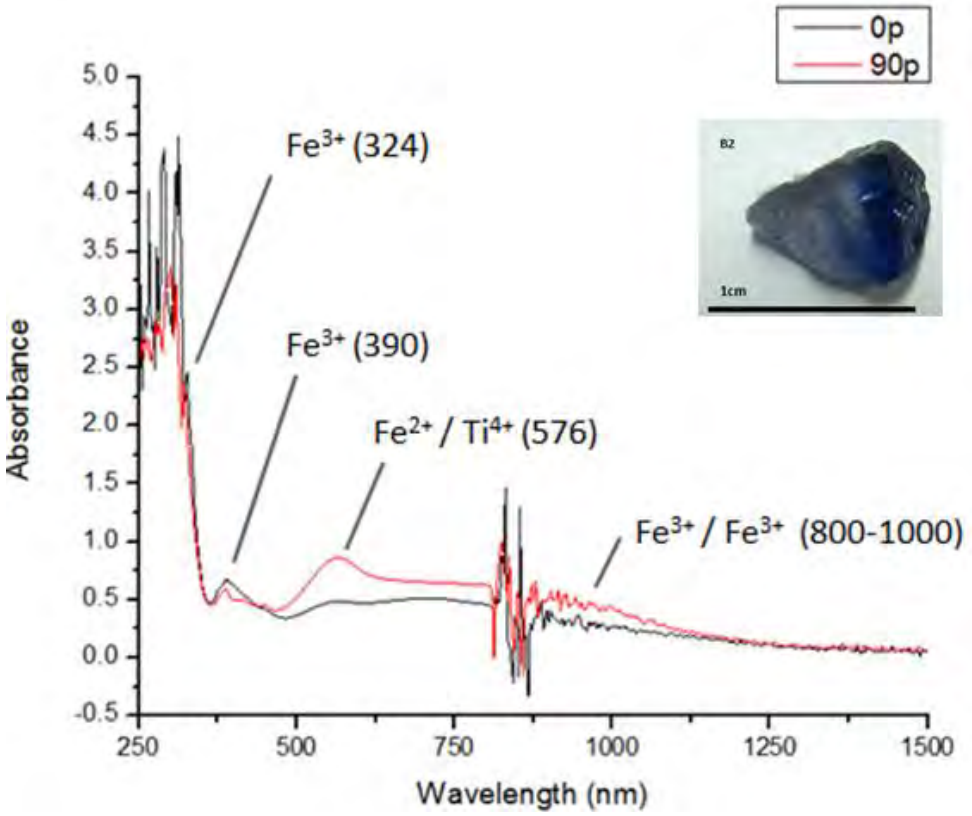

Figure 4.21 UV-Vis-NIR spectrum from sample B2 showing the absorption of Fe^{3+}, Fe^{2+}/Ti^{4} and $Fi^{3+}Fi^{3+}$

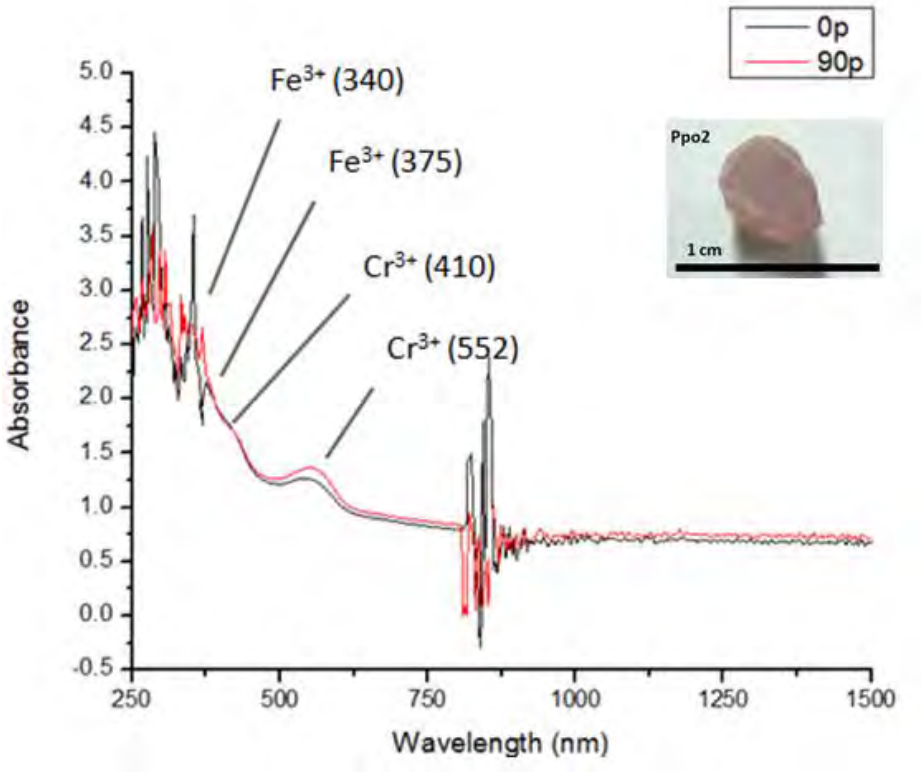

Figure 4.22 UV-Vis-NIR spectrum from sample Ppo2 showing the absorption of $Fe^{3+}$and Cr^{3+}

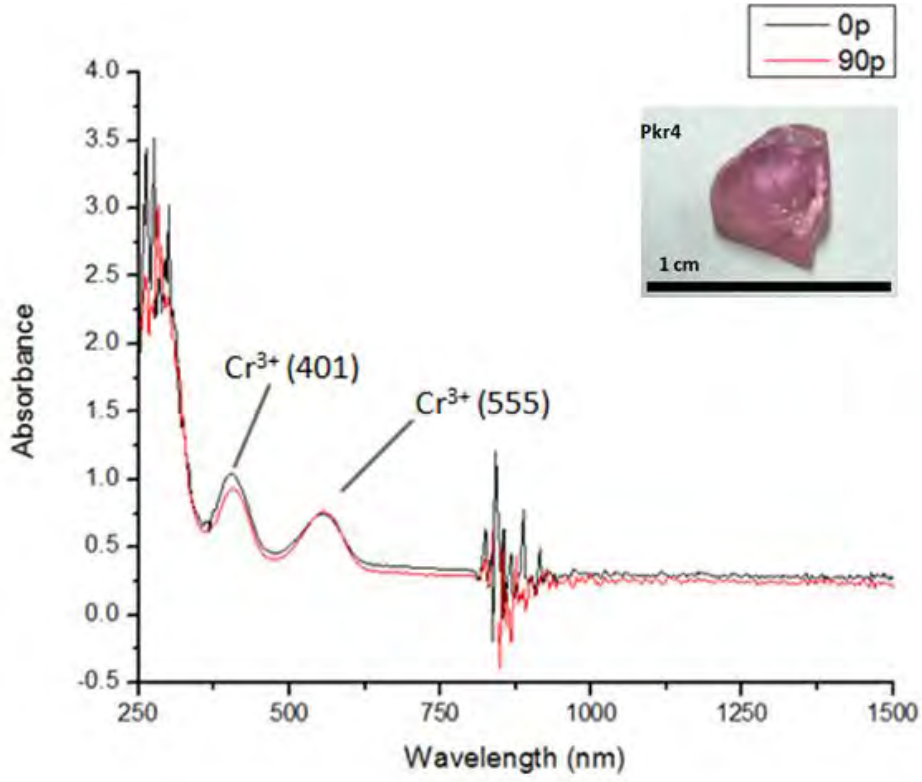

Figure 4.23 UV-Vis-NIR spectrum from sample Pkr4 showing the absorption of Cr^{3+}

4.6 Chemical Composition

EDXRF Analysis

EDXRF analysis is calculated for the chemical composition of sapphires which consist mainly of Al_2O_3. Other elements inputted during the process are those commonly found inside the gemstone and are partly responsible for providing colors such as TiO_2, V_2O_5, Cr_2O_3, Fe_2O_3 and Ga_2O_3. The calculation displays in the form of weight percentage (%wt). Table 4.3 and Appendix D represent the summarization of chemical composition of the samples.

Table 4.3 Summary of chemical EDXRF Analyses of Quy Chau sapphire samples.

Element	Blue Samples	Orangey Pink Samples	Reddish Pink Samples
Al_2O_3	88.65-99.86 (99.71±0.08)	99.67-99.93 (99.85±0.07)	99.55-99.91 (99.82±0.097)
TiO_2	0.03-0.08 (0.04±0.02)	0.0039-0.144 (0.06±0.05)	0.011-0.10 (0.02±0.02)
V_2O_5	0.01-0.01 (0.01±0.00)	0.00-0.01 (0.01±0.00)	0.00-0.03 (0.01±0.01)
Cr_2O_3	0.01-0.05 (0.03±0.02)	0.02-0.05 (0.03±0.01)	0.04-0.27 (0.10±0.06)
Fe_2O_3	0.026-0.254 (0.20±0.10)	0.011-0.289 (0.00±0.08)	0.01-0.14 (0.00±0.04)
Ga_2O_3	0.00-0.01 (0.01±0.00)	0.00-0.02 (0.01±0.00)	0.00-0.03 (0.01±0.01)

The main composition of sapphire is Al_2O_3, approximately 99.8%. However, for the blue samples, Fe_2O_3 content is higher than the other groups. This is the reason behind the blue color. The presence of vanadium (V_2O_5) also influences the color by adding a deep violet tone to the blue samples (Sutherland, 2014). In contrast, the reddish pink samples are calculated to have the highest quantity of chromium (Cr_2O_3) and contain the lowest amount of iron. Meanwhile, the orangey pink samples include considerable amounts of both iron and chromium giving orangey tone of color.

Proportional plots between Cr_2O_3/Ga_2O_3 and Fe_2O_3 in Figure 4.23 can be used to separate sapphires between metamorphic origin and basaltic origin. It suggests that the ratios exceeding 1 belong to metamorphic region while their counterpart is basaltic origin (Diep, 2015).

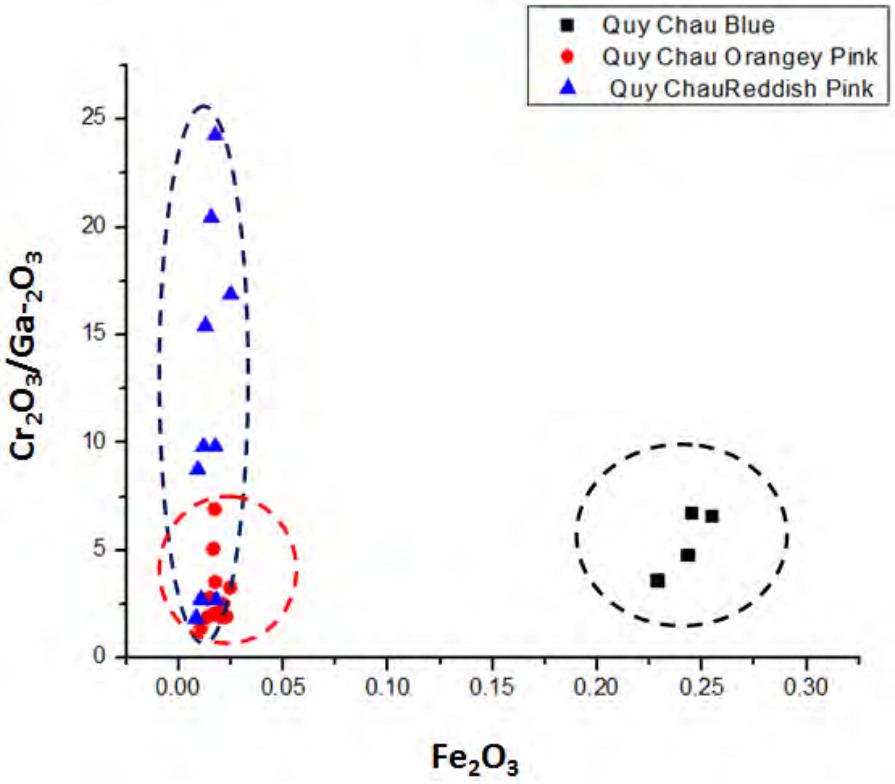

Figure 4.24 Cr_2O_3/Ga_2O_3 vs. Fe_2O_3 plots of Quy Chau samples

As illustrated, most of the sapphire samples from Quy Chau deposit have high Cr_2O_3/Ga_2O_3 exceeding 1. Moreover, each sample group has its own distinctive trend. The blues samples have the highest content of iron while the reddish pink samples have the highest content of chromium. The orangey pink samples fall between the ranges of the previous groups

$LogCr_2O_3/Ga_2O_3$ vs $LogFe_2O_3/TiO_2$ and $LogCr_2O_3/V_2O_5$ vs Log Fe_2O_3/Ga_2O_3 (Figures 4.24 and 4.25) plots also differentiate these sample groups.

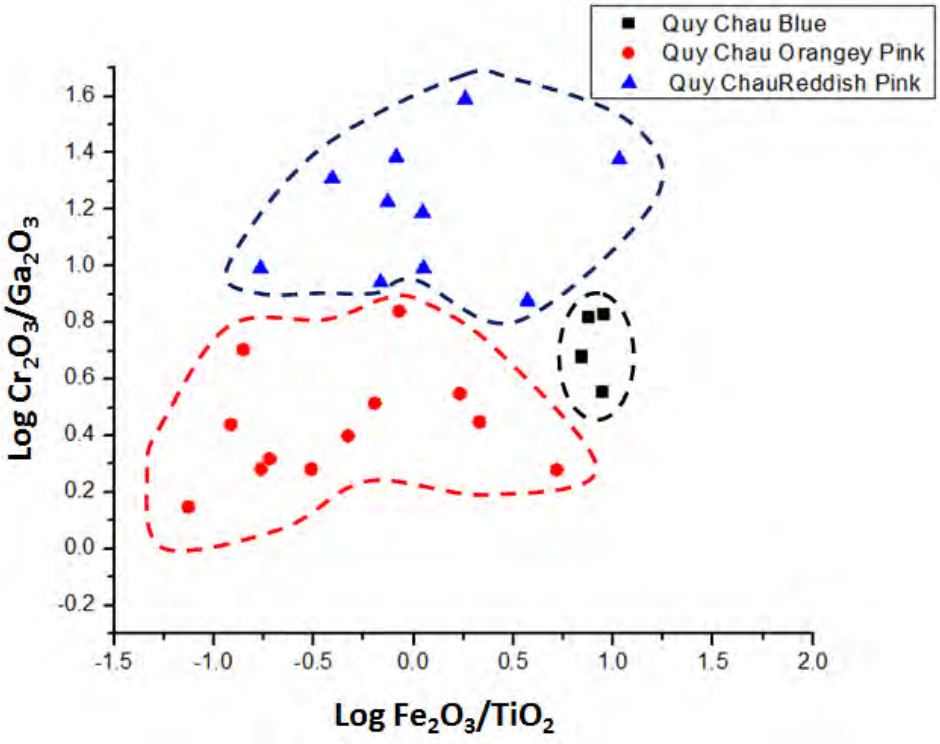

Figure 4.25 Log Cr_2O_3/Ga_2O_3 vs Log Fe_2O_3/TiO_2 plots of Quy Chau sapphires.

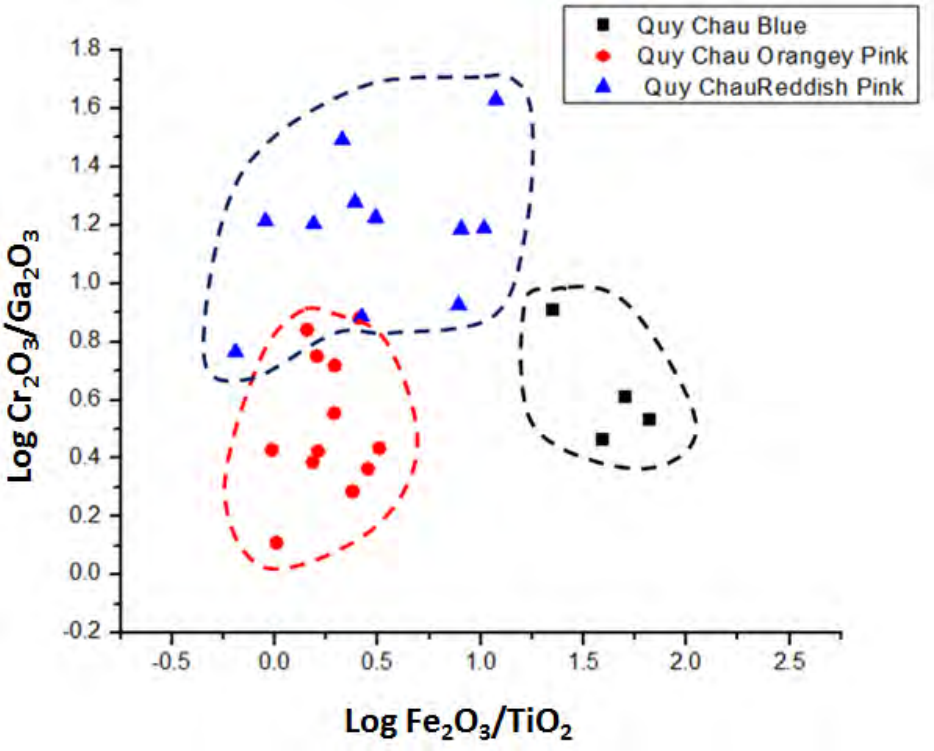

Figure 4.26 Log Cr_2O_3/V_2O_5 vs Log Fe_2O_3/Ga_2O_3 plots of Quy Chau sapphires.

The trends are similar to the previous plots. Blue samples are of the highest iron content; reddish pink samples are of the highest chromium content and orangey pink samples contain moderate contents of both iron and chromium.

EPMA Analysis

EPMA analyses also show similar results to that of EDXRF. The main composition is Al_2O_3. Trace elements of sapphire samples are re-calculated on the basis of stoichiometry and concluded on Table 4.4 and all data are reported in Appendix E.

Table 4.4 Representatives of EPMA analyses of Quy Chau sapphire samples.

Element	B2-1	B2-2	B2-3	Ppo9-1	Ppo9-2	Ppo9-3	Ppo10-1	Ppo10-2	Ppo10-3	Pkr3-1	Pkr3-2	Pkr3-3	Pkr4-1	Pkr4-2	Pkr4-3
SiO2	0.0000	0.0000	0.0000	0.0000	0.0002	0.0004	0.0000	0.0000	0.0000	0.0002	0.0001	0.0000	0.0000	0.0000	0.0000
TiO2	0.0003	0.0001	0.0000	0.0018	0.0017	0.0011	0.0011	0.0005	0.0010	0.0001	0.0002	0.0004	0.0006	0.0000	0.0003
Al2O3	1.9964	1.9965	1.9963	1.9969	1.9965	1.9972	1.9966	1.9991	1.9982	1.9981	1.9988	1.9984	1.9970	1.9984	1.9979
FeO	0.0040	0.0039	0.0044	0.0001	0.0000	0.0004	0.0003	0.0000	0.0002	0.0003	0.0005	0.0000	0.0000	0.0007	0.0002
Mn	0.0003	0.0006	0.0000	0.0000	0.0006	0.0000	0.0001	0.0000	0.0002	0.0005	0.0000	0.0000	0.0004	0.0000	0.0000
Mg	0.0000	0.0001	0.0000	0.0000	0.0000	0.0000	0.0001	0.0001	0.0000	0.0001	0.0000	0.0000	0.0000	0.0000	0.0001
Ca	0.0000	0.0000	0.0002	0.0001	0.0000	0.0002	0.0000	0.0002	0.0000	0.0000	0.0001	0.0001	0.0001	0.0000	0.0000
K	0.0001	0.0001	0.0001	0.0001	0.0004	0.0001	0.0000	0.0000	0.0000	0.0002	0.0001	0.0000	0.0000	0.0000	0.0000
Cr	0.0002	0.0003	0.0006	0.0003	0.0004	0.0003	0.0014	0.0000	0.0003	0.0006	0.0003	0.0005	0.0017	0.0009	0.0011
V	0.0000	0.0000	0.0000	0.0002	0.0000	0.0000	0.0002	0.0000	0.0000	0.0002	0.0000	0.0003	0.0001	0.0001	0.0002
Formula	3(O)	3(O)	3(O)	3(O)	3(O)	3(O)	3(O)	3(O)	3(O)	3(O)	3(O)	3(O)	3(O)	3(O)	3(O)
Si	0.000	0.000	0.000	0.000	0.000	0.000	0.000	0.000	0.000	0.000	0.000	0.000	0.000	0.000	0.000
Ti	0.000	0.000	0.000	0.002	0.002	0.001	0.001	0.000	0.001	0.000	0.000	0.000	0.001	0.000	0.000
Al	1.996	1.996	1.996	1.997	1.997	1.997	1.997	1.999	1.998	1.998	1.999	1.998	1.997	1.998	1.998
Fe	0.004	0.004	0.004	0.000	0.000	0.000	0.000	0.000	0.000	0.000	0.000	0.000	0.000	0.001	0.000
Mn	0.000	0.001	0.000	0.000	0.001	0.000	0.000	0.000	0.000	0.000	0.000	0.000	0.000	0.000	0.000
Mg	0.000	0.000	0.000	0.000	0.000	0.000	0.000	0.000	0.000	0.000	0.000	0.000	0.000	0.000	0.000
Ca	0.000	0.000	0.000	0.000	0.000	0.000	0.000	0.000	0.000	0.000	0.000	0.000	0.000	0.000	0.000
K	0.000	0.000	0.000	0.000	0.000	0.000	0.000	0.000	0.000	0.000	0.000	0.000	0.000	0.000	0.000
Cr	0.000	0.000	0.001	0.000	0.000	0.000	0.001	0.000	0.000	0.001	0.000	0.000	0.002	0.001	0.001
V	0.000	0.000	0.000	0.000	0.000	0.000	0.000	0.000	0.000	0.000	0.000	0.000	0.000	0.000	0.000

CHAPTER 5

DISCUSSION AND CONCLUSIONS

Thirty one rough samples from Quy Chau deposit, Vietnam, have been categorized into 3 groups including blue samples, orangey pink samples and reddish pink samples.

Five blue samples are highly fractured and the transparency is considered as high to opaque. Color zone and crystal inclusion are usually found in these samples.

Thirteen orangey pink samples are cloudy due to the high accumulation of small inclusion. Blue color zoning can be found in some samples which indicate the presence of iron or vanadium (Sutherland, 2014).

Thirteen reddish pink samples are the most transparent among the other groups. Black mineral inclusion and colorless inclusion are found and located near the surface of the samples.

The fluorescence phenomenon can be used to identify sapphire from some specific deposit such as Mozambique or Madagascar. However, most of the samples from Quy Chau display inert fluorescence under ultraviolet region. Only reddish pinks samples show weak red fluorescence under short wave ultraviolet. Anyhow, since the proper mechanism behind this effect is still not well understood, it is difficult to identify the cause of fluorescence. However, most heat treated sapphires appear to have chalky fluorescence (Crowningshield, 1966). Therefore, it may assume that all the samples have never been heat treated.

Crystal inclusions found inside the gemstone are identified as calcite and apatite which may indicate protolith of the sapphire. Calcite can be found normally as a main composition of carbonate rock. Since the literature reviews (Garnier, 2008) imply that the Quy Chau sapphires are marble-hosted. The presence of calcite can confirm carbonate environment. Along with apatite, it can relate to the lagoonal environment with evaporite crystallization feeding the chlorine and sulfide ion to the system to form apatite (Li, 2015). Other unidentified crystal such as black tubular crystals or black crystals can be interpreted as amphibole which is commonly found in the amphibolites facies metamorphism or spinel which is the initial substance for forming corundum from the destabilization process along the retrograde metamorphism (Garnier, 2008). Rutle is also possible to occur since it widespread crystalline under high pressure and temperature metamorphic condition.

Fingerprint is found associated with plane-arranged crystals as a result of fracture healing process. As the fractures are healed, the solution left at the plane can become curvy and result in fingerprint patterns. However, as the process continues, those solutions will gradually crystalline and form small crystals (Roedder, 1962).

The heterogeneity of color is commonly observed inside the blue samples. The principle which is responsible for this feature is the immobility of titanium. To create blue color, a charge transferring between iron and titanium ion is required. Yet, due to the high oxidation state of titanium, it requires a high energy condition such as magmatic chamber to move freely (Baalen, 1993). The energy from contact metamorphism is not enough for titanium to flow resulting in a colorless area inside the gem with only titanium. Unable to move to the lattice point, titanium would later oxidize into rutile (TiO_2).

FTIR results show a varying amount of AlOOH at about 3300, 2900 and 2850 cm^{-1} in Quy Chau deposit. An absence of AlOOH normally indicates heat treatment or basaltic sapphire. However, all the studied samples possess particular quantity of AlOOH which means that it crystalline under non magmatic condition.

Three groups of samples also share the same trend of high CO_2 at approximately 2350 cm^{-1}. The evidence fit the model of Garnier et al, 2008 which suggest that sapphire from northern Vietnam were formed under a high CO_2 condition within a retrograde metamorphism caused during the Himalayan orogeny. It is clear that the high level of CO_2 will reduce the pH of the system contributing to a suitable condition for oxidative reaction to take place. This includes the reaction of AlOOH $\rightarrow$ $H_2O + Al_2O_3$. Nevertheless, Due to the retrogradational condition, this reaction tended to slow down as the temperature and pressure decrease contributing to the leftover of AlOOH in some samples (Fillali, 2011).

H_2O is normally found between 3960 – 3520 cm^{-1} along with C-H stretching of alkane group generally at 2922 and 2850 cm^{-1}

UV-Vis-NIR results pointed out the cause of color in Quy Chau sapphire. In blue samples, a strong peak of Fe^{3+} at 324 and 390 nm and a 576 nm peak of Fe^{2+}/Ti^{4+} deliver blue color to this sample group. Absorption of both Fe^{3+} detected at 340 and 375 nm and Cr^{3+} shown at 410 and 522 nm represent the combination of yellow and pink color resulting in orangey zone of the orangey pink group. Finally, reddish pink group consist of Cr^{3+} peak in common appearing at 401 and 555 nm.

EDXRF results reveal that the main composition of corundum is Al_2O_3. The highest Fe_2O_3 content is found in blue samples. Reddish pink group, on the other hand, shows the lowest iron content but is rich in Cr_2O_3.

Moreover, plotted graph of Cr_2O_3/Ga_2O_3 shows values which exceed 1. It can assume that these samples are controlled by metamorphic mechanism. The plot also divided the 3 groups of samples into 3 zones due to the different compositions. The zones of Quy Chau at the same time differ from other deposits such as Mozambique, Rawanda, Nigeria, Thailand, Madagascar and Myanmar from unknown mines on logarithm plots of $LogCr_2O_3/Ga2O3$ vs $LogFe_2O_3/TiO_2$ as seen in Figures 5.1 to 5.3.

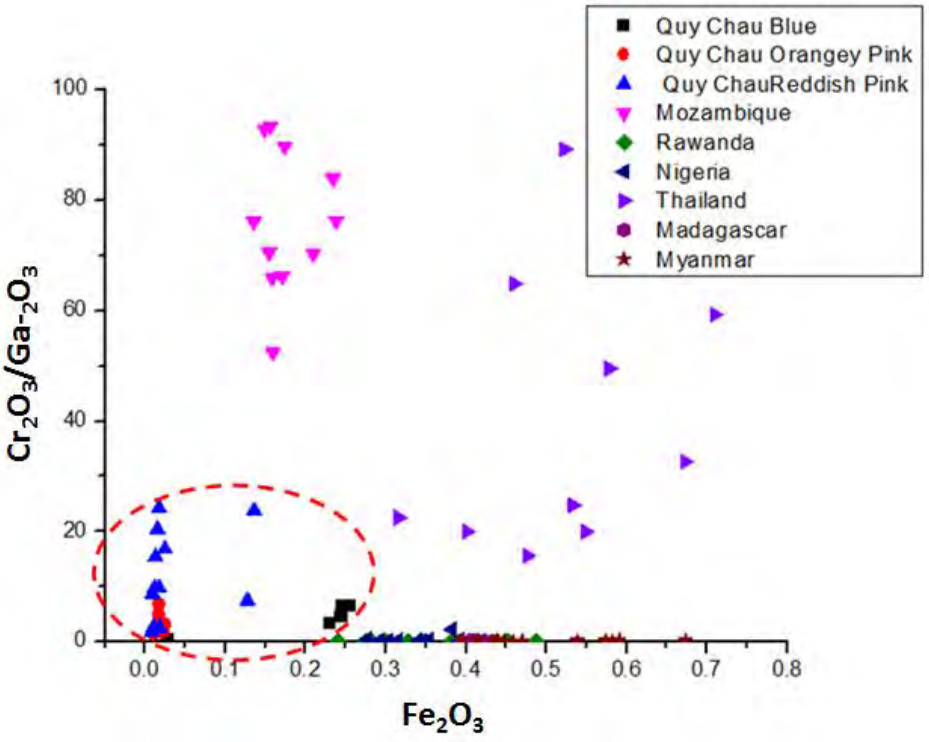

Figure 5.1 Cr_2O_3/Ga_2O_3 VS Fe_2O_3 plot of Quy Chau sapphire samples compared to other deposits.

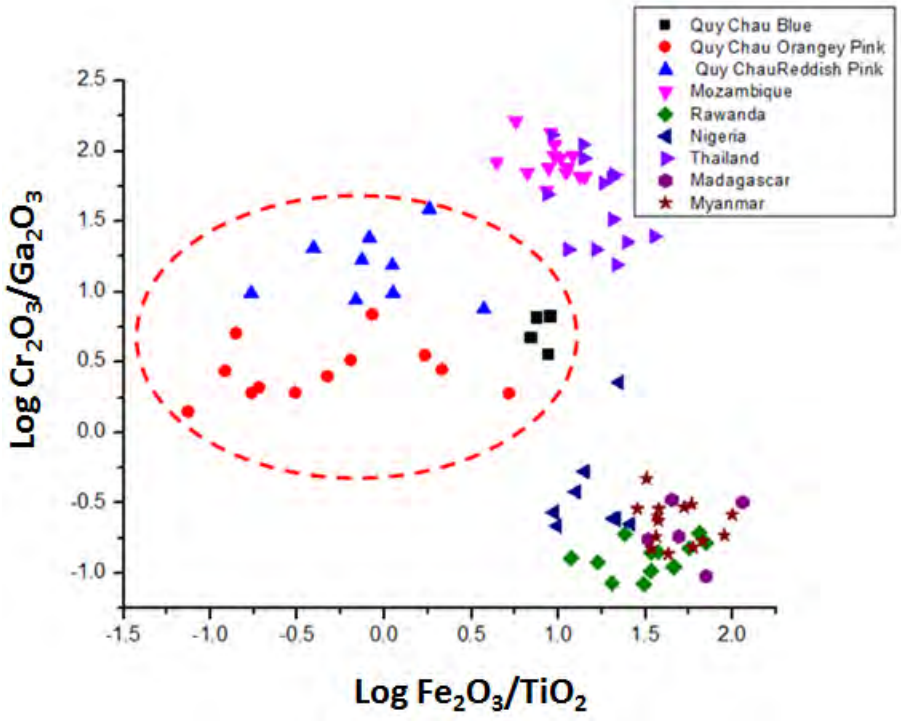

Figure 5.2 Log Cr_2O_3/Ga_2O_3 vs Log Fe_2O_3/TiO_2 plot of Quy Chau sapphires compared to other deposits.

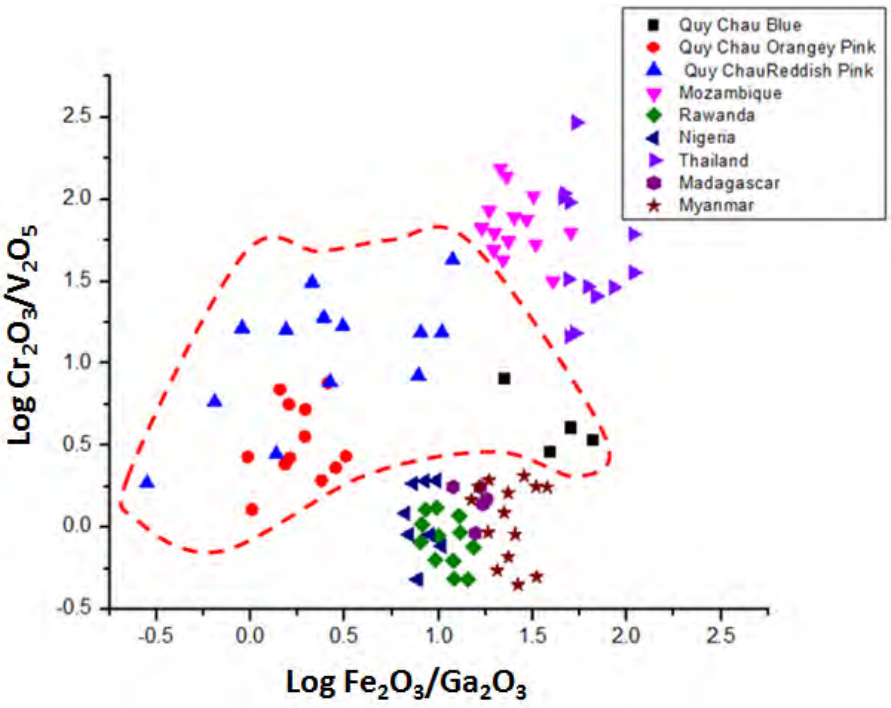

Figure 5.3 Log Cr_2O_3/V_2O_5 vs Log Fe_2O_3/Ga_2O_3 plot of Quy Chau sapphires compared to other deposits.

Chemical compositions gathered from EPMA resemble that of EDXRF. Stoichiometry re-calculation provides quantity of iron, magnesium and titanium atoms which can be plotted into ternary plots (Figure 5.1).

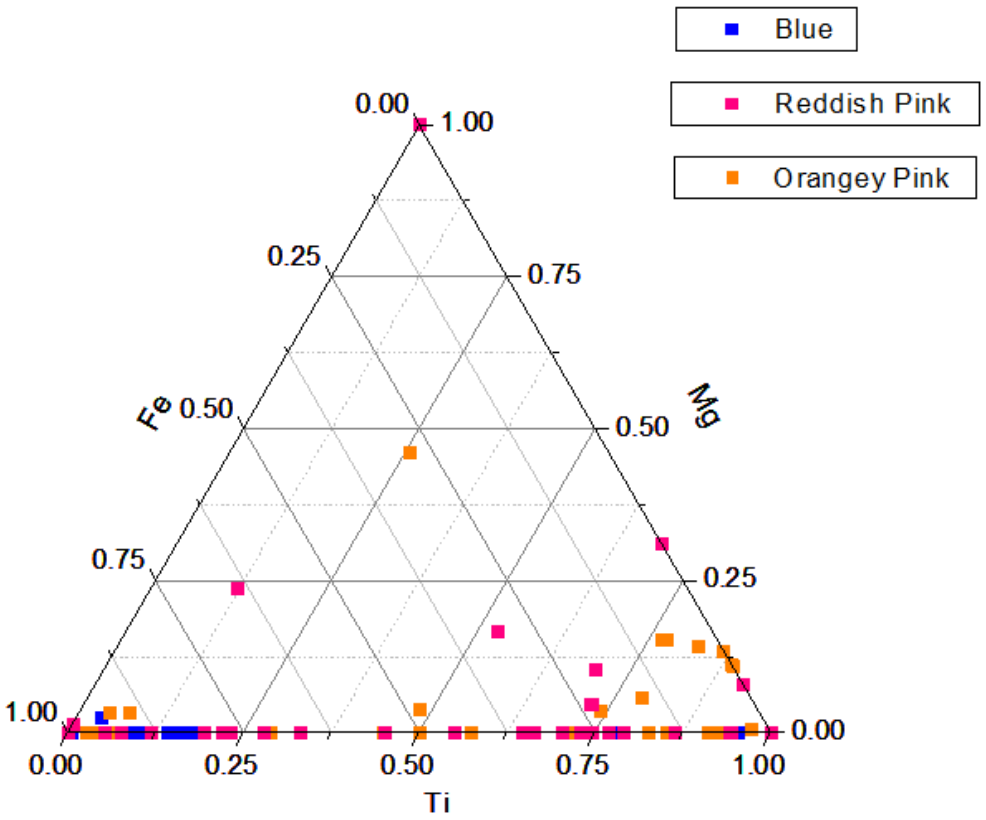

Figure 5.4 Ternary Ti-Mg-Fe plots of Qua Chau sapphires

According to Häger (2001), blue samples fall into blue color zone, which is sensible since the samples display dark blue tone. However, orangey and reddish pink samples spread show no systematically trends. This phenomenon is explained by the fact the coloring elements of both categories depend mainly on chromium instead of iron and titanium

In conclusion, with a presence of calcite and apatite, high CO_2 content and a spotty presence of AlOOH, the origin of these sapphires can be interpreted matching the new genetic model (Garnier et al, 2008). The model suggests that the protoliths of the sapphires were impure limestone which was deposited on a lagoonal platform. The platform is enriched in alumina from continental feed. Pressure and temperature later derived from Himalayan orogeny which caused many sapphire depositions along the mountain range. Therefore, the sapphire has been mainly formed during the retrograde process with high CO_2 extracted from carbonate. The CO_2 reduced the overall pH level and influenced any oxidative reaction such as alumina oxide formation (corundum) (Fyfe, 1958).

APPENDICES

SECTION A: SAMPLE COLLECTION

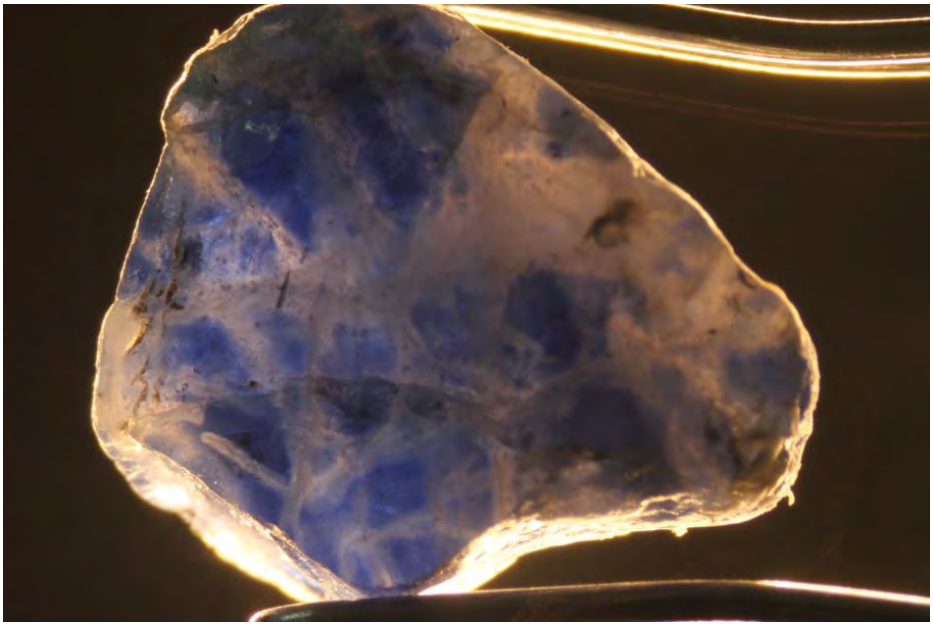

Figure A1 Sample B1 with 0.65x magnification

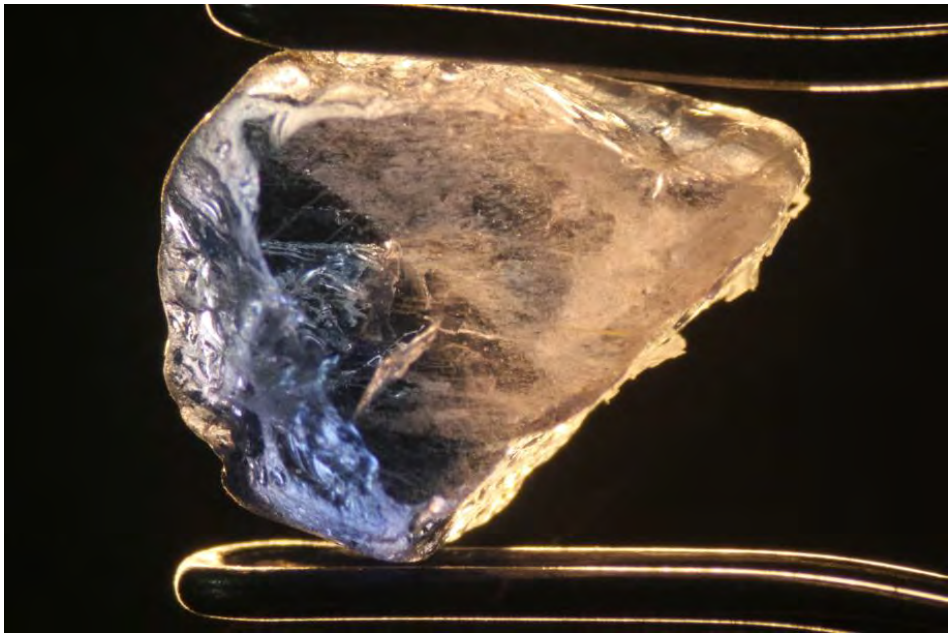

Figure A2 Sample B2 with 0.8x magnification

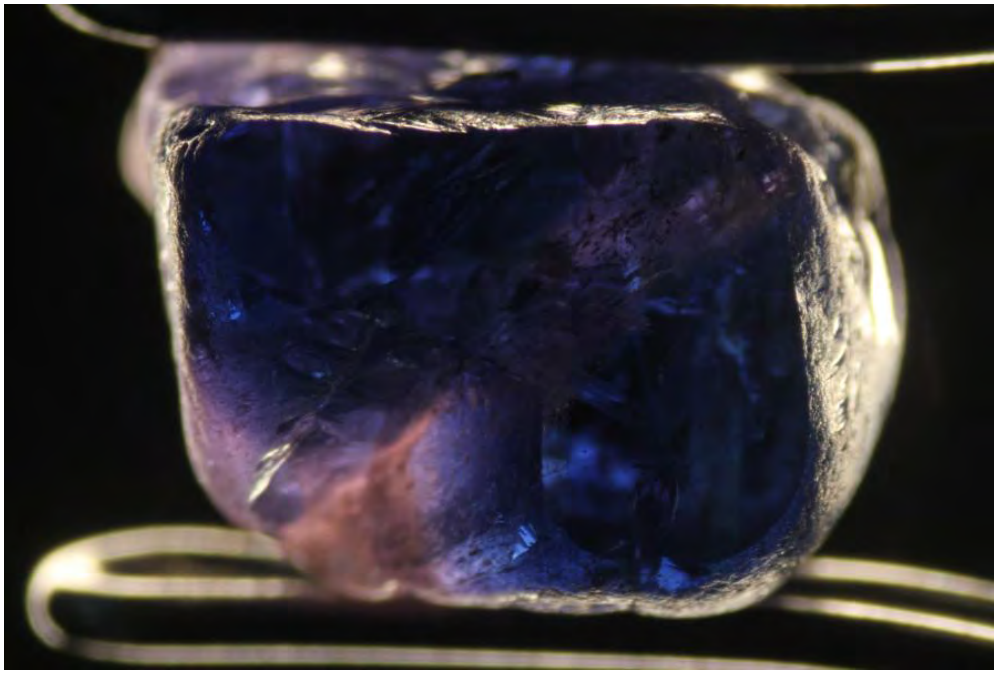

Figure A3 Sample B3 with 0.8x magnification

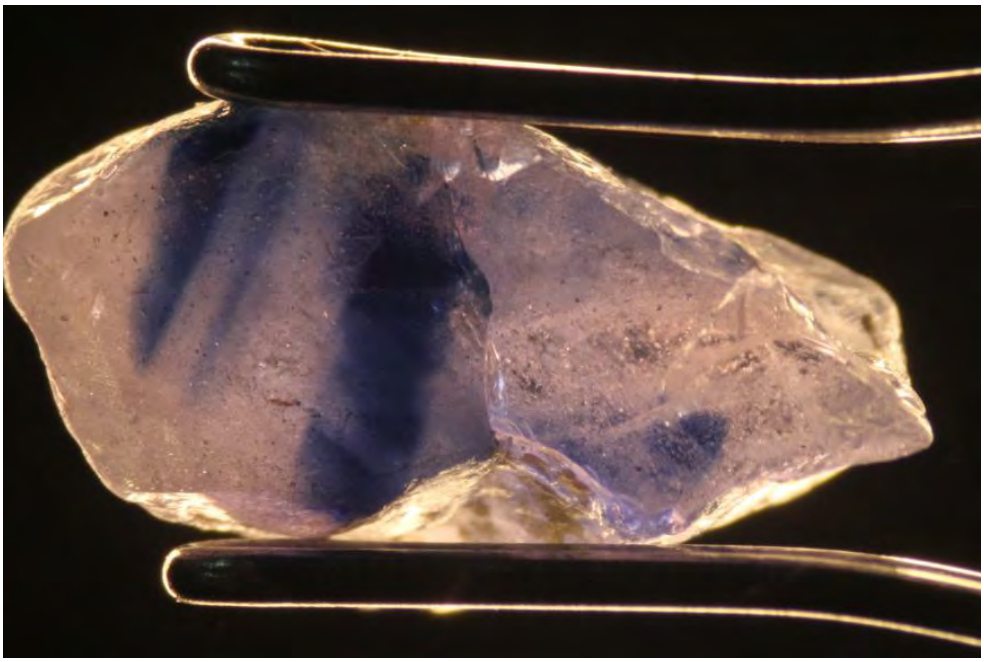

Figure A4 Sample B4 with 0.8x magnification

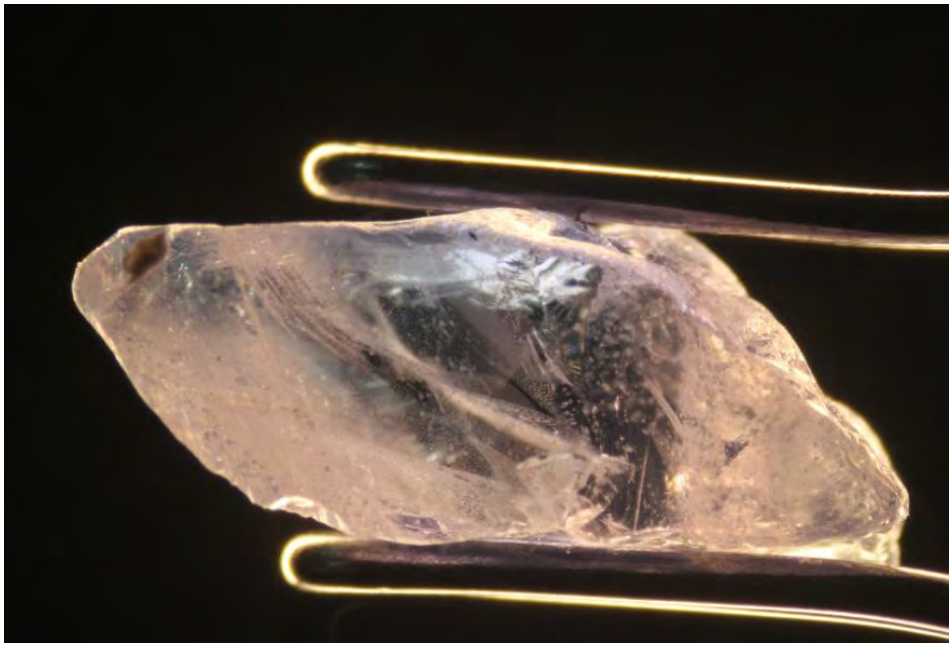

Figure A5 Sample B5 with 0.8x magnification

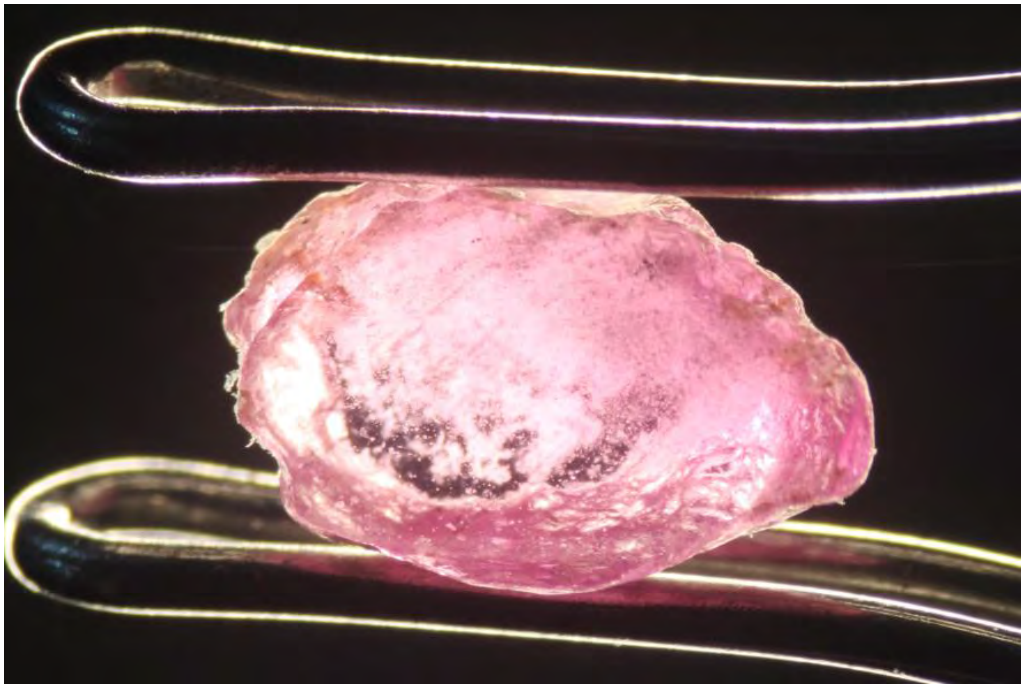

Figure A6 Sample Pkr1 with 1.0x magnification

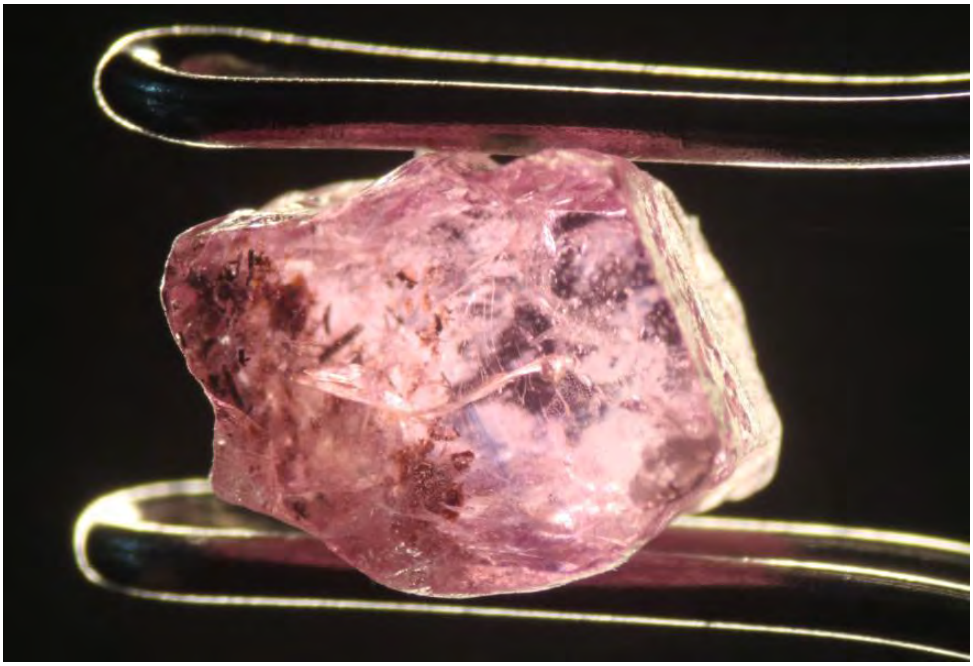

Figure A7 Sample Pkr2 with 1.0x magnification

Figure A8 Sample Pkr3 with 1.0x magnification

Figure A9 Sample Pkr4 with 1.0x magnification

Figure A10 Sample Pkr5 with 1.0x magnification

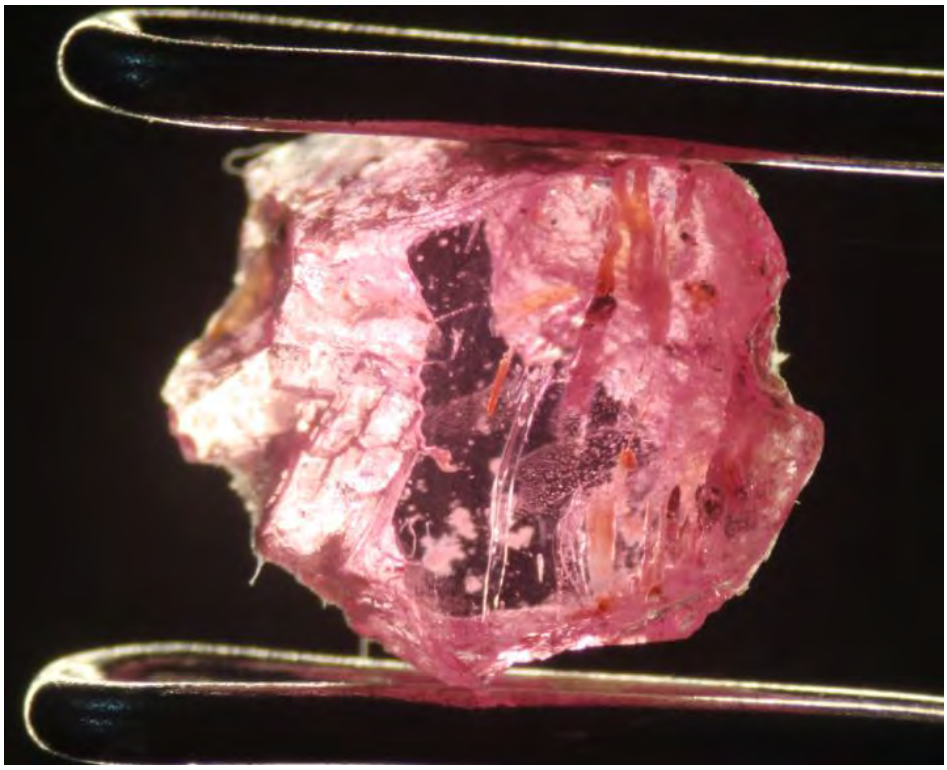

Figure A11 Sample Pkr6 with 1.0x magnification

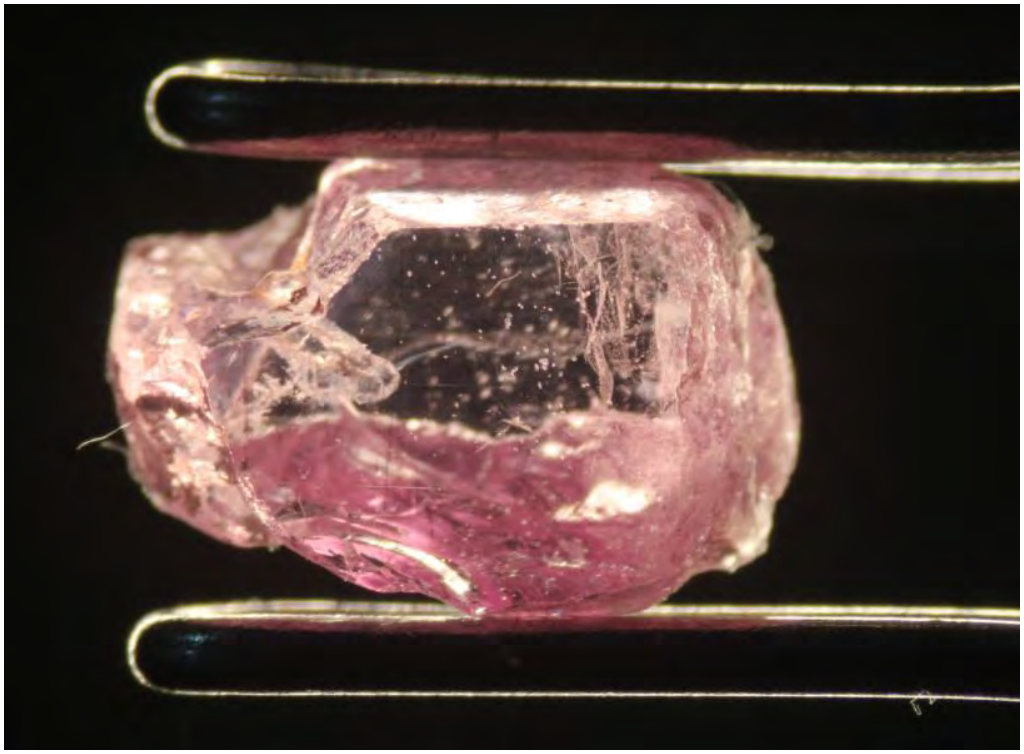

Figure A12 Sample Pkr7 with 1.0x magnification

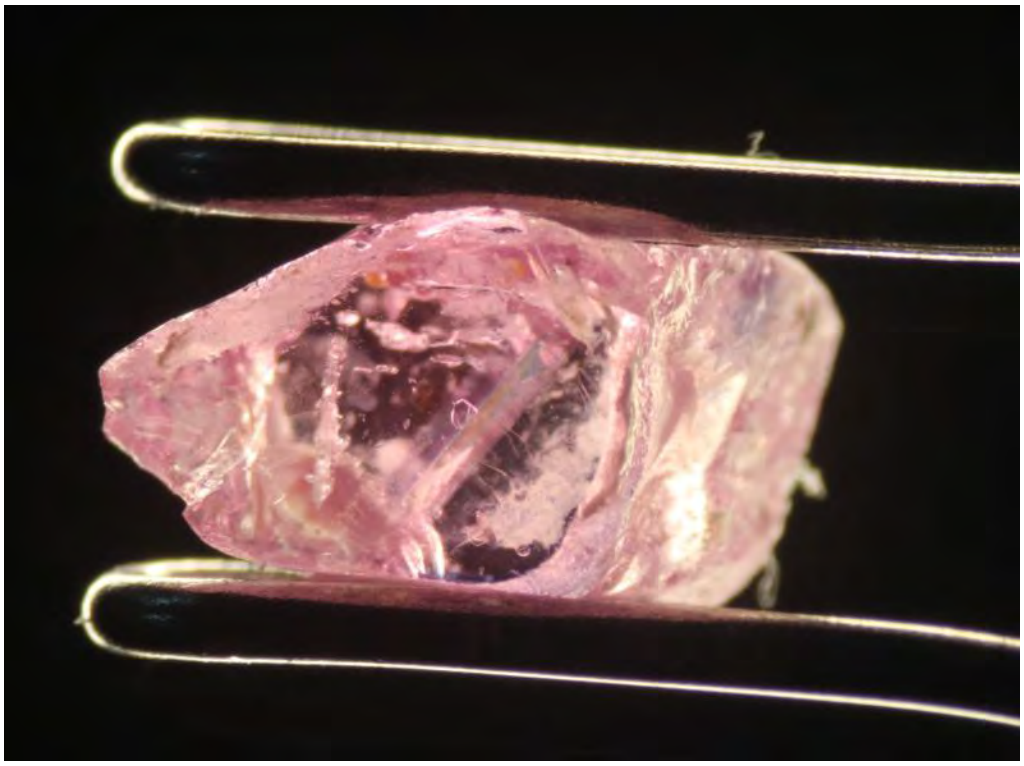

Figure A13 Sample Pkr8 with 1.0x magnification

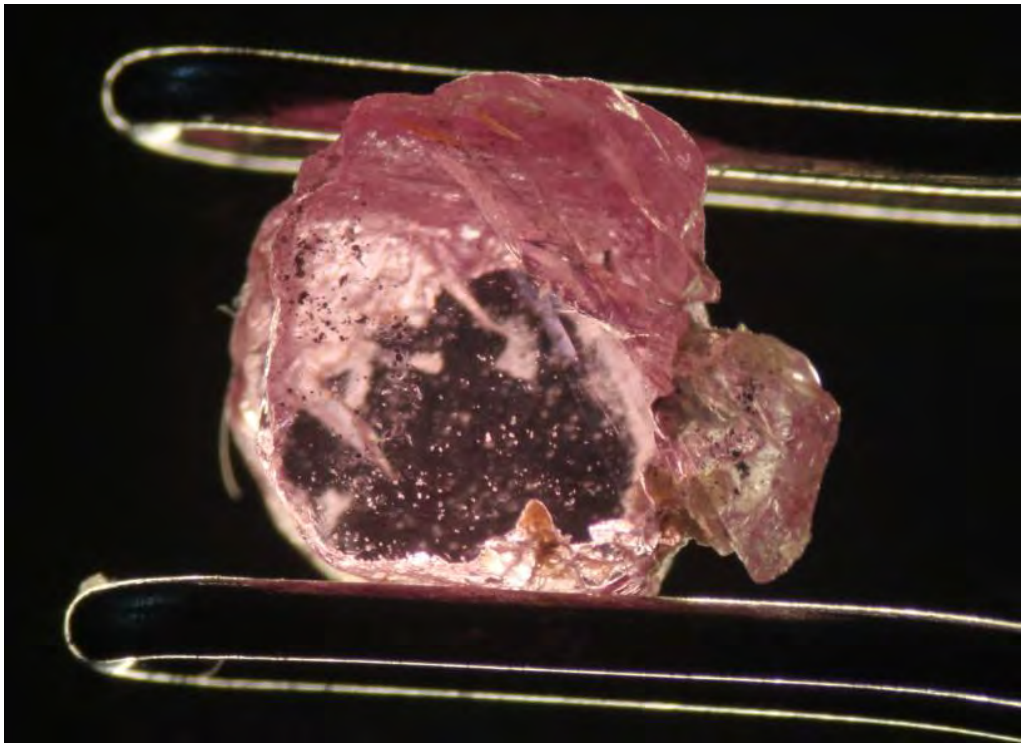

Figure A14 Sample Pkr9 with 1.0x magnification

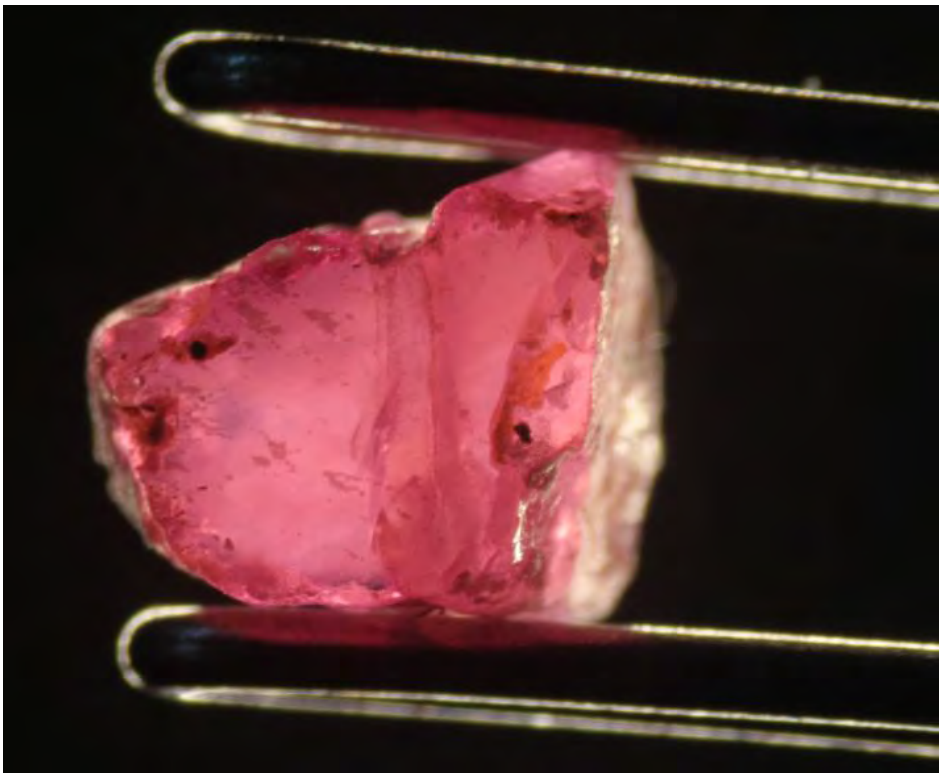

Figure A15 Sample Pkr10 with 1.0x magnification

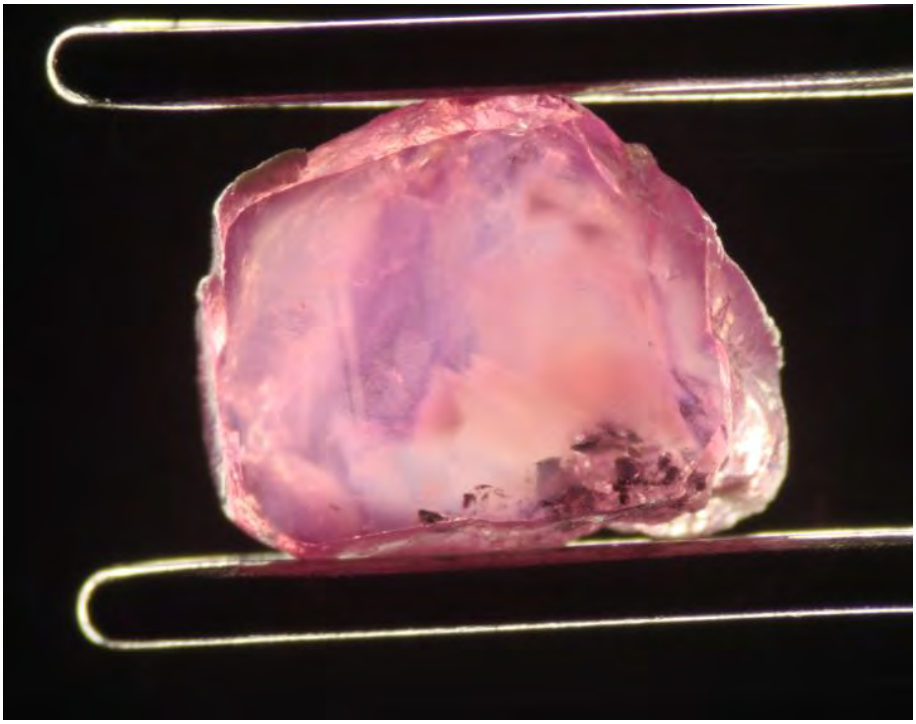

Figure A16 Sample Pkr11 with 1.0x magnification

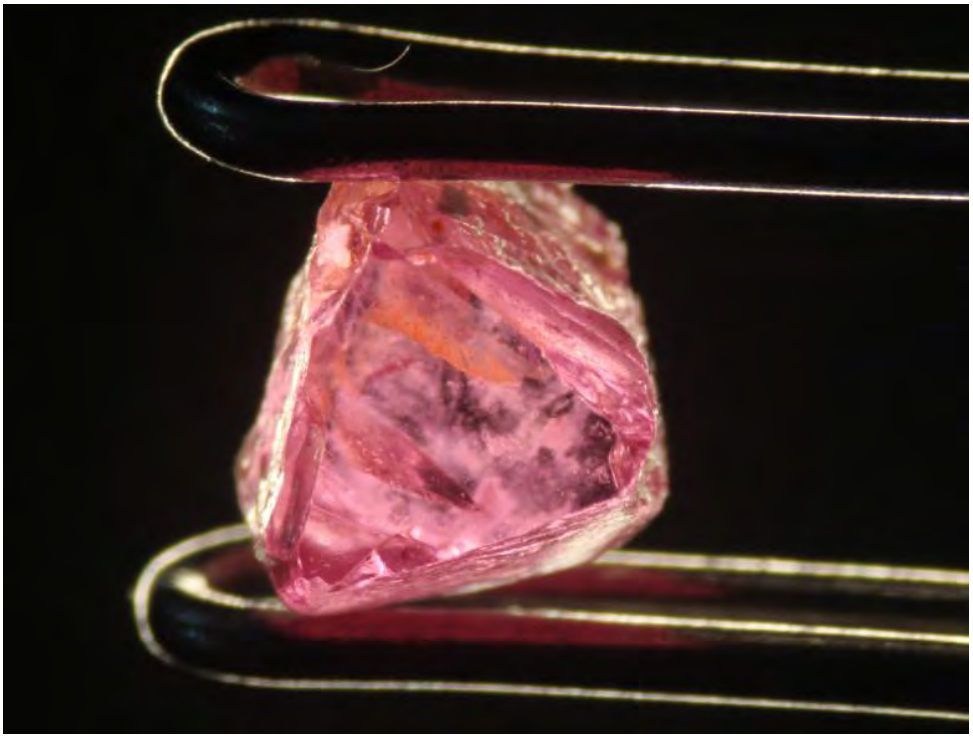

Figure A17 Sample Pkr12 with 1.0x magnification

Figure A18 Sample Pkr13 with 1.0x magnification

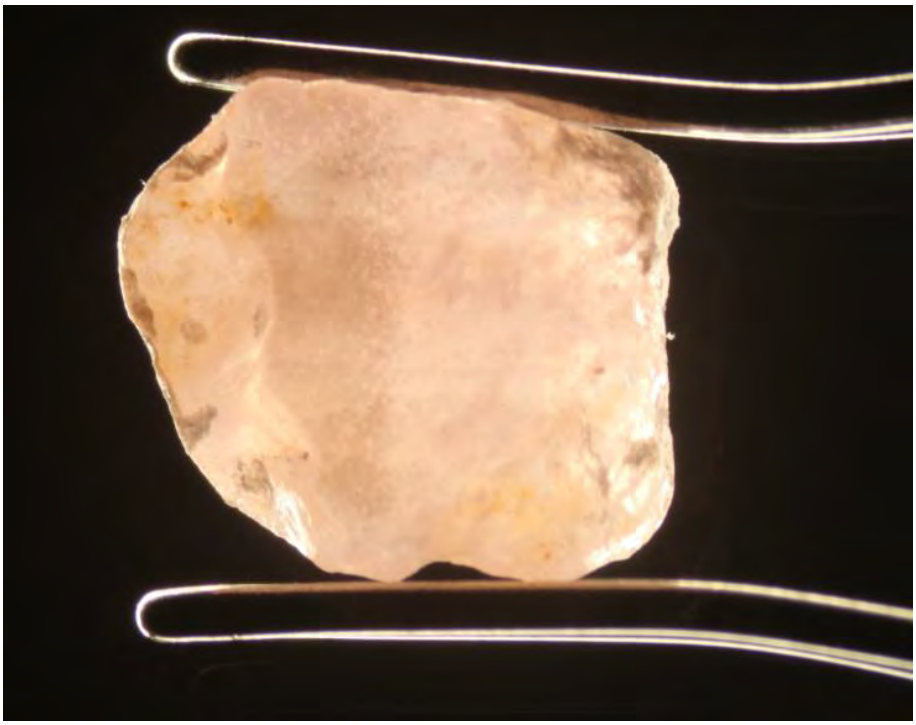

Figure A19 Sample Ppo1 with 0.65x magnification

Figure A20 Sample Ppo2 with 0.8x magnification

Figure A21 Sample Ppo3 with 0.8x magnification

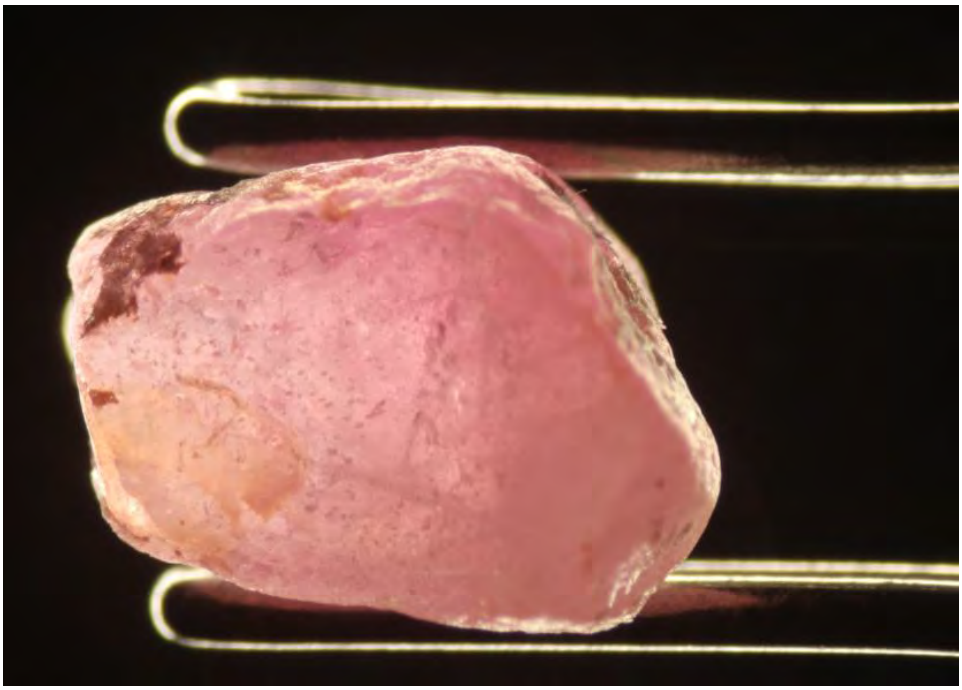

Figure A22 Sample Ppo4 with 1.0x magnification

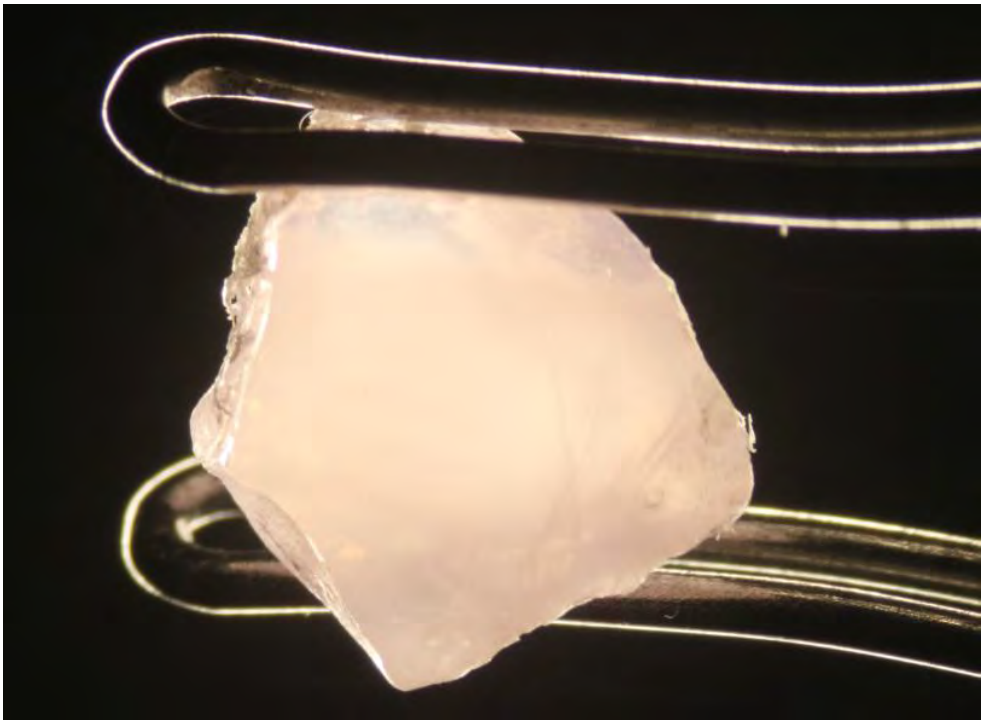

Figure A23 Sample Ppo5 with 0.8x magnification

Figure A24 Sample Ppo6 with 1.0x magnification

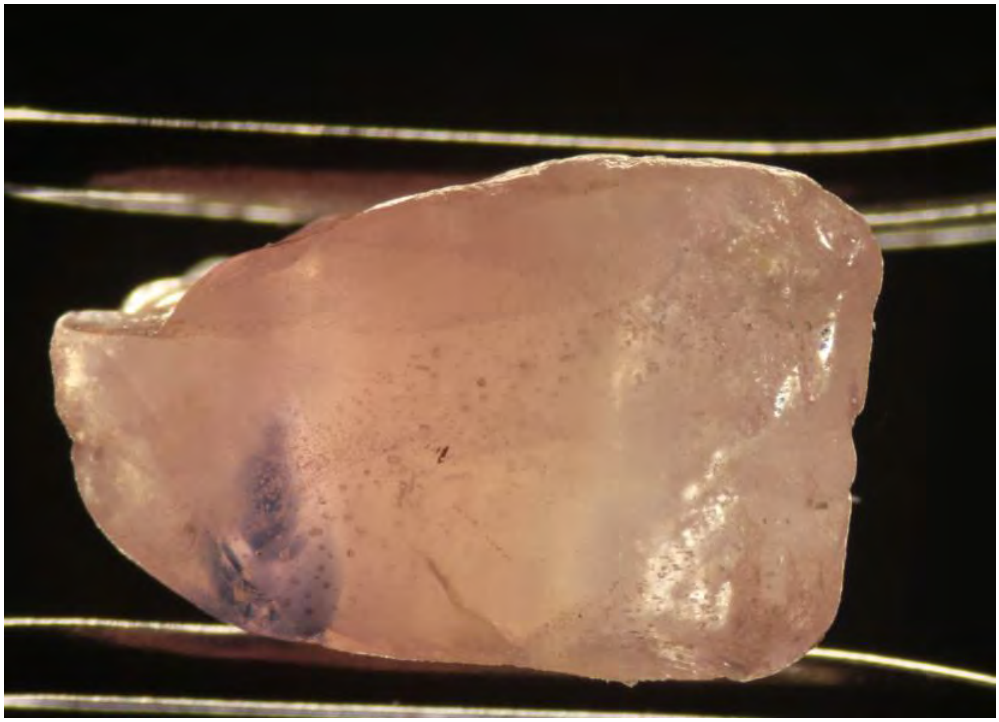

Figure A25 Sample Ppo7 with 1.0x magnification

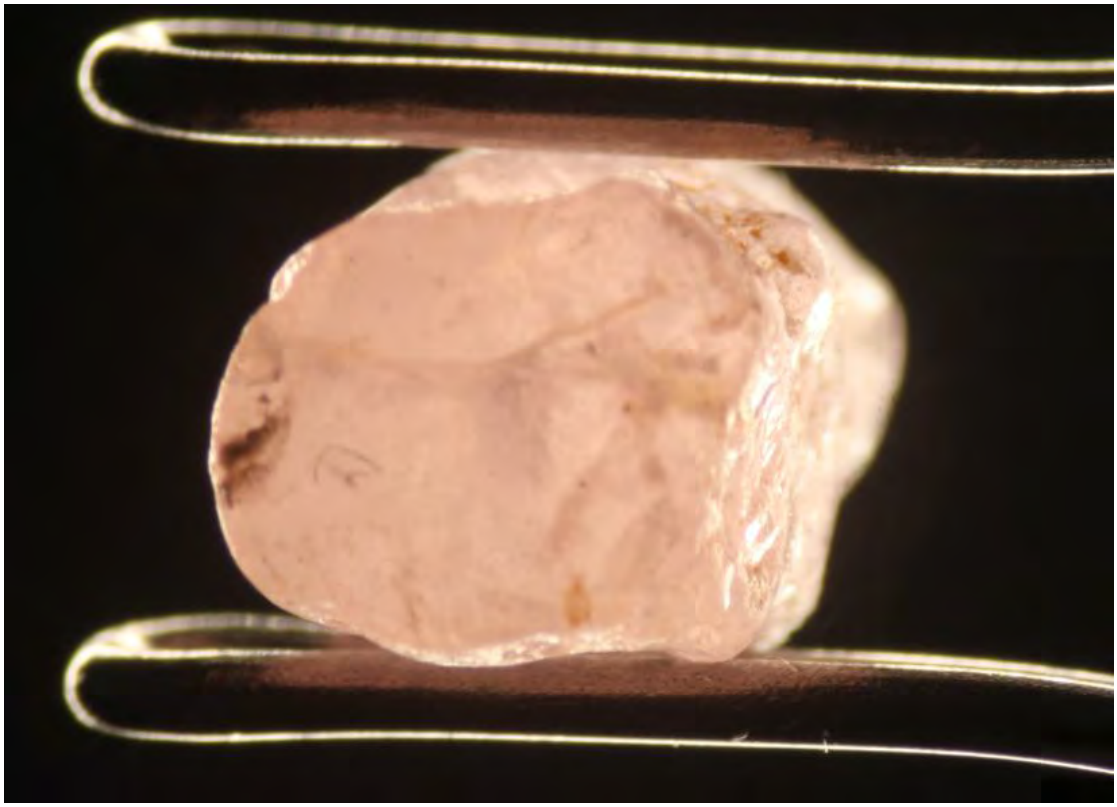

Figure A26 Sample Ppo8 with 1.0x magnification

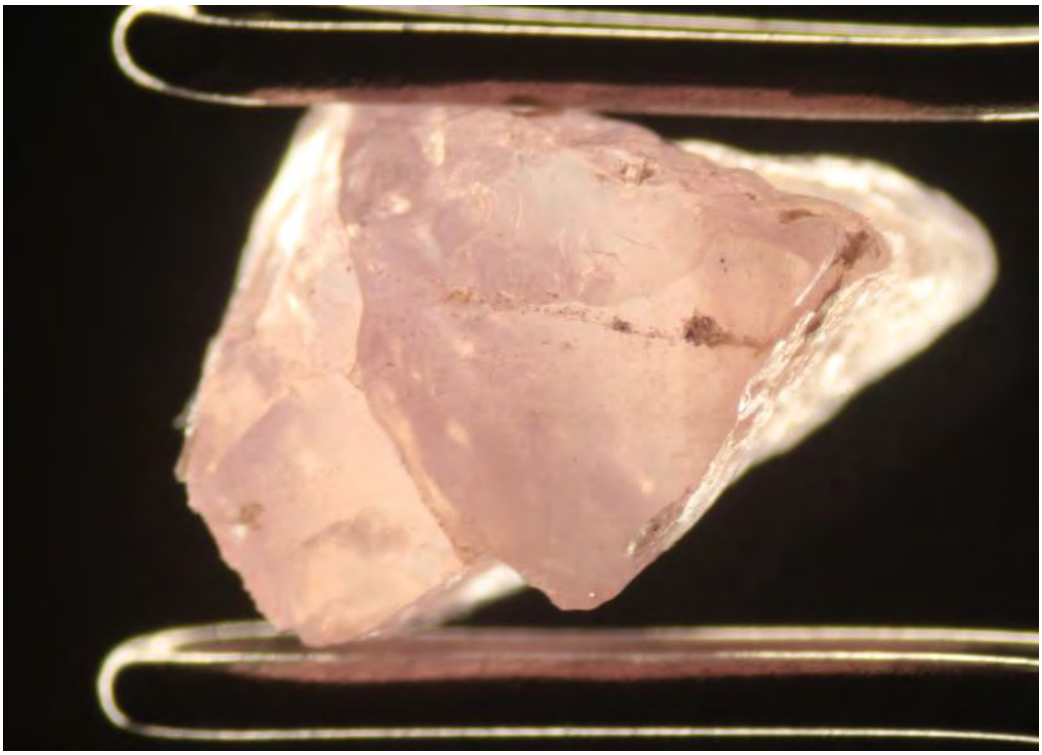

Figure A27 Sample Ppo9 with 1.0x magnification

Figure A28 Sample Ppo10 with 1.0x magnification

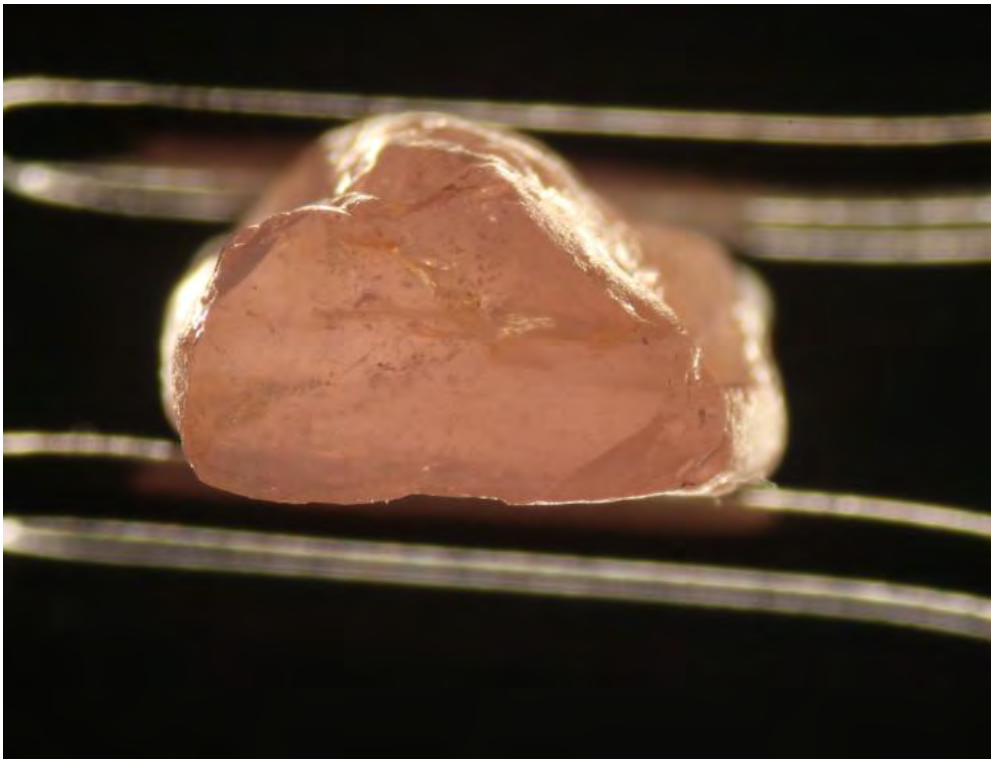

Figure A29 Sample Ppo11 with 1.0x magnification

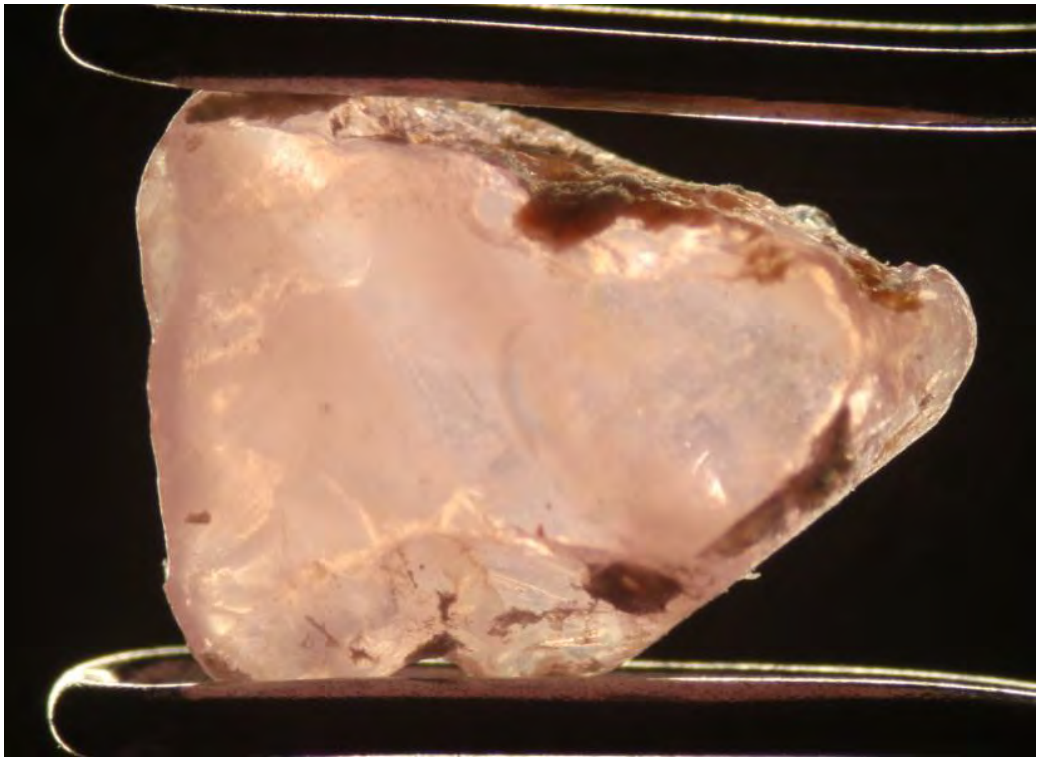

Figure A30 Sample Ppo12 with 1.0x magnification

Figure A31 Sample Ppo13 with 1.0x magnification

Figure A32 Purple color zone from B3 with 1.6x magnification

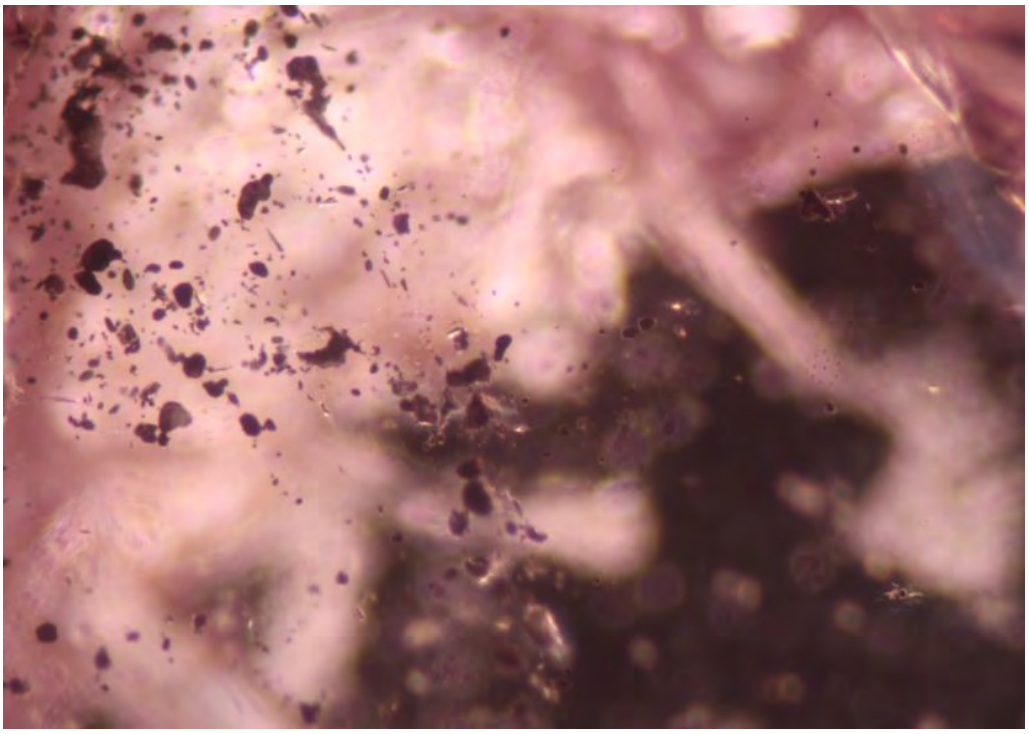

Figure A33 Black mineral inclusions from Pkr9 with 4.0x magnification

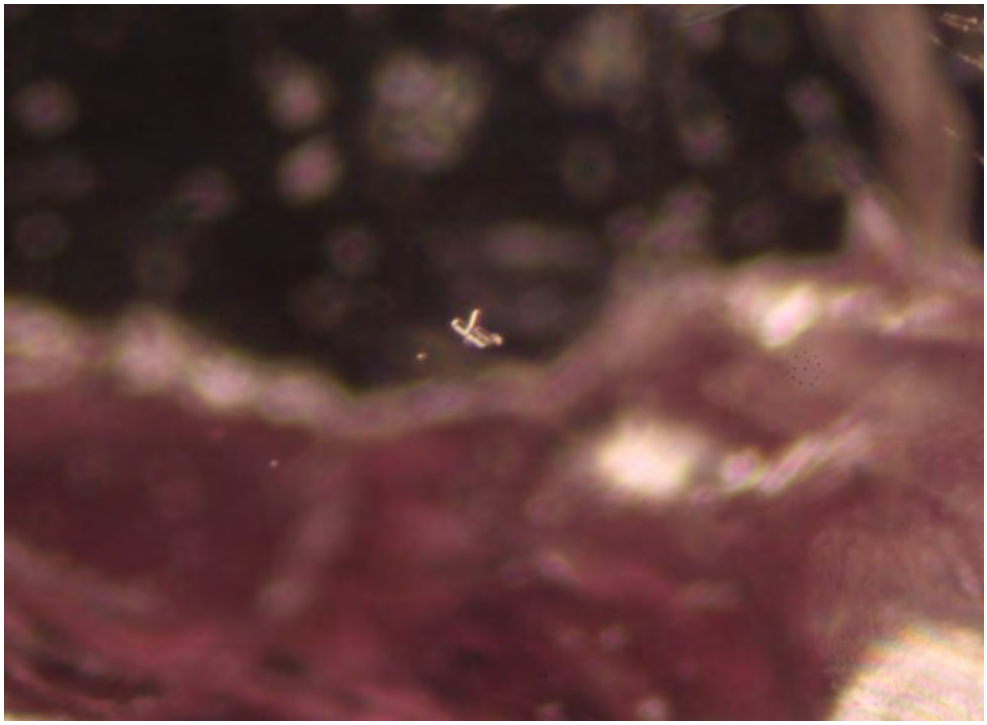

Figure A34 Crystal inclusion from Pkr9 with 5.0x magnification

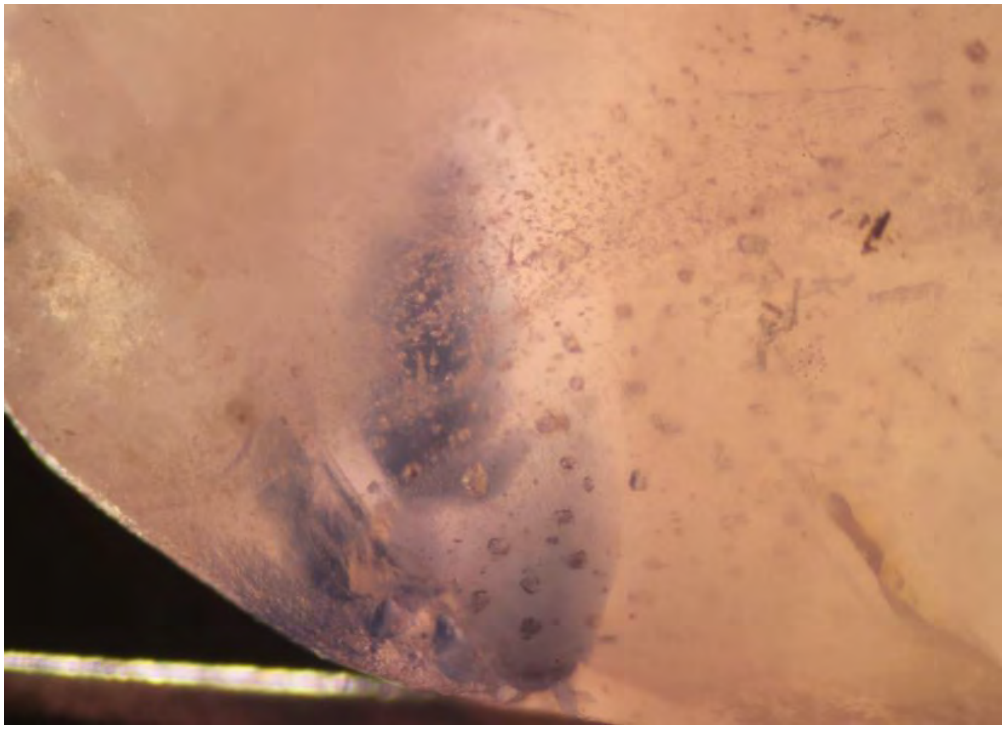

Figure A35 Blue color zoning with crystal from Ppo7 with 2.5x magnification

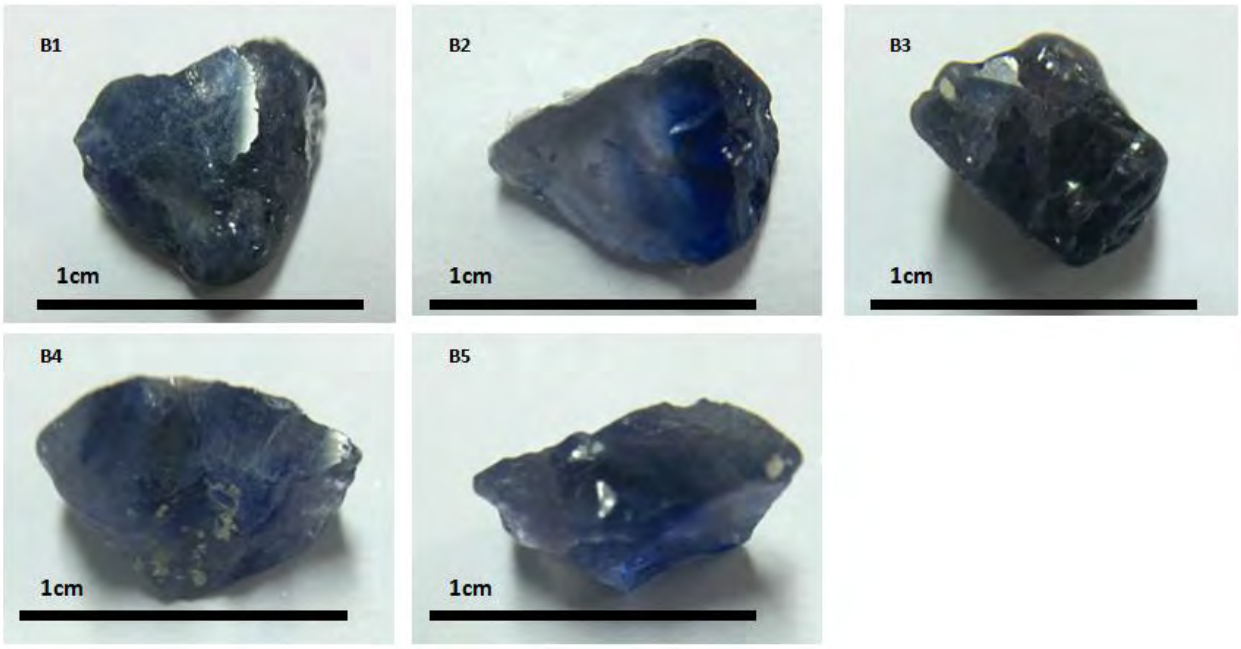

Figure A36 Blue Samples

B1: 4.96 ct, B2: 1.50 ct, B3: 2.91 ct, B4: 2.67 ct, B5: 2.49 ct

Figure A37 Orangey Pink Samples

Ppo1: 1.39 ct, Ppo2: 1.42 ct, Ppo3: 1.63 ct, Ppo4: 1.24 ct, Ppo5: 0.77 ct, Ppo6: 0.89 ct, Ppo7: 1.28 ct, Ppo8: 1.35 ct, Ppo9: 1.20ct, Ppo10: 1.00 ct, Ppo11: 1.03 ct, Ppo12: 0.87 ct, Ppo13: 0.61 ct

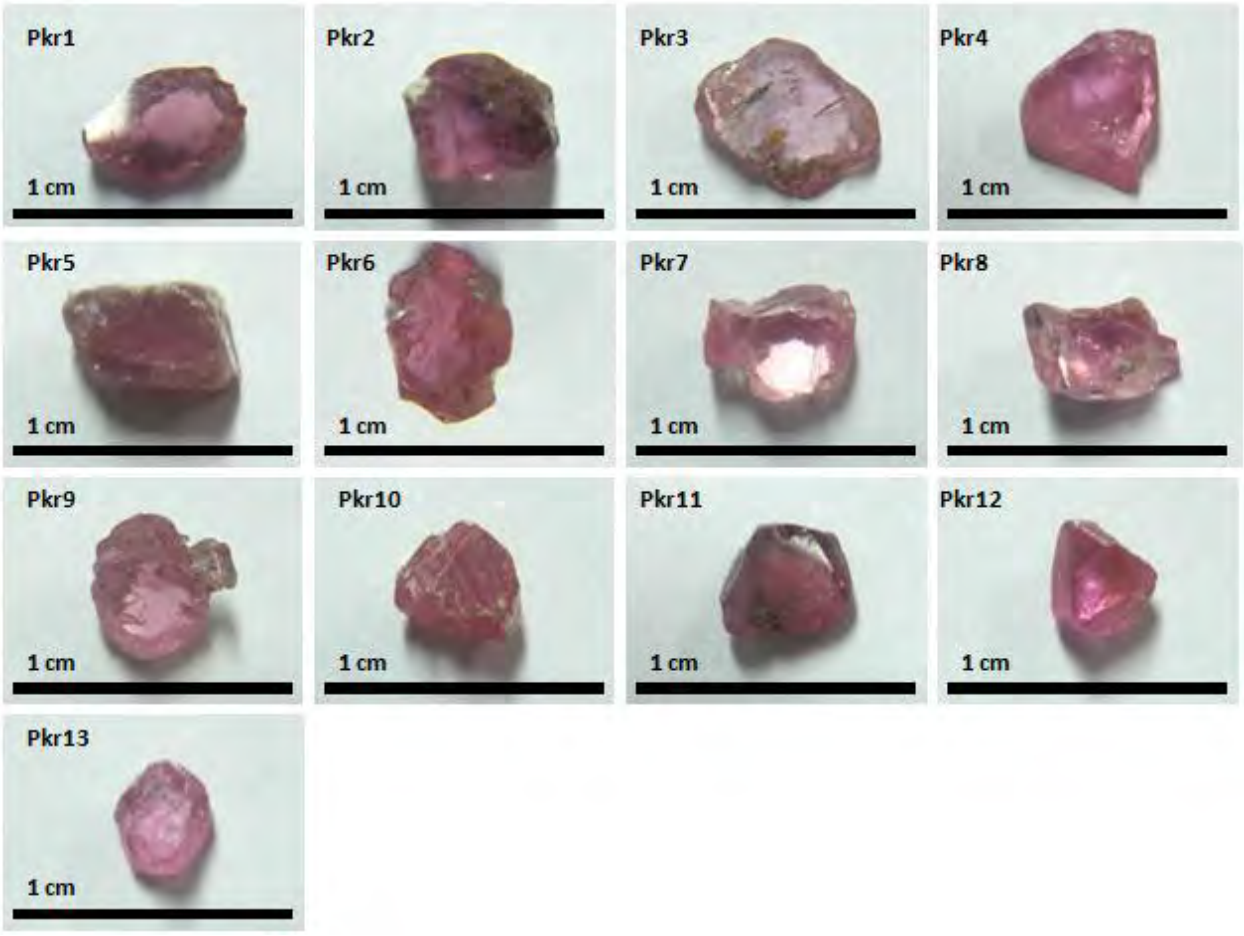

Figure A38 Orangey Pink Samples

Pkr1: 0.51 ct, Pkr2: 0.97 ct, Pkr3: 0.79 ct, Pkr4: 0.62 ct, Pkr5: 0.84 ct, Pkr6: 0.49 ct, Pkr7: 0.62 ct, Pkr8: 0.60 ct, Pkr9: 0.65 ct, Pkr10: 0.60 ct, Pkr11: 0.44 ct, Pkr12: 0.46 ct, Pkr13: 0.36 ct

SECTION B: FTIR SPECTRUM

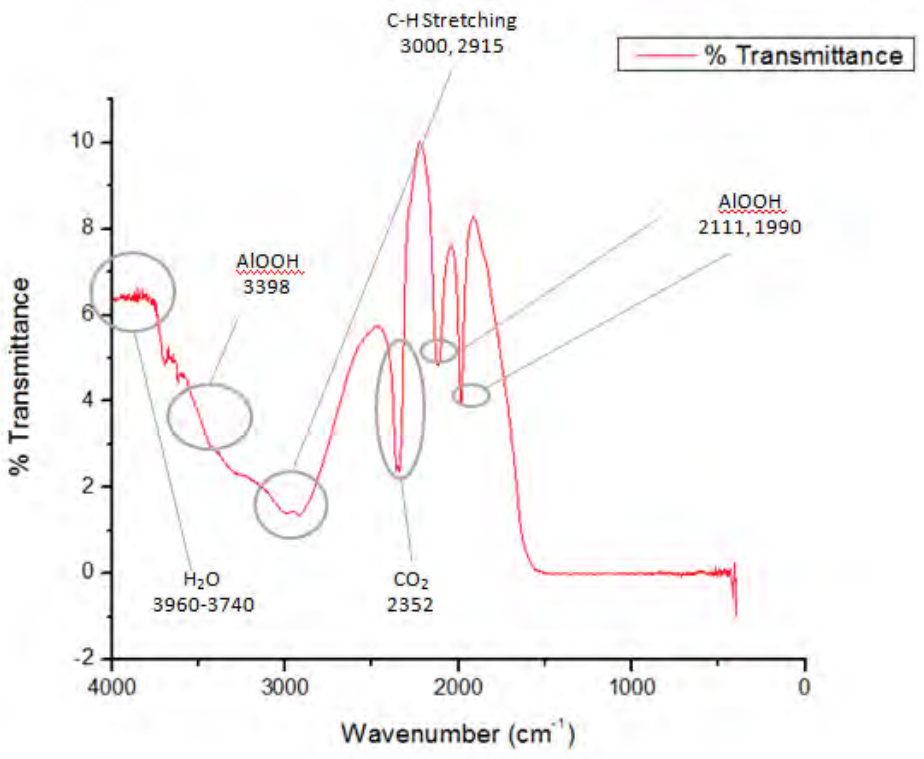

Figure B1 FTIR Result of B1

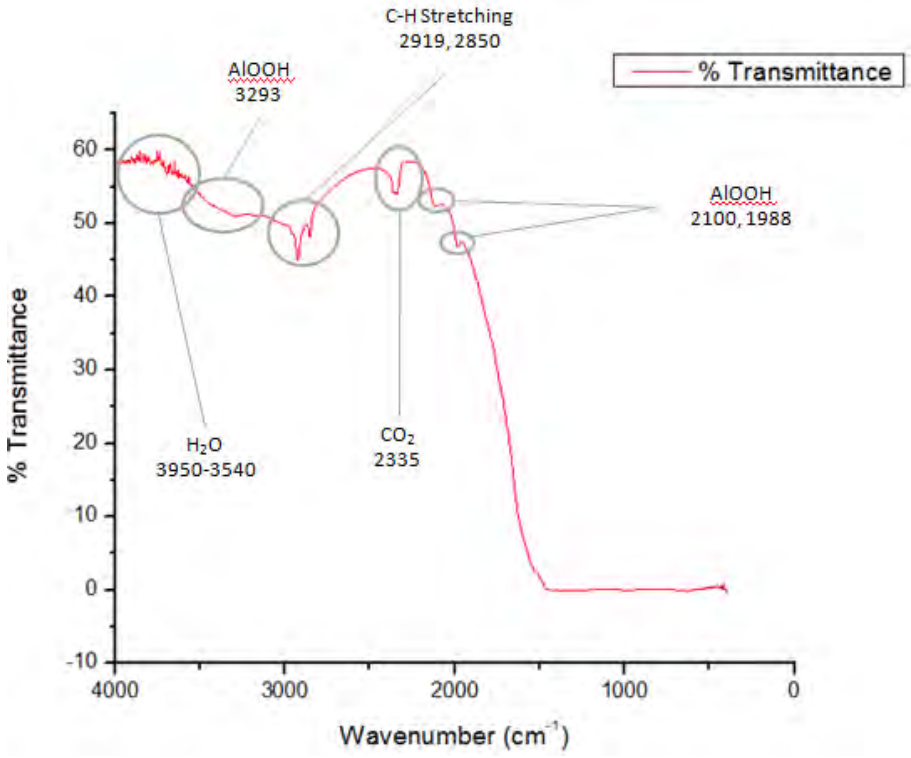

Figure B2 FTIR Result of B2

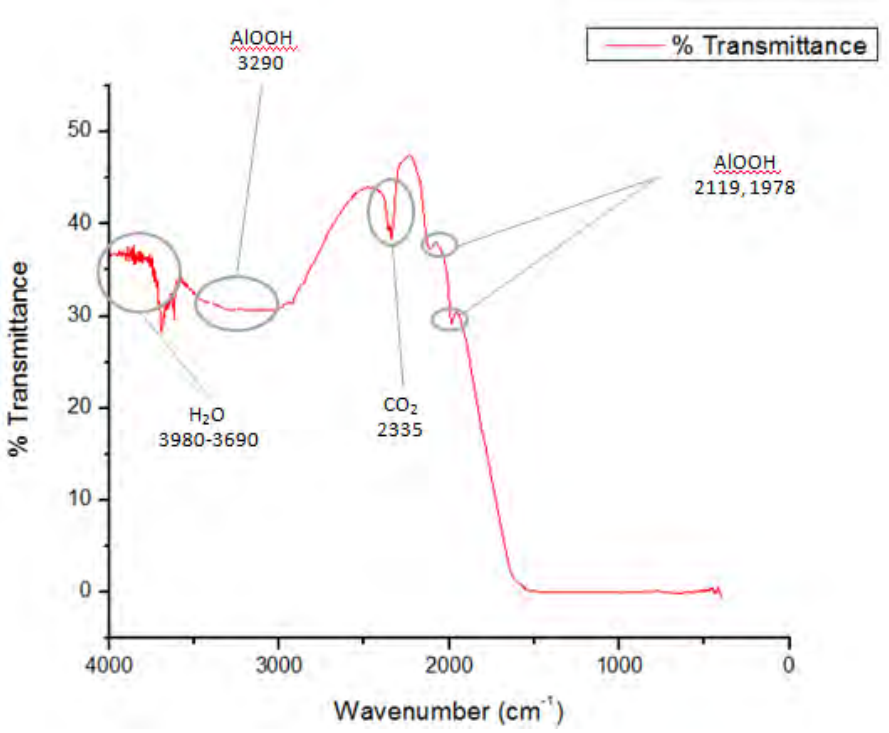

Figure B3 FTIR Result of B3

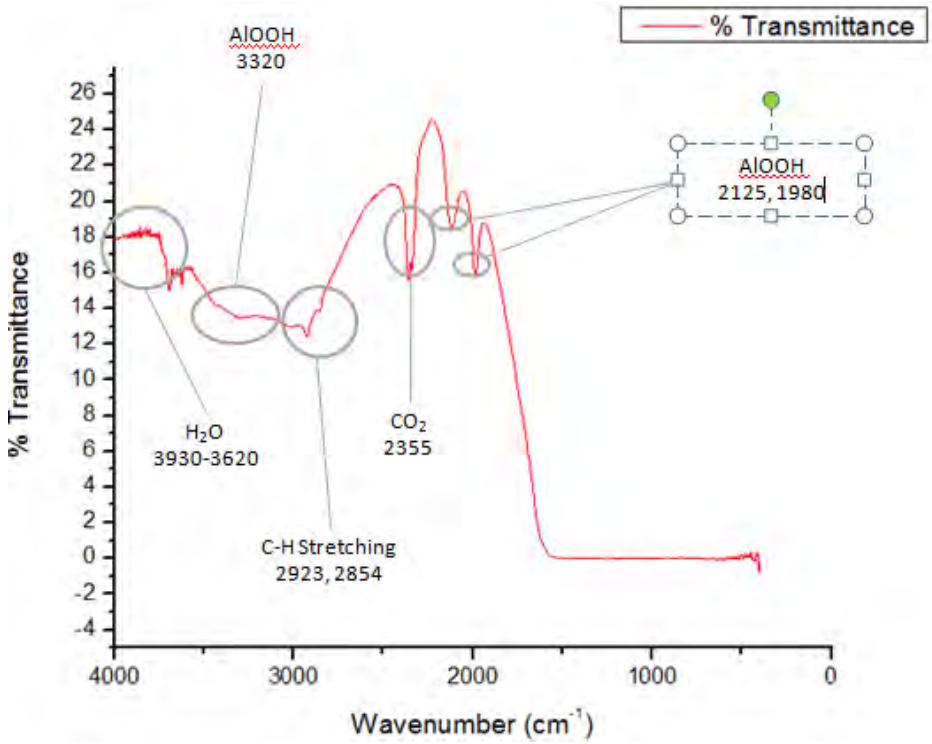

Figure B4 FTIR Result of B4

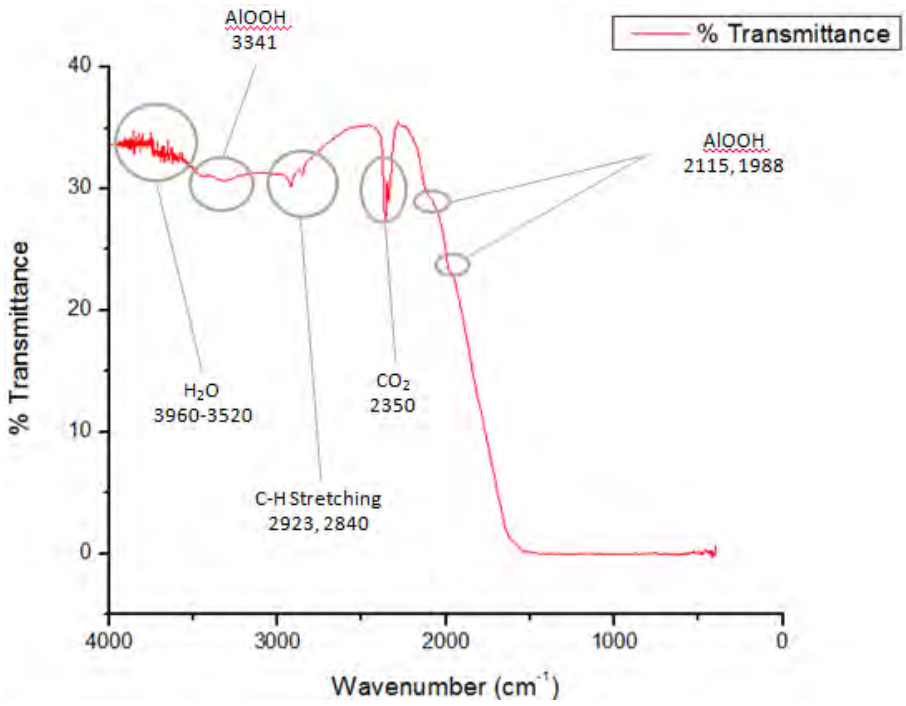

Figure B5 FTIR Result of B5

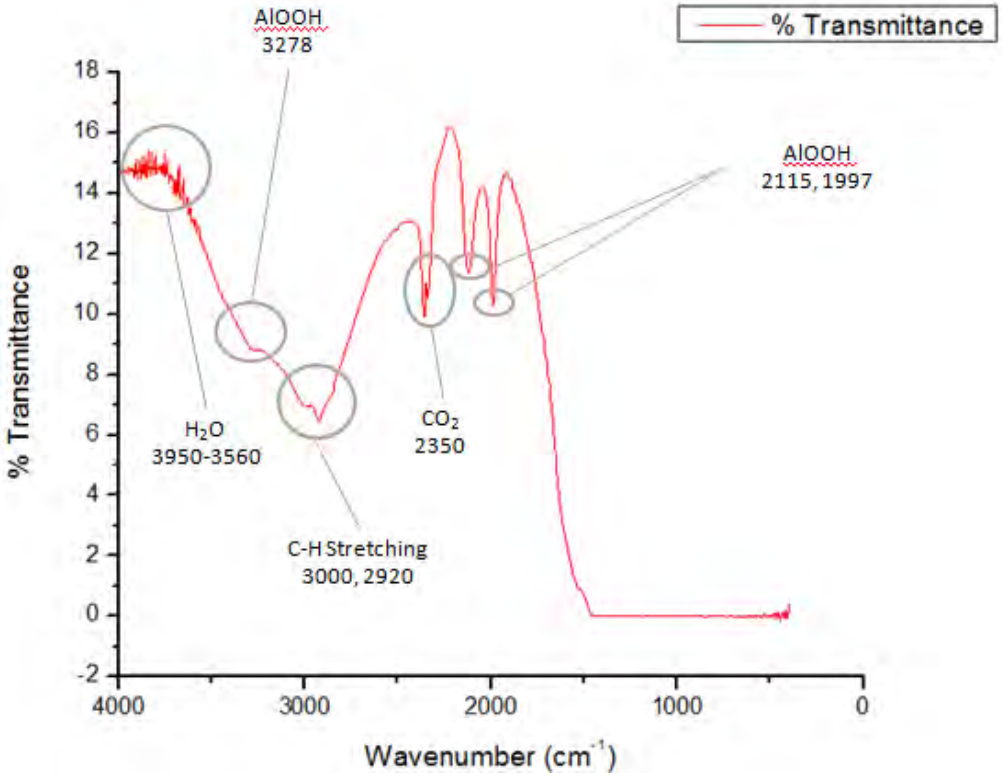

Figure B6 FTIR Result of Ppo1

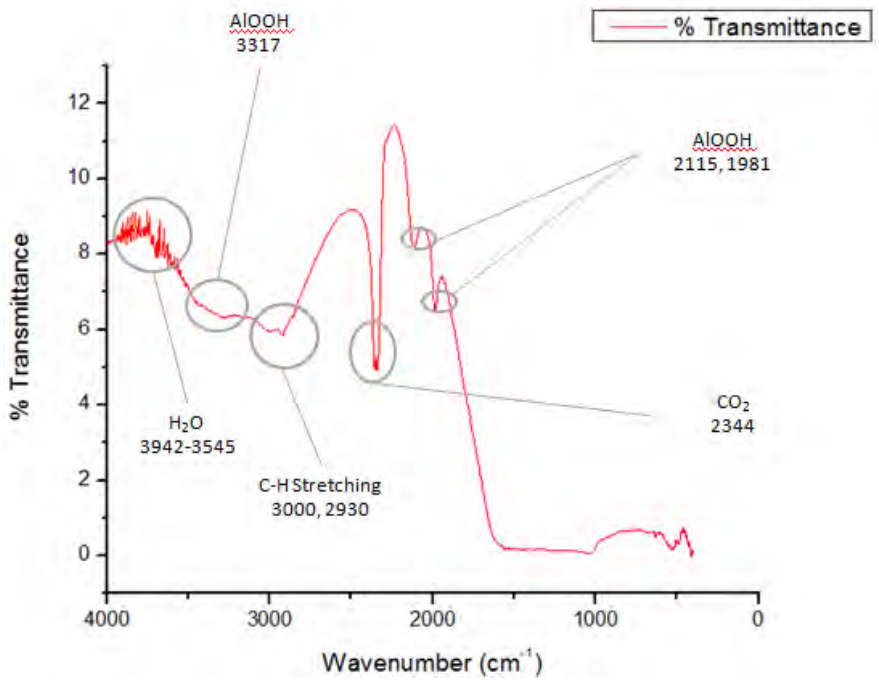

Figure B7 FTIR Result of Ppo2

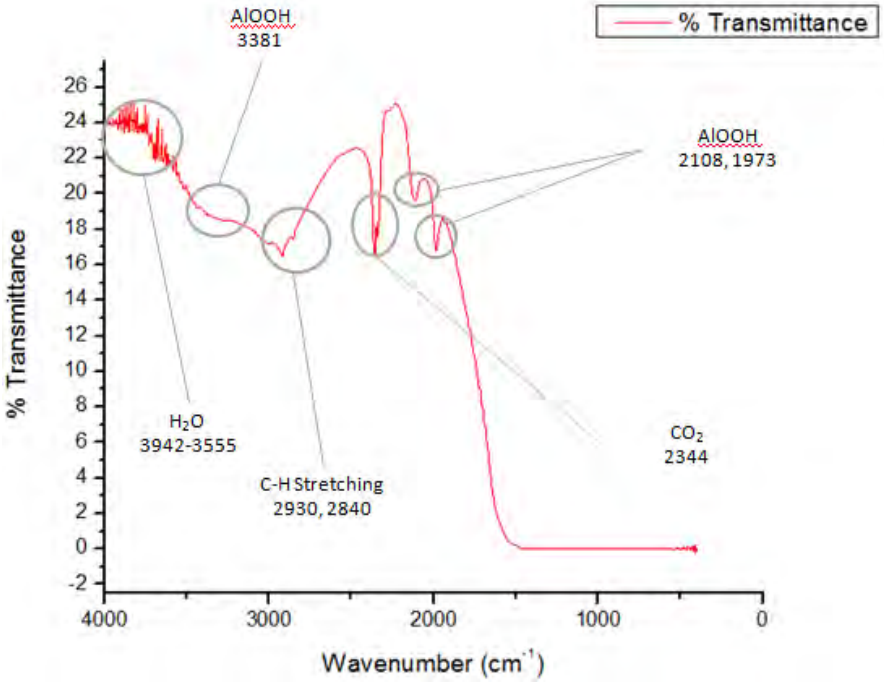

Figure B8 FTIR Result of Ppo3

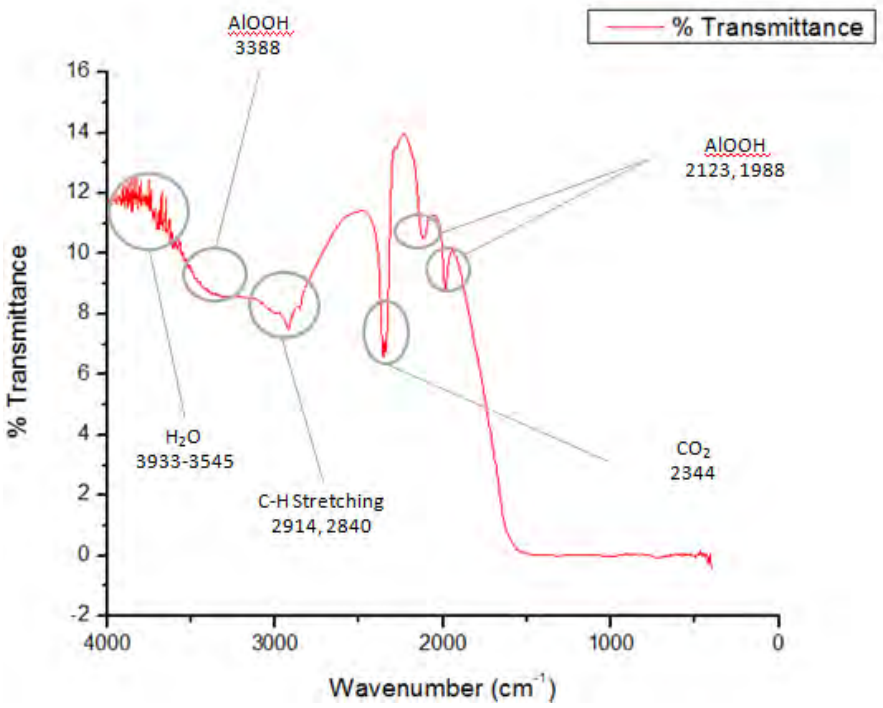

Figure B9 FTIR Result of Ppo4

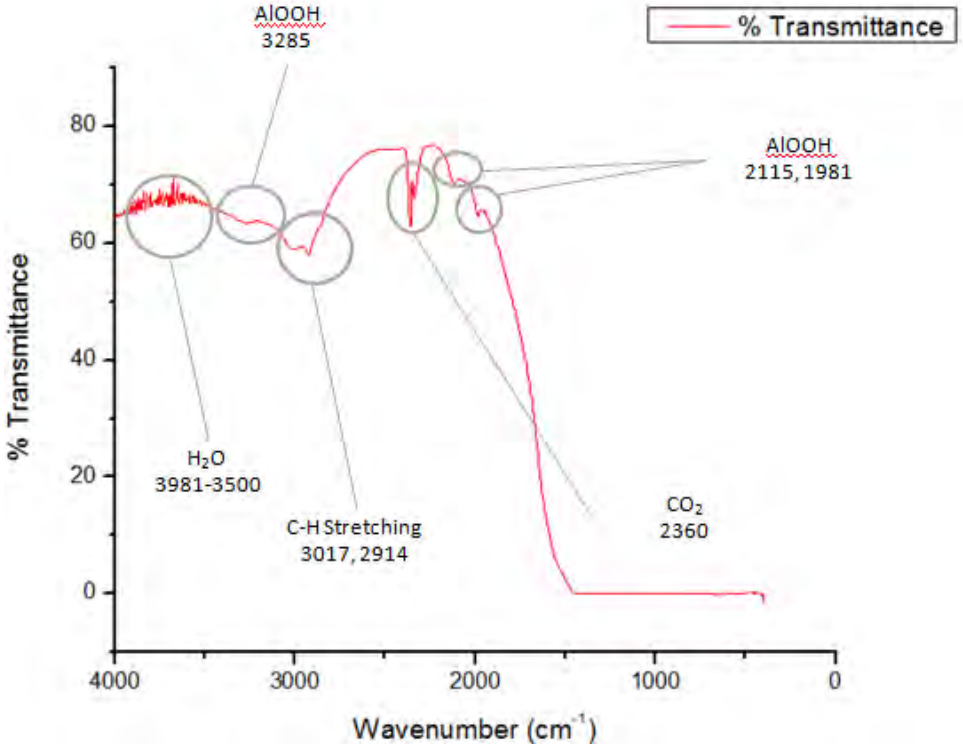

Figure B10 FTIR Result of Ppo5

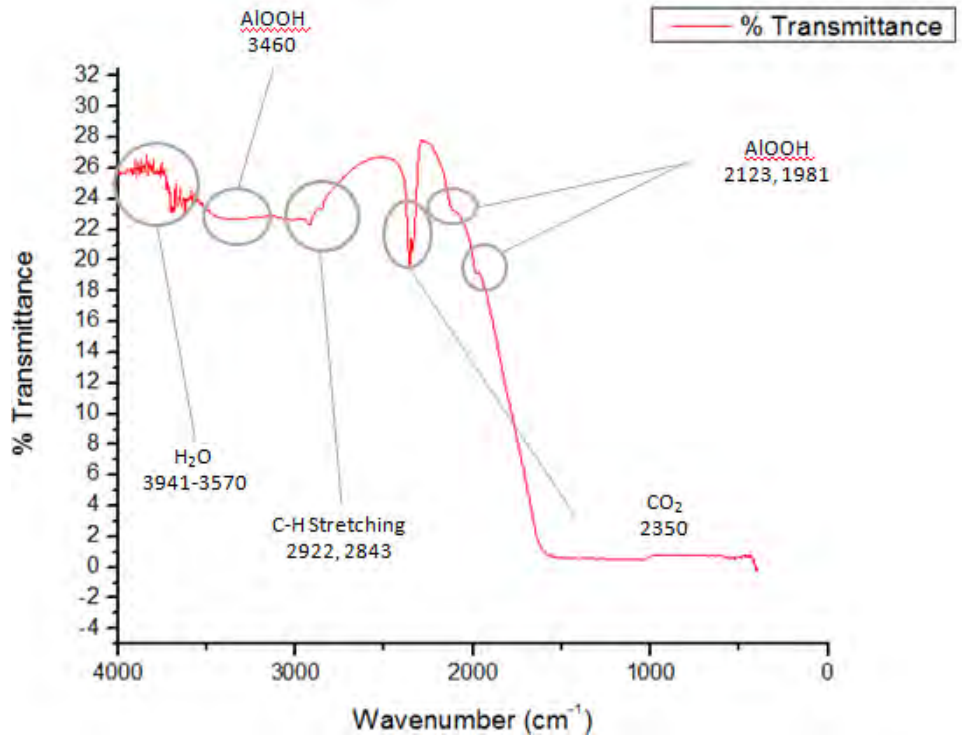

Figure B11 FTIR Result of Ppo6

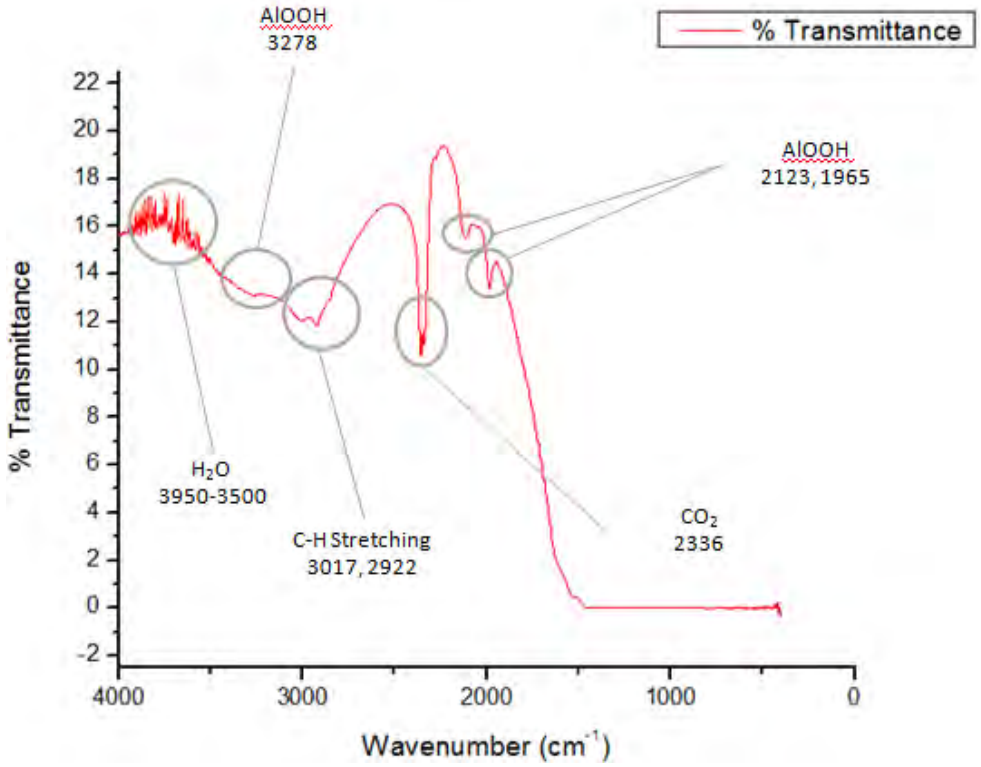

Figure B12 FTIR Result of Ppo7

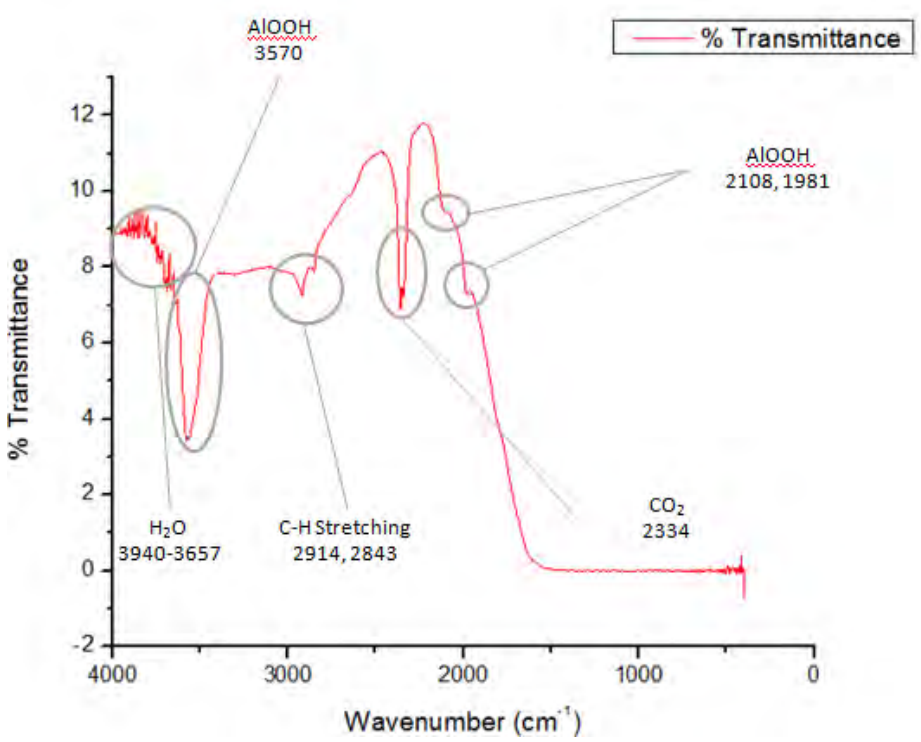

Figure B13 FTIR Result of Ppo8

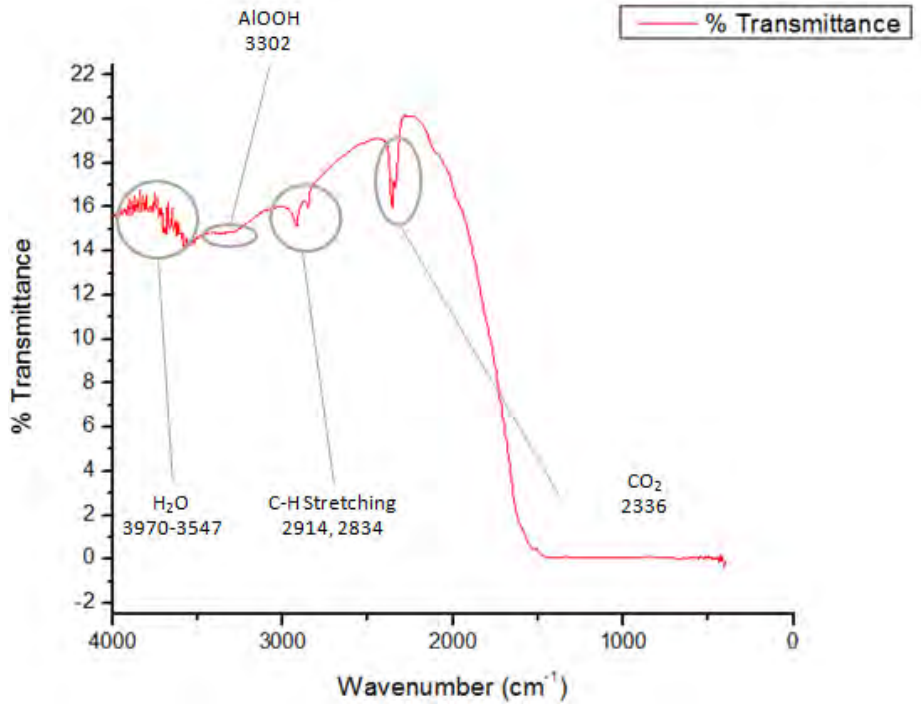

Figure B14 FTIR Result of Ppo9

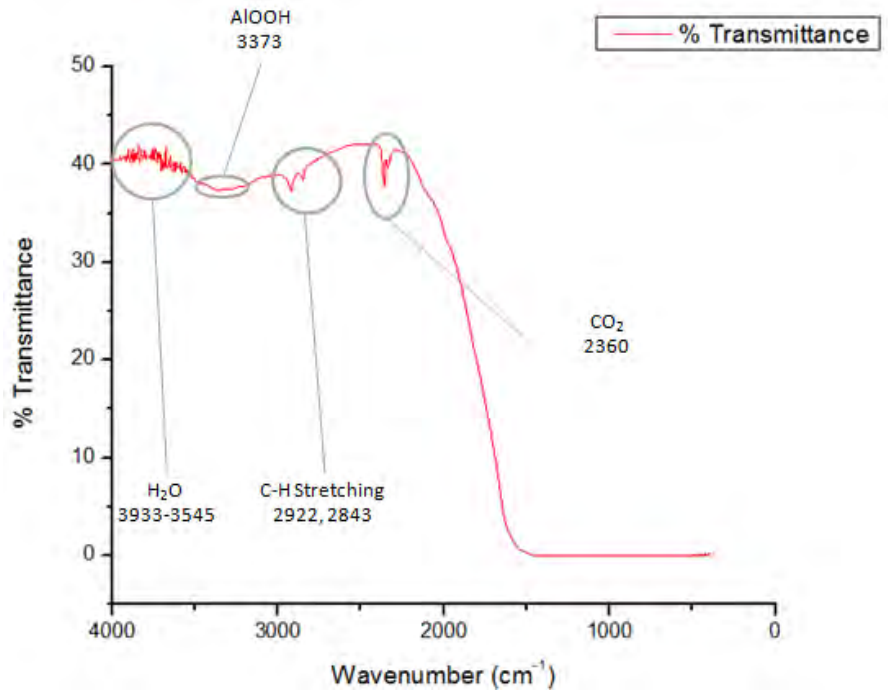

Figure B15 FTIR Result of Ppo10

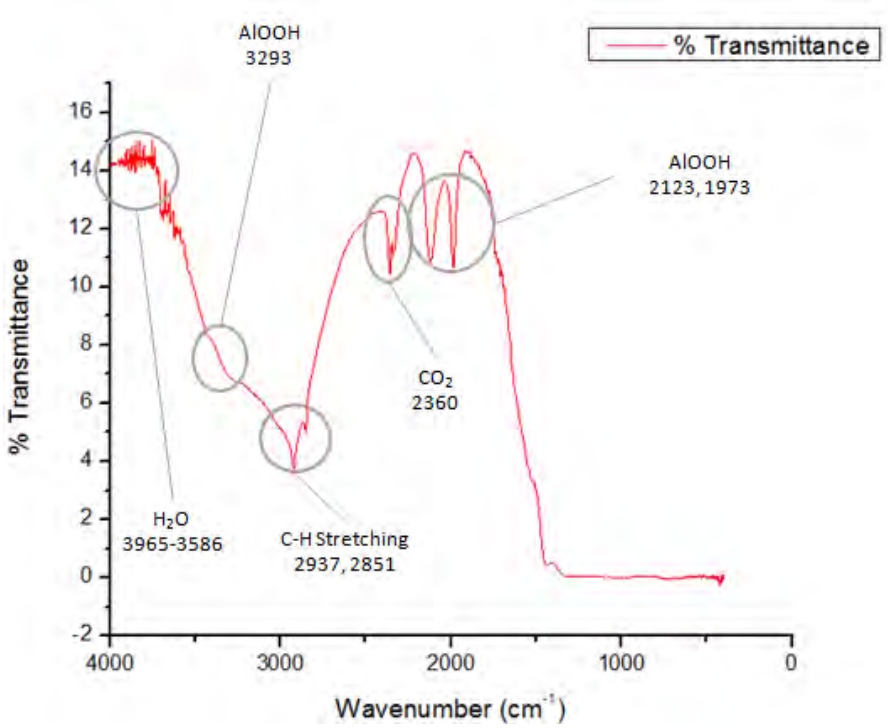

Figure B16 FTIR Result of Ppo11

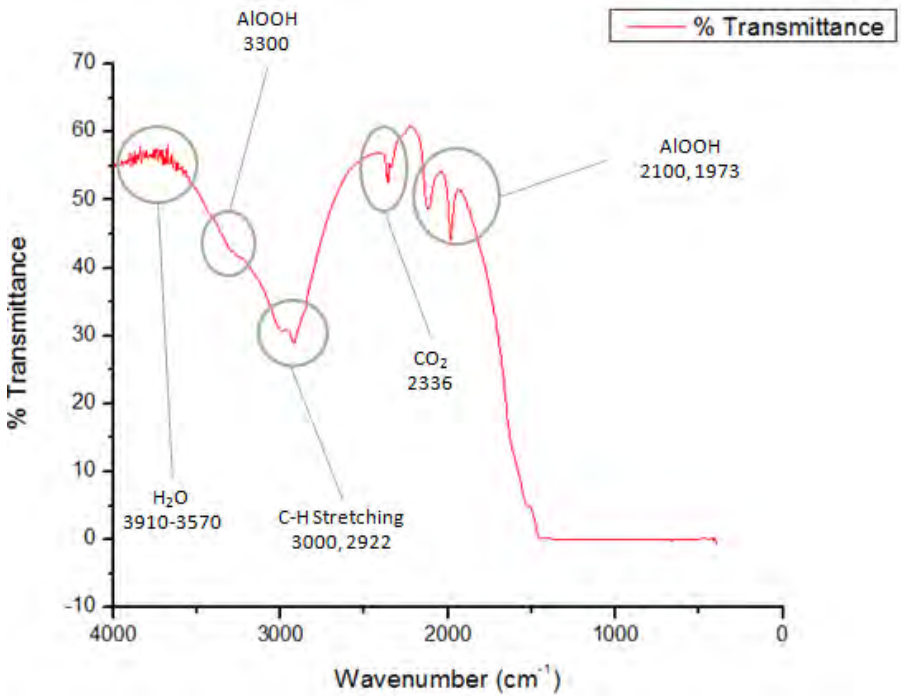

Figure B17 FTIR Result of Ppo12

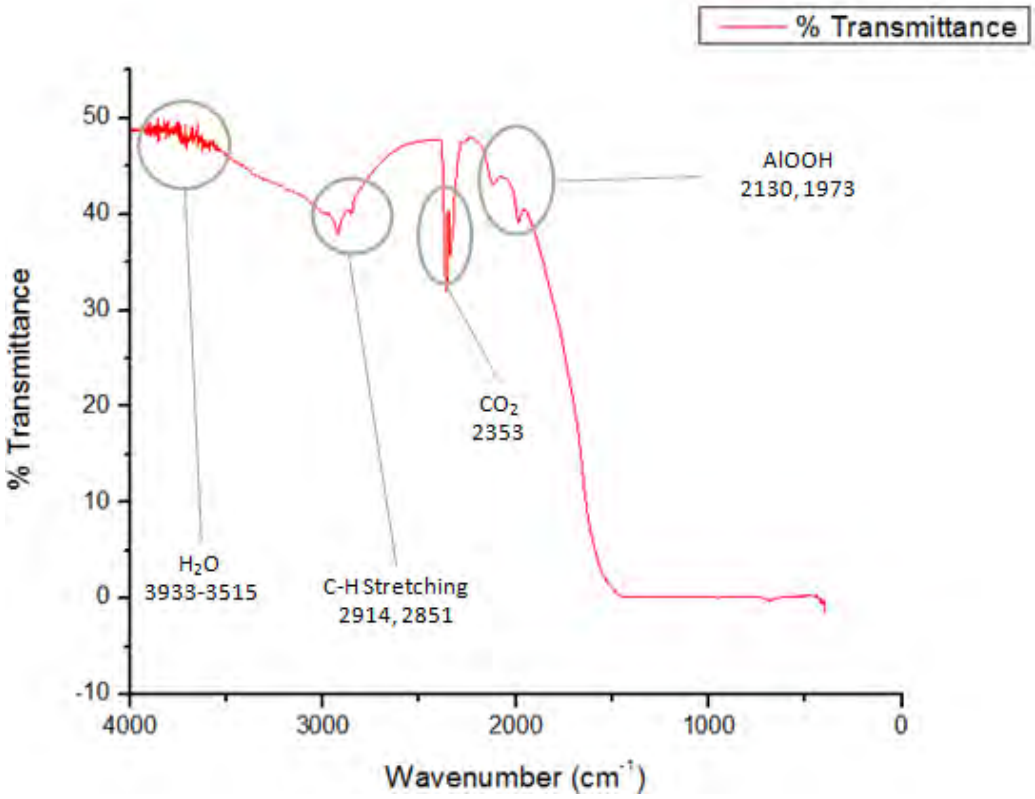

Figure B18 FTIR Result of Ppo13

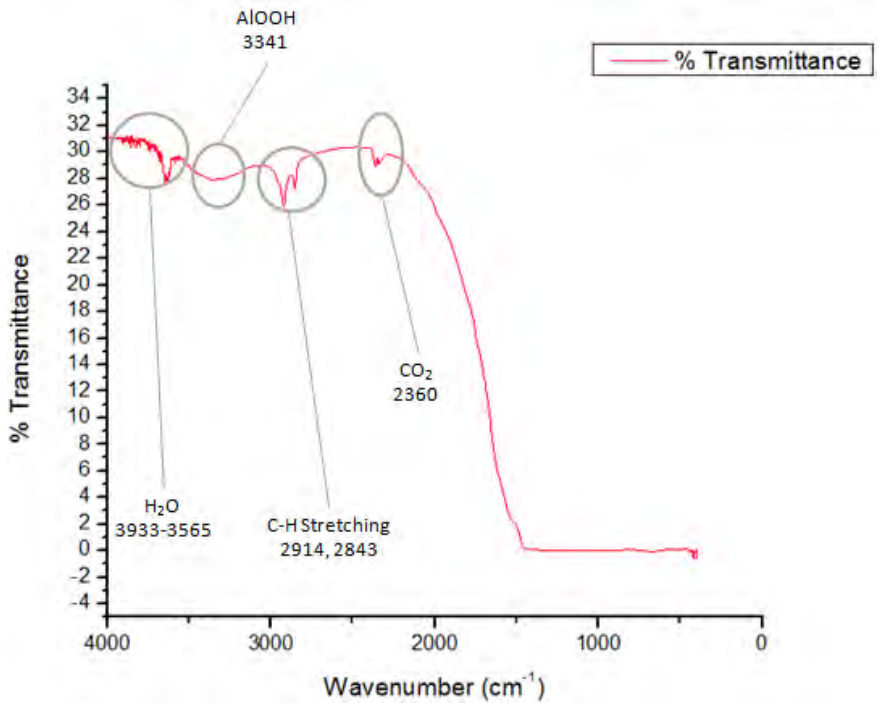

Figure B19 FTIR Result of Pkr1

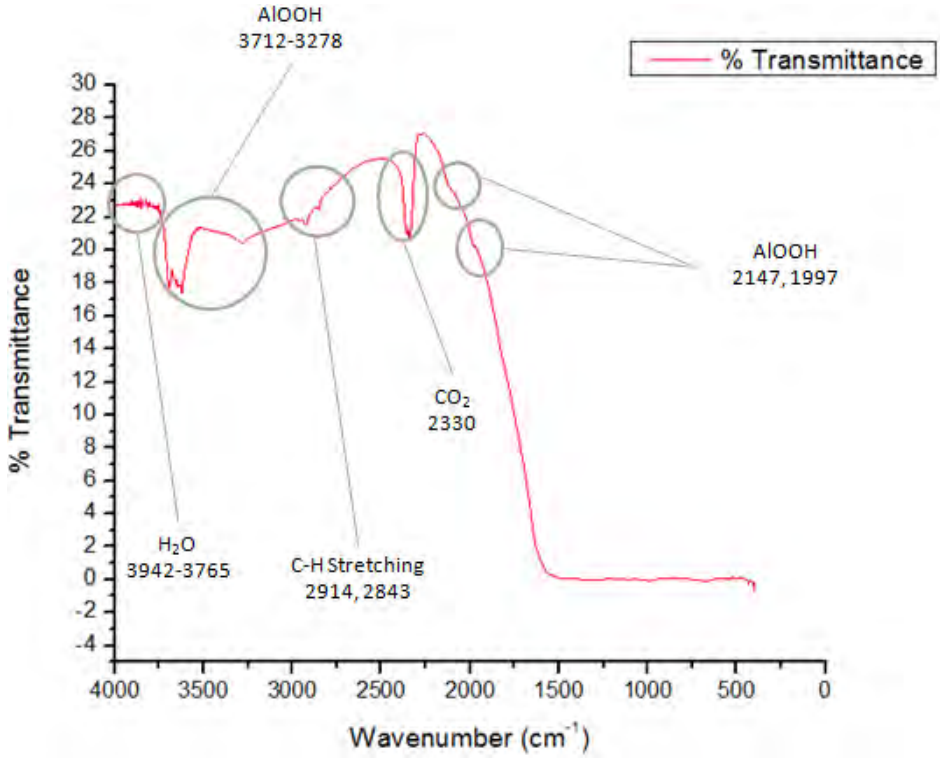

Figure B20 FTIR Result of Pkr2

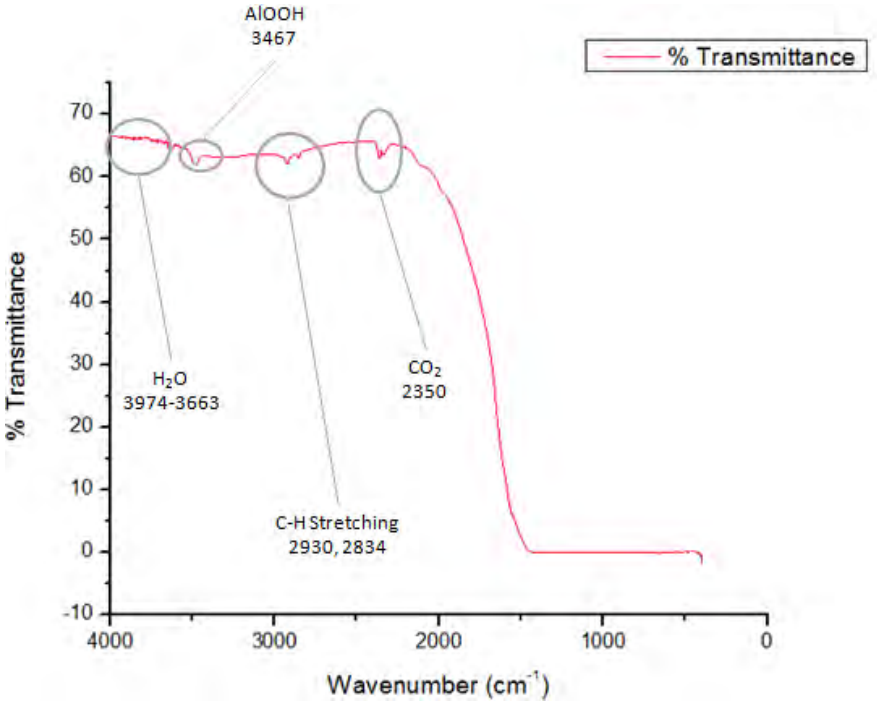

Figure B21 FTIR Result of Pkr3

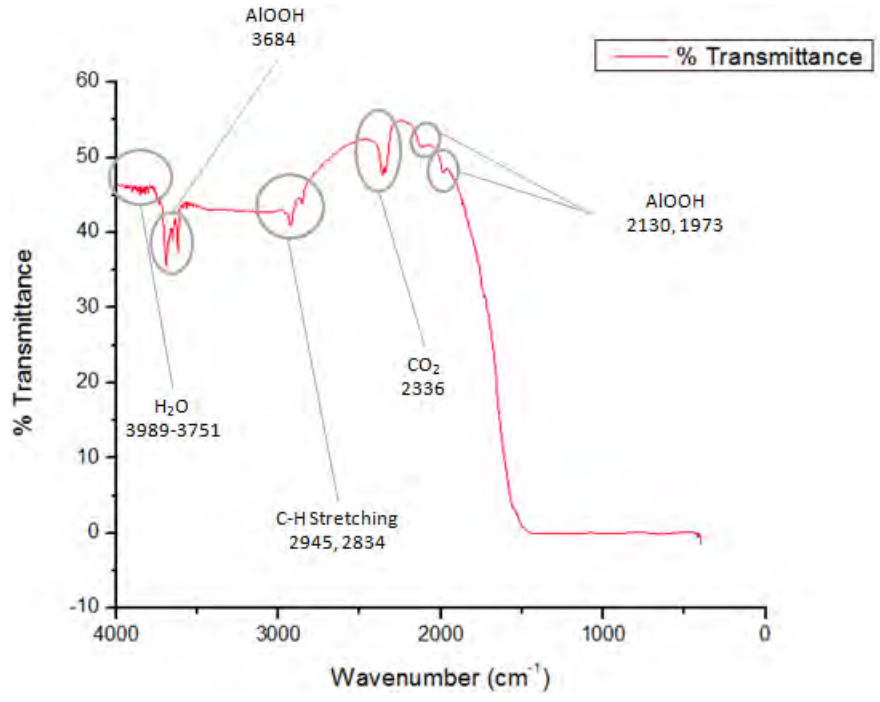

Figure B22 FTIR Result of Pkr4

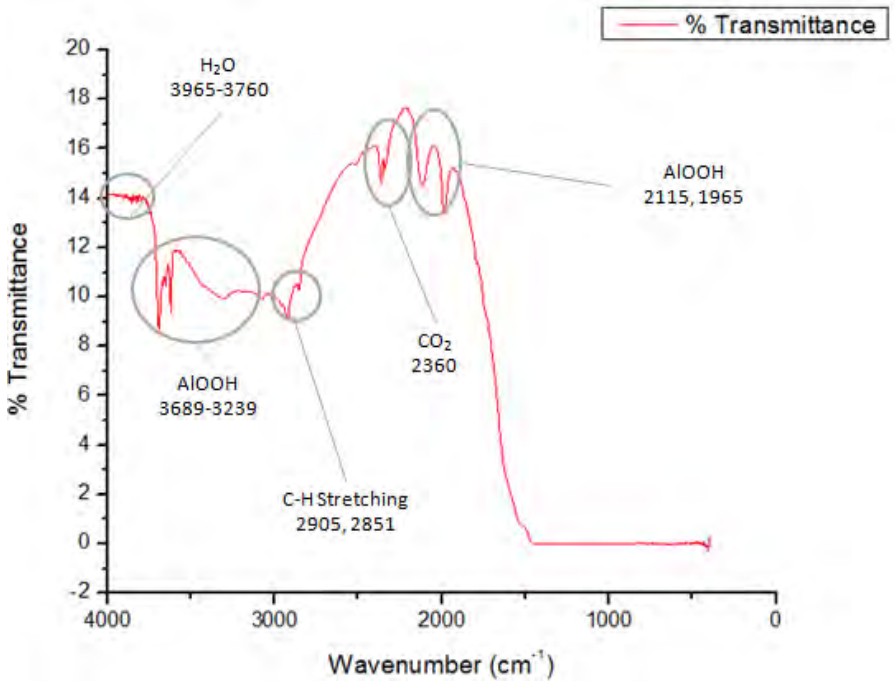

Figure B23 FTIR Result of Pkr5

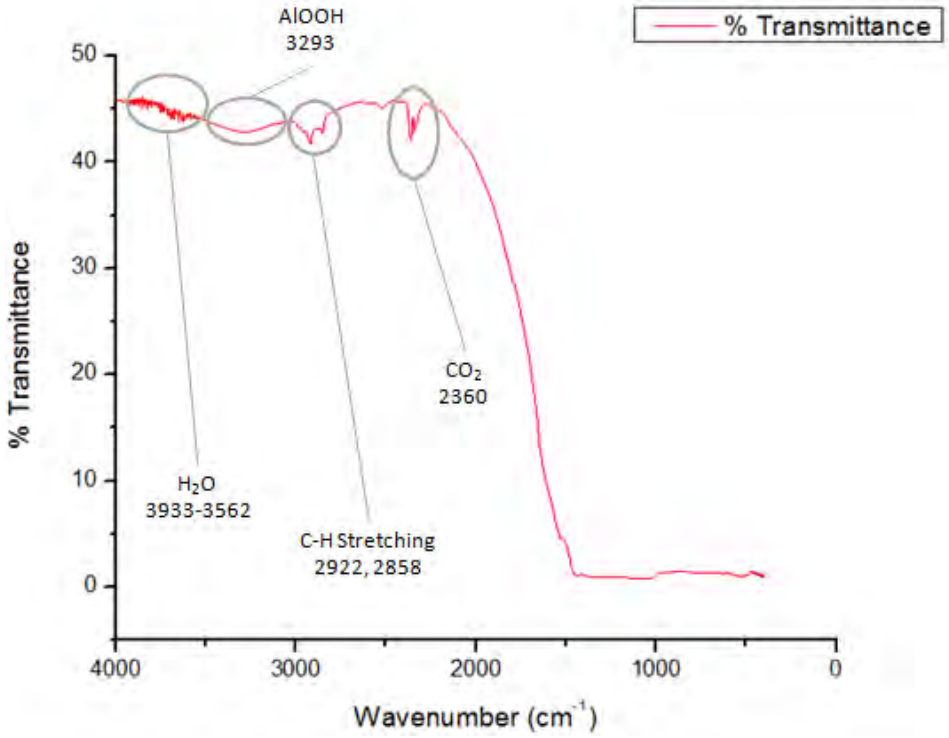

Figure B24 FTIR Result of Pkr6

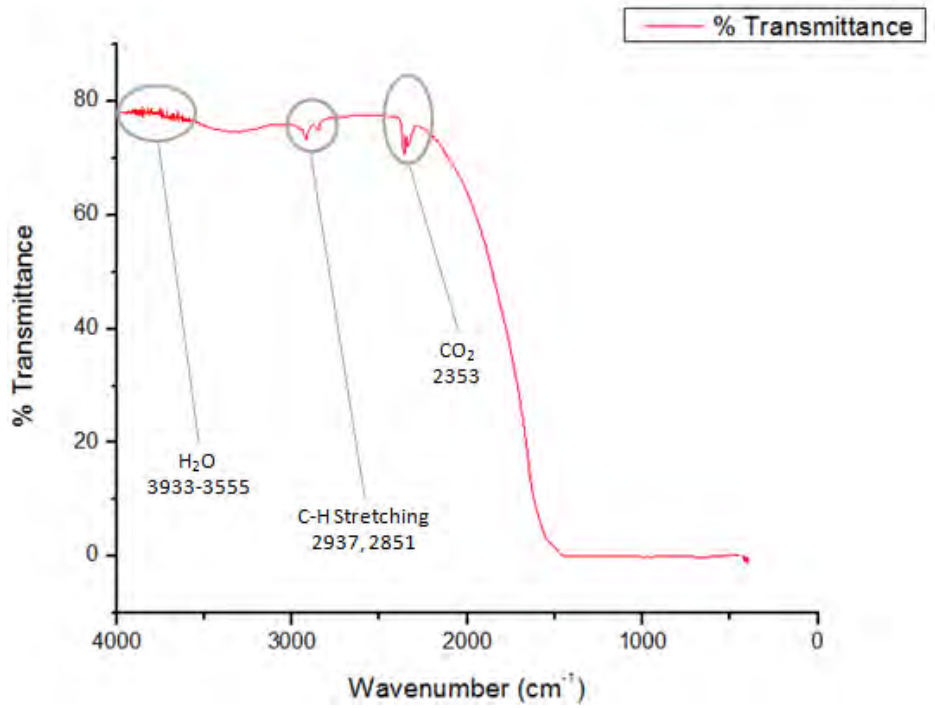

Figure B25 FTIR Result of Pkr7

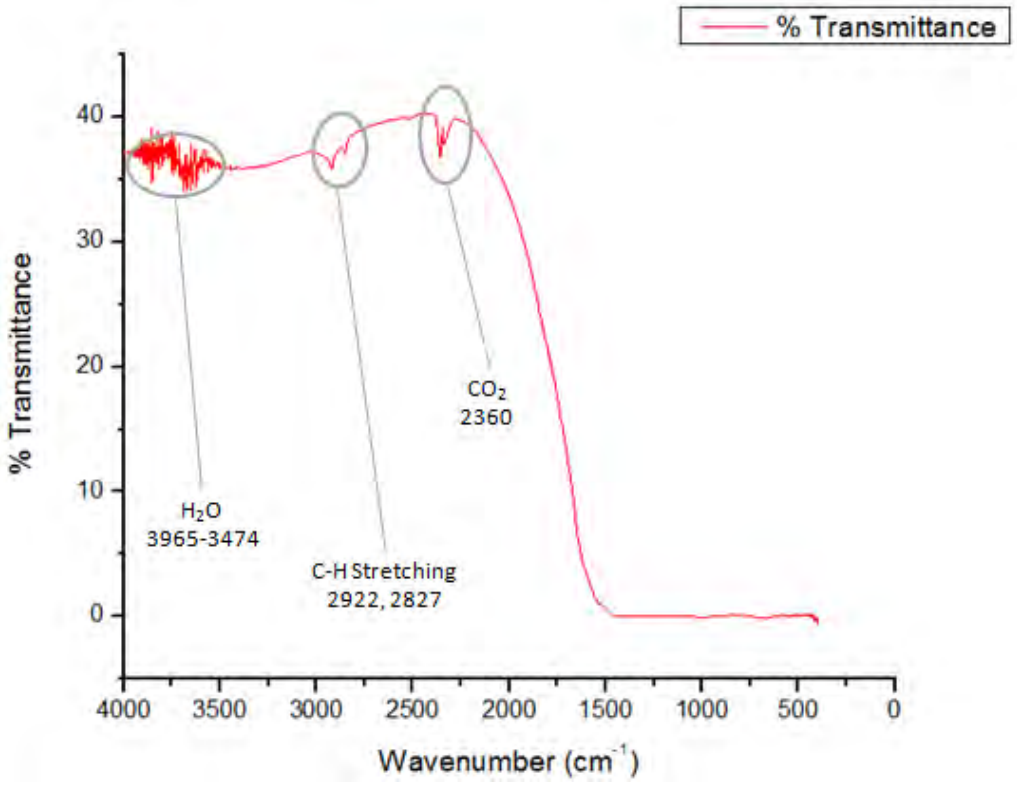

Figure B26 FTIR Result of Pkr8

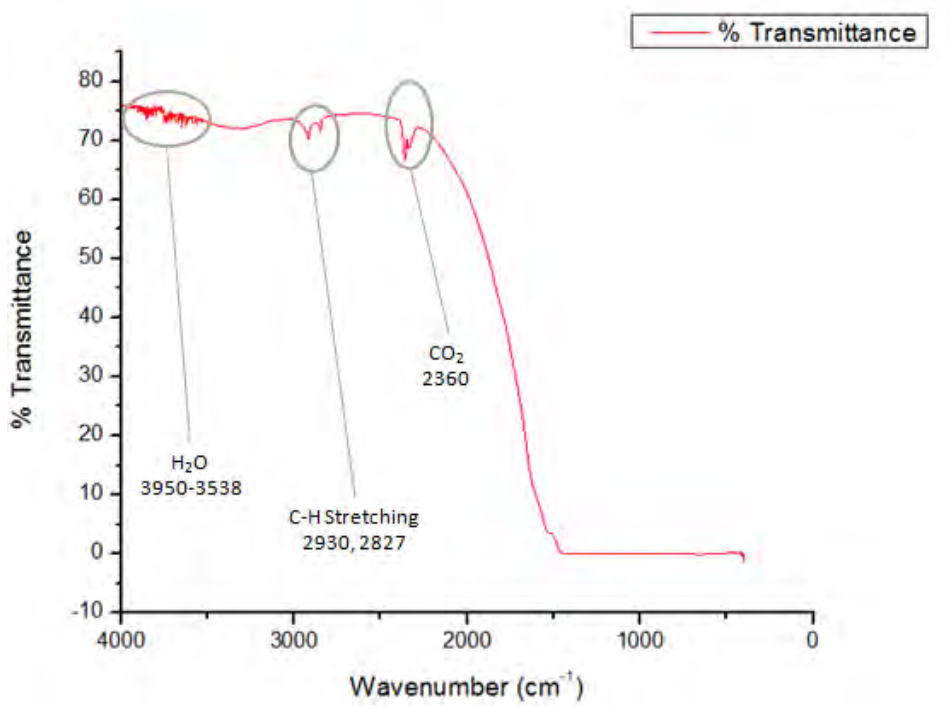

Figure B27 FTIR Result of Pkr9

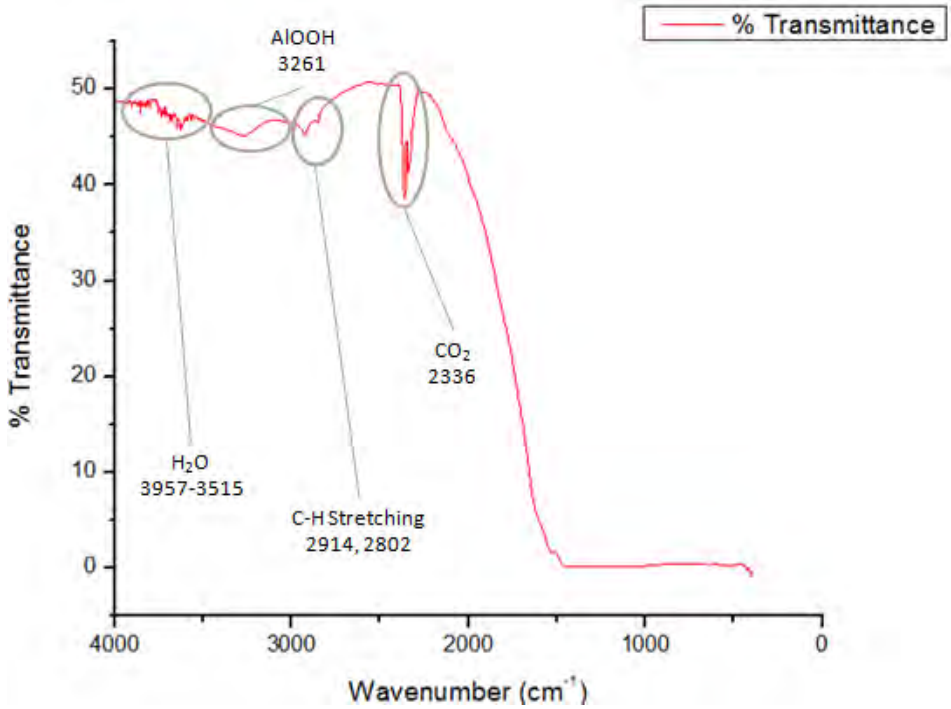

Figure B28 FTIR Result of Pkr10

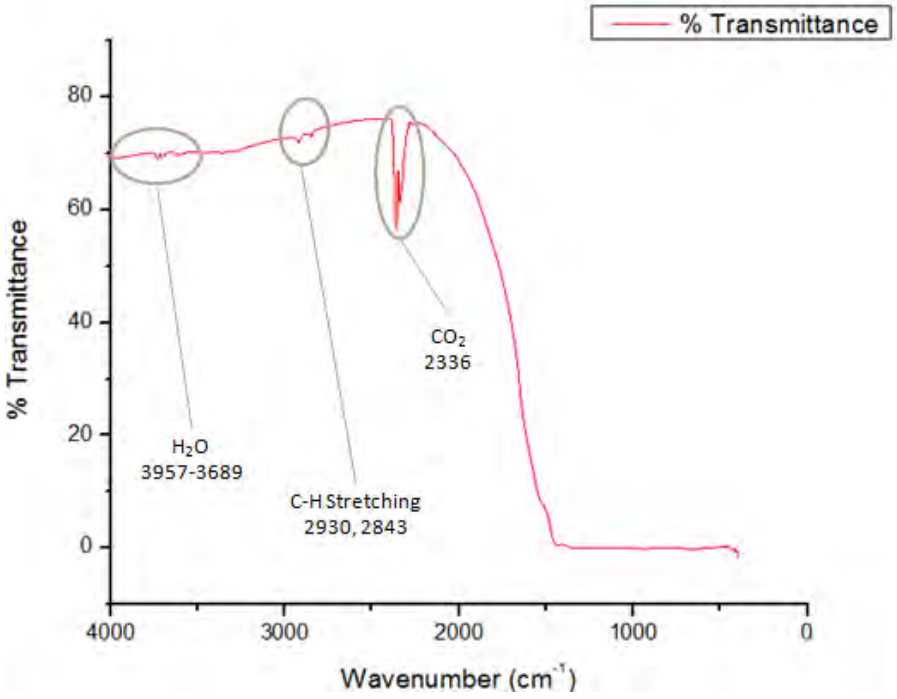

Figure B29 FTIR Result of Pkr11

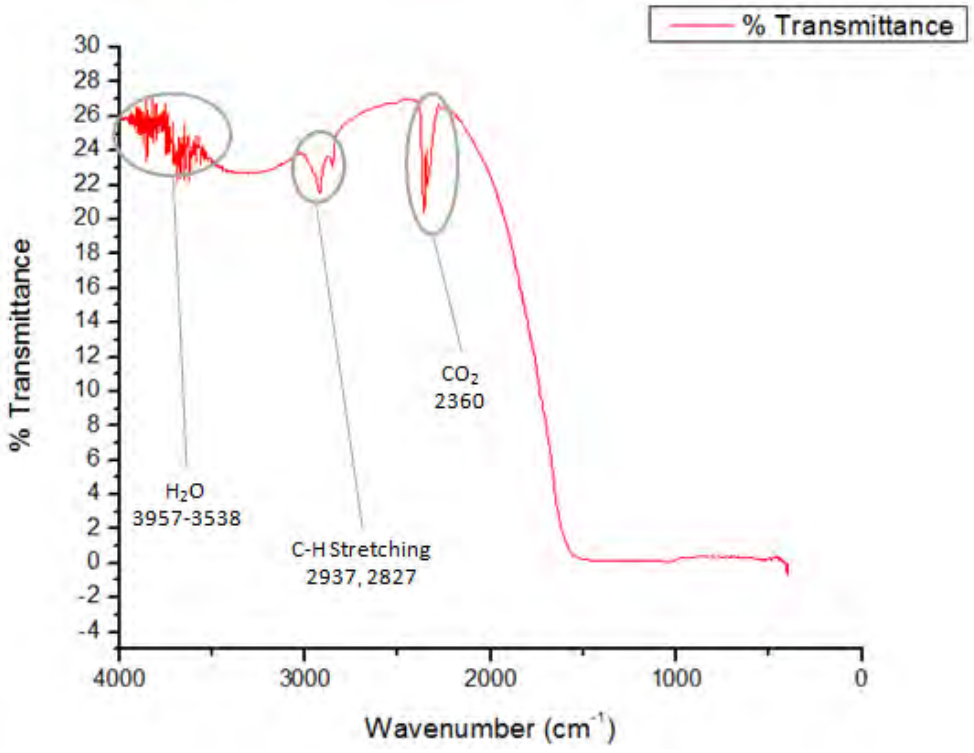

Figure B30 FTIR Result of Pkr12

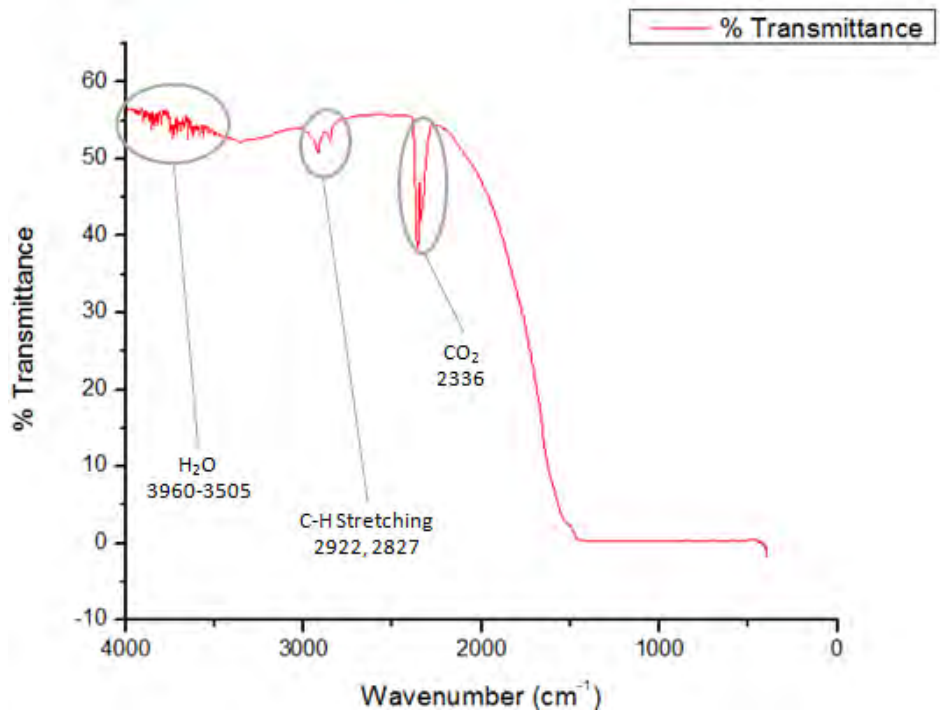

Figure B31 FTIR Result of Pkr13

SECTION C: UV-Vis-NIR SPECTRUM

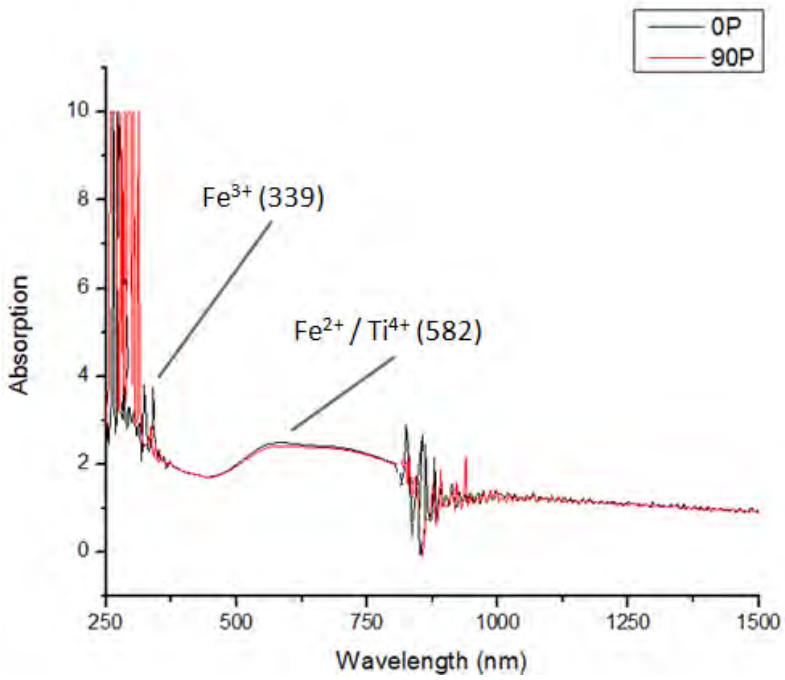

Figure C1 UV-Vis-NIR Result of B1

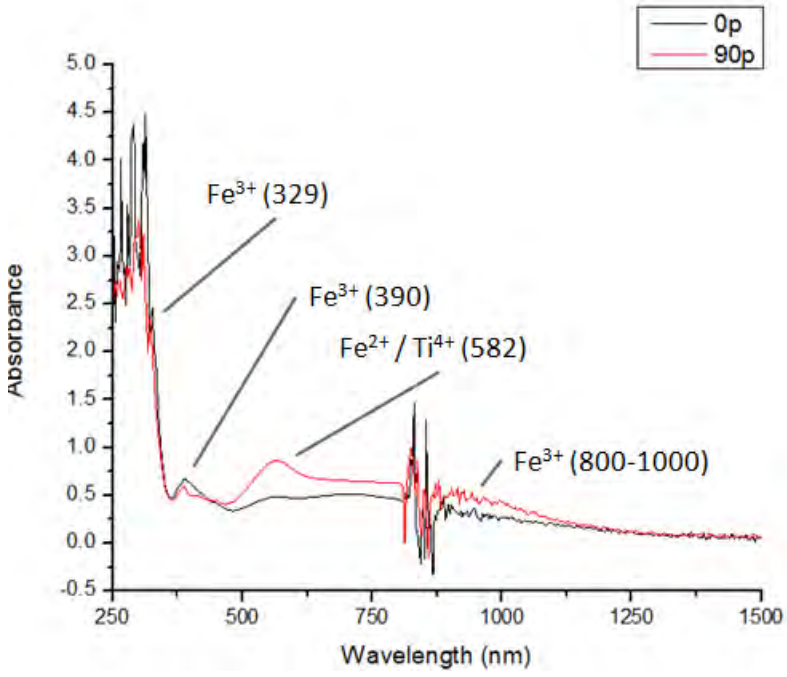

Figure C2 UV-Vis-NIR Result of B2

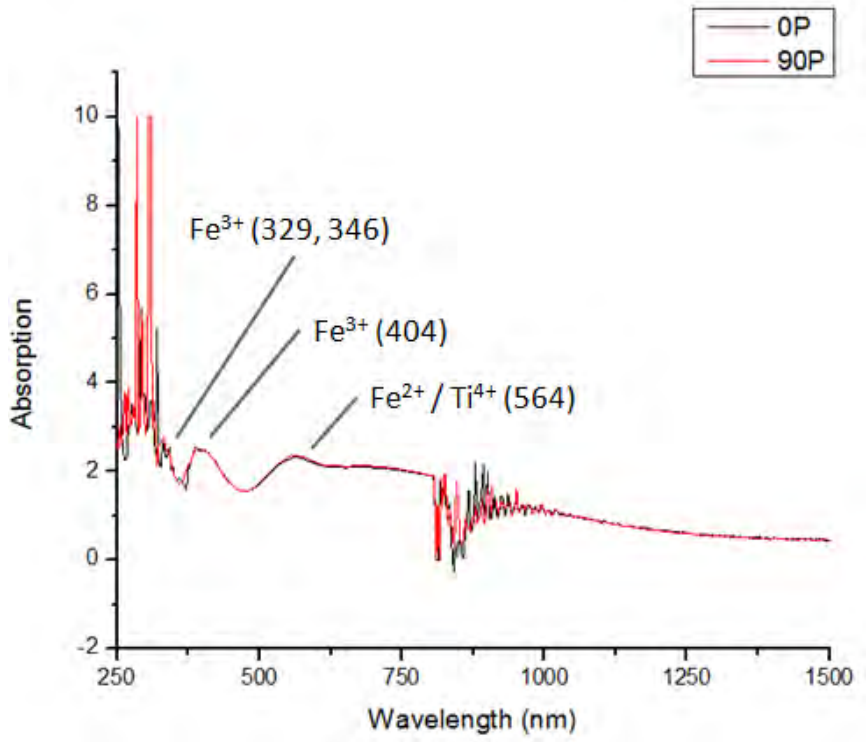

Figure C3 UV-Vis-NIR Result of B3

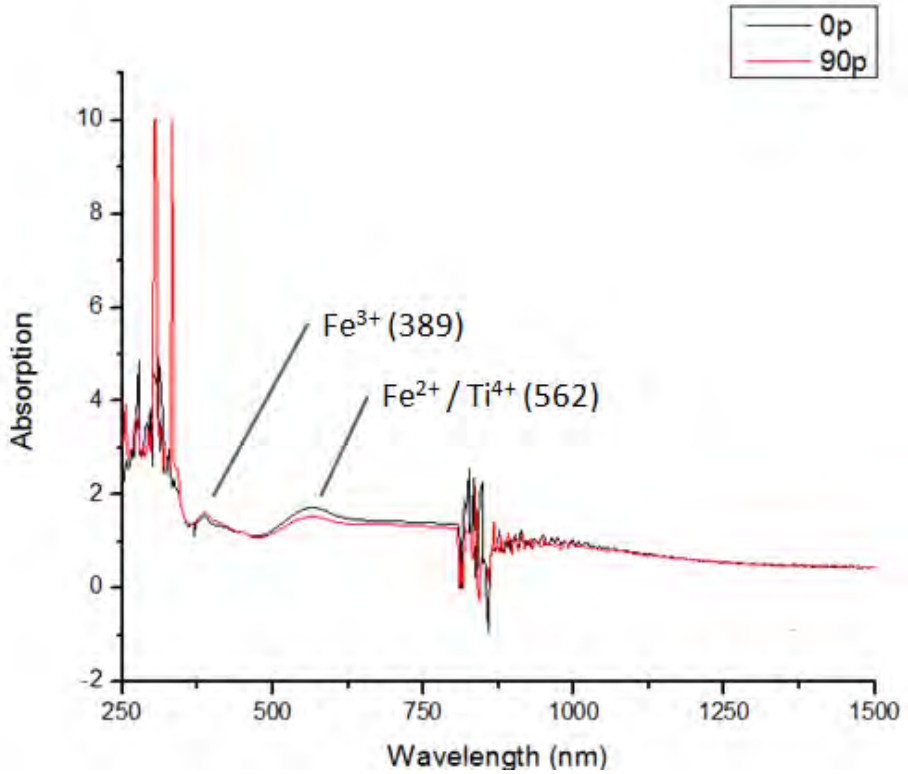

Figure C4 UV-Vis-NIR Result of B4

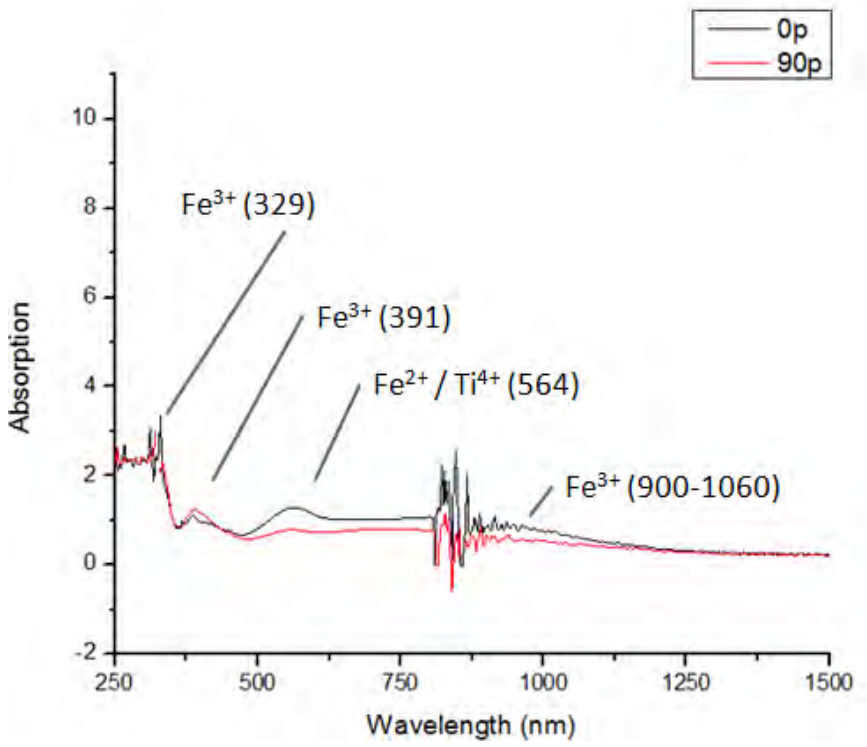

Figure C5 UV-Vis-NIR Result of B5

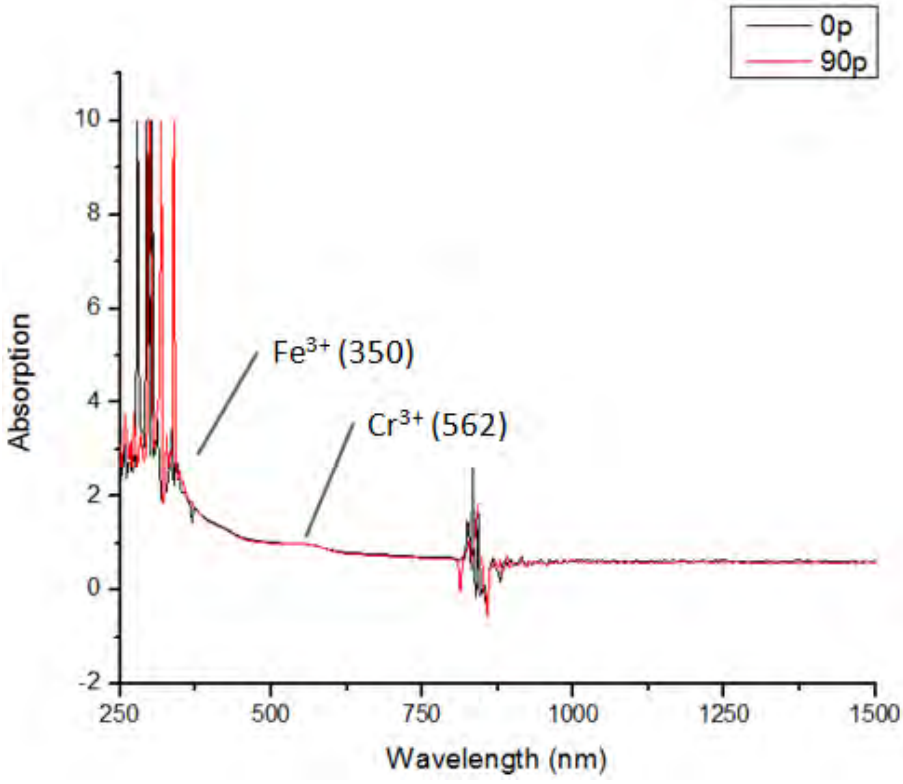

Figure C6 UV-Vis-NIR Result of Ppo1

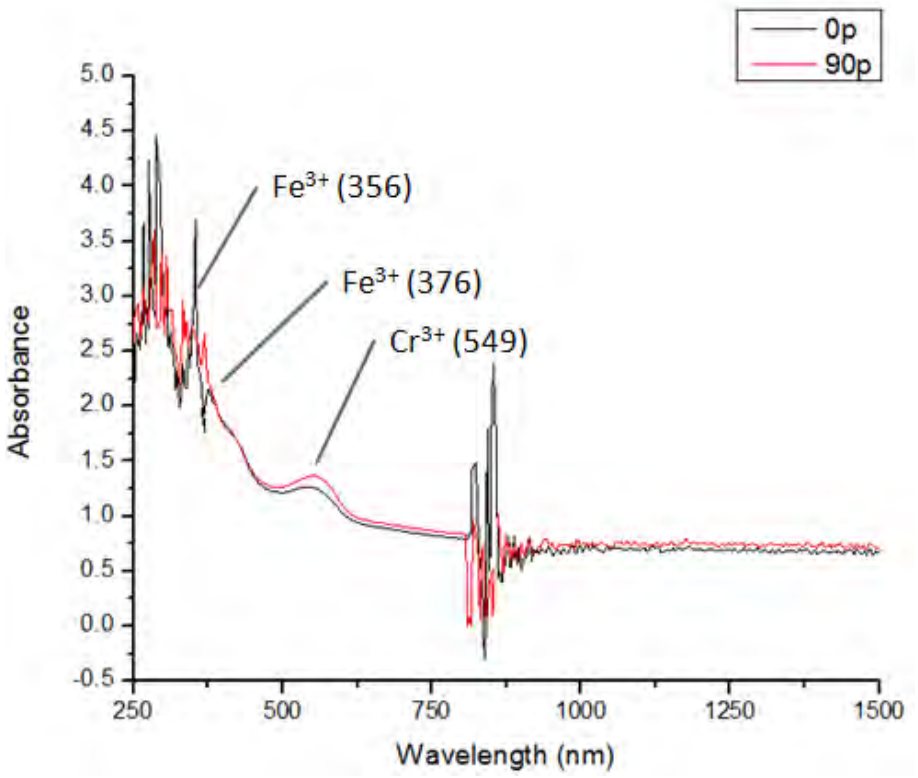

Figure C7 UV-Vis-NIR Result of Ppo2

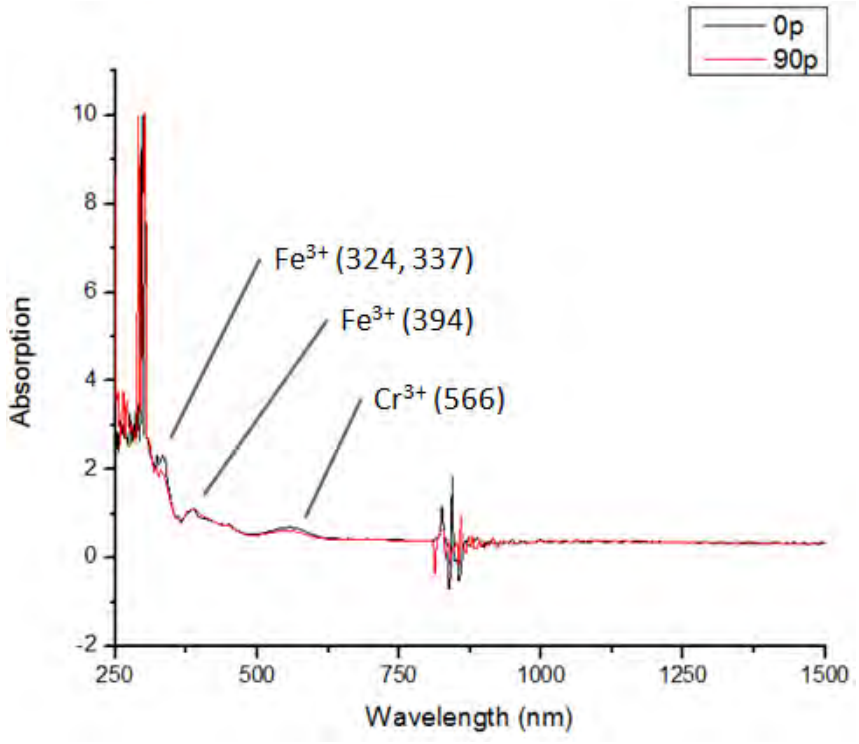

Figure C8 UV-Vis-NIR Result of Ppo3

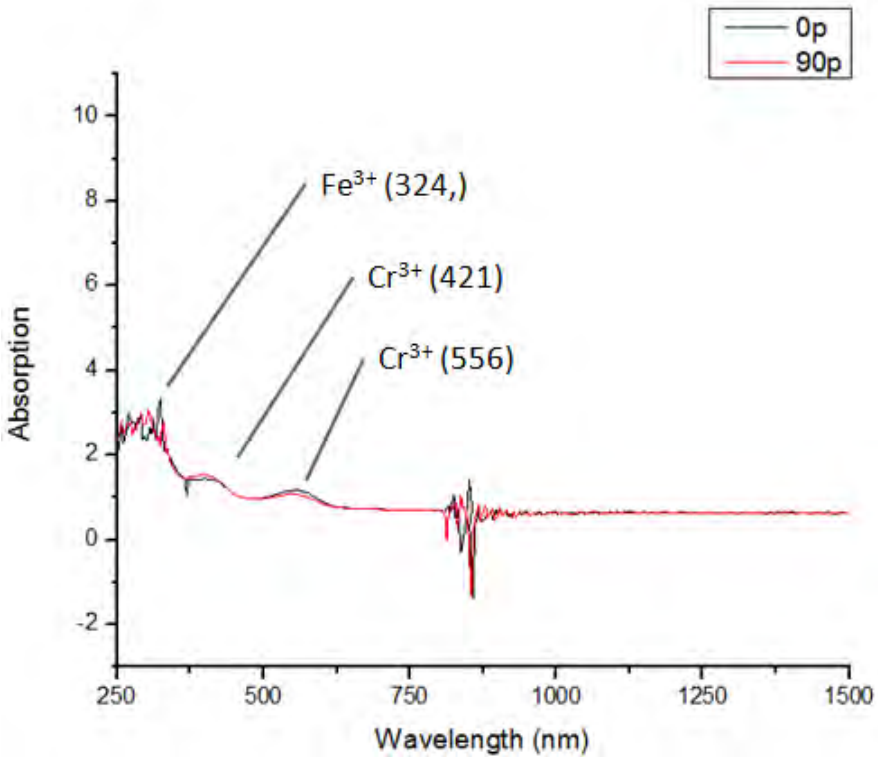

Figure C9 UV-Vis-NIR Result of Ppo4

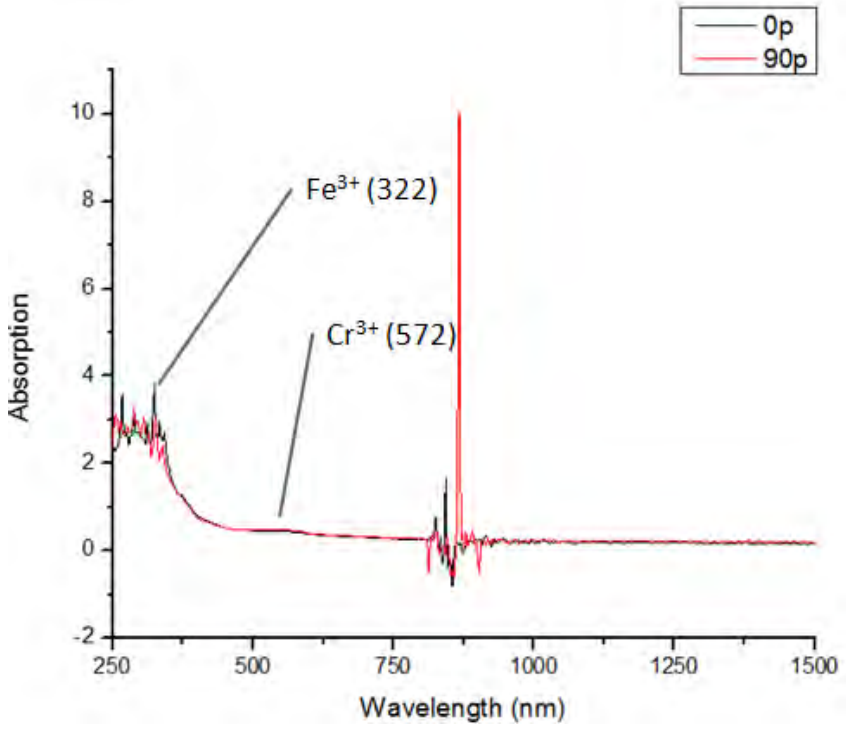

Figure C10 UV-Vis-NIR Result of Ppo5

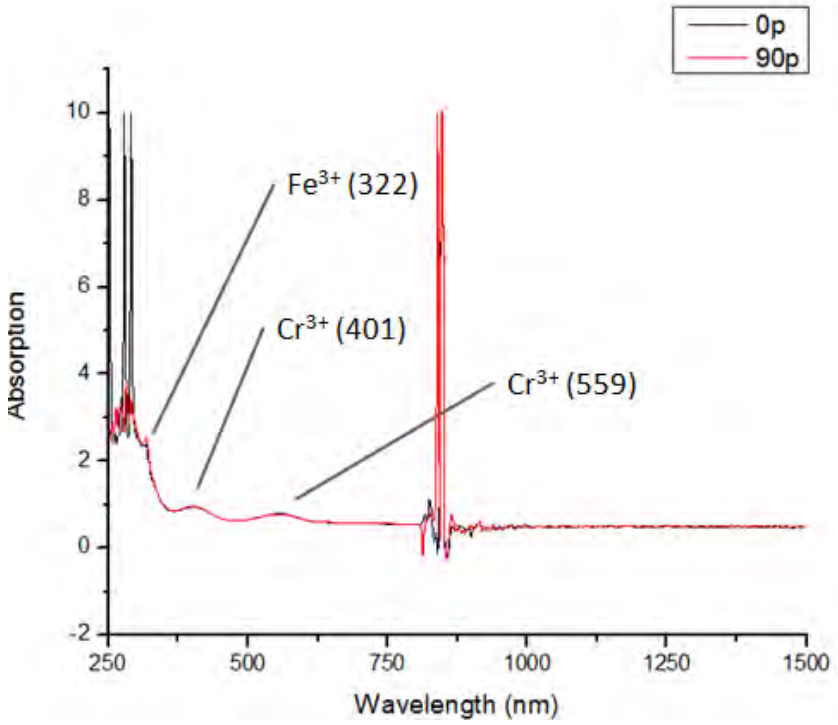

Figure C11 UV-Vis-NIR Result of Ppo6

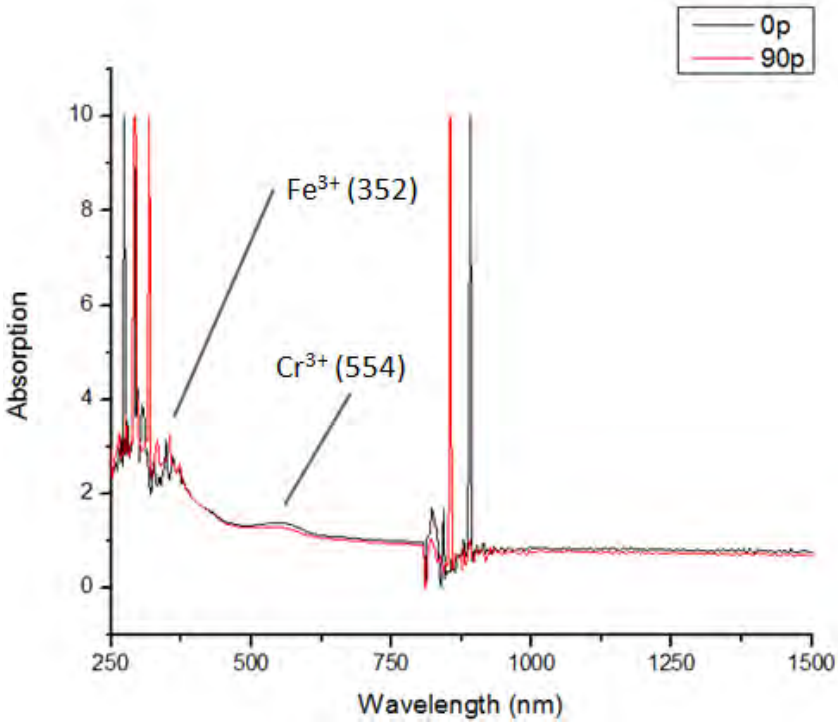

Figure C12 UV-Vis-NIR Result of Ppo7

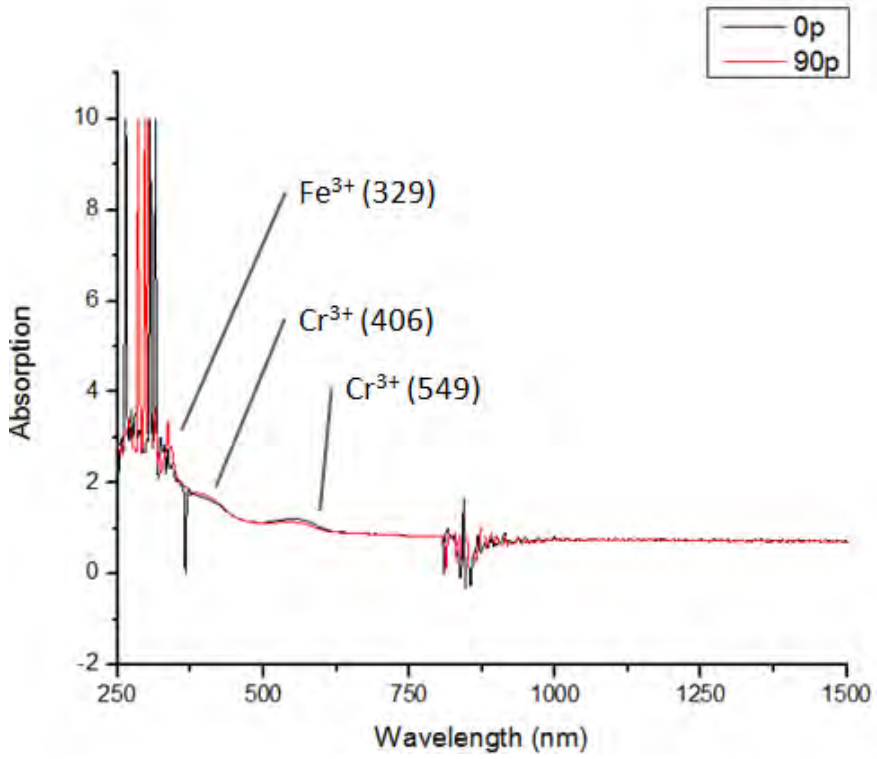

Figure C13 UV-Vis-NIR Result of Ppo8

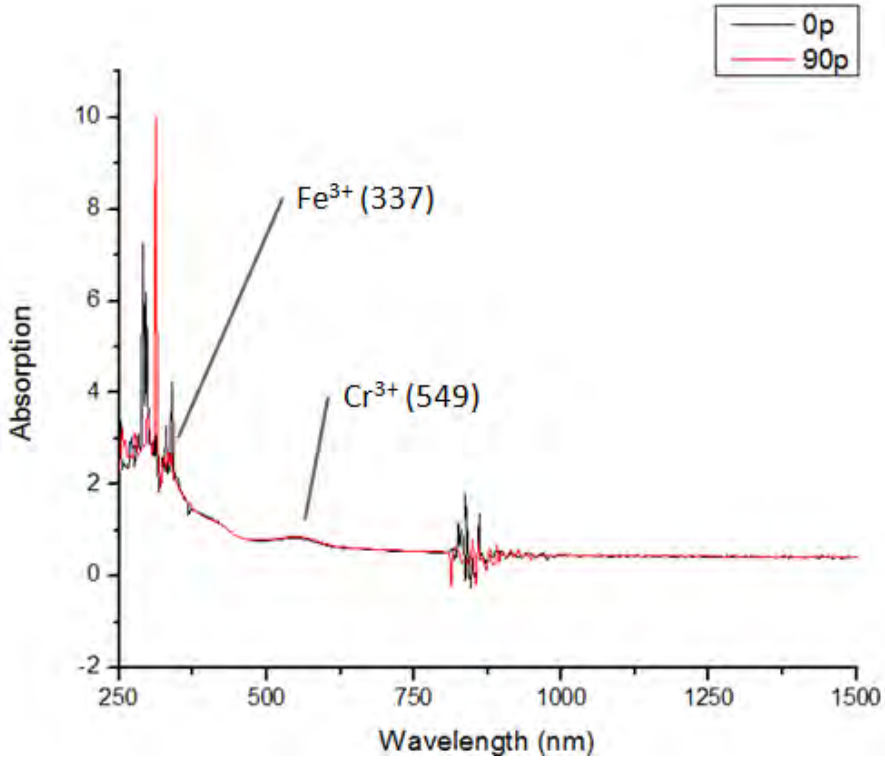

Figure C14 UV-Vis-NIR Result of Ppo9

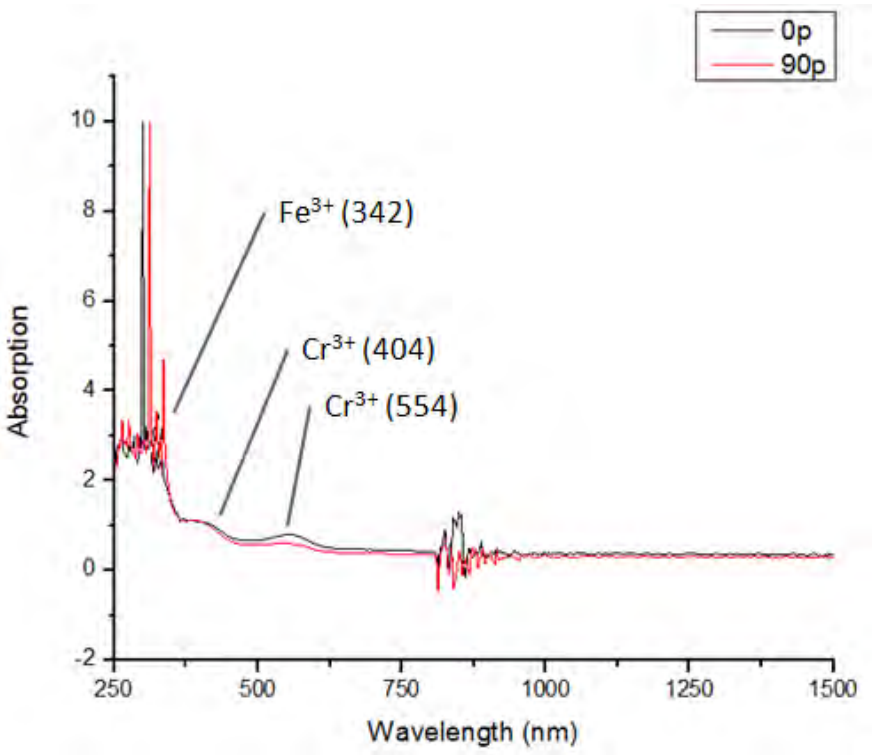

Figure C15 UV-Vis-NIR Result of Ppo10

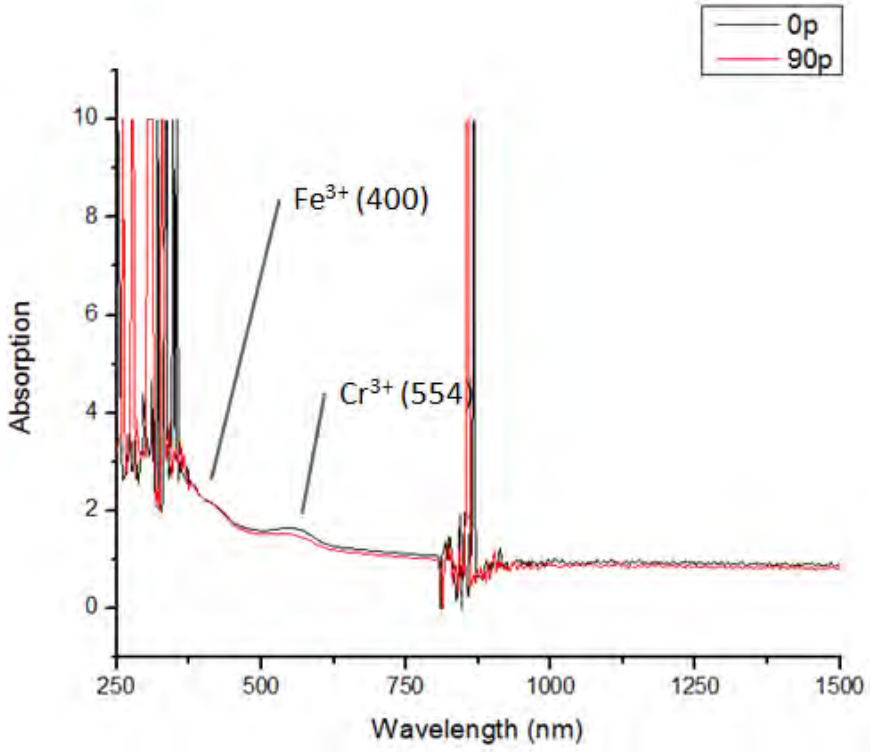

Figure C16 UV-Vis-NIR Result of Ppo11

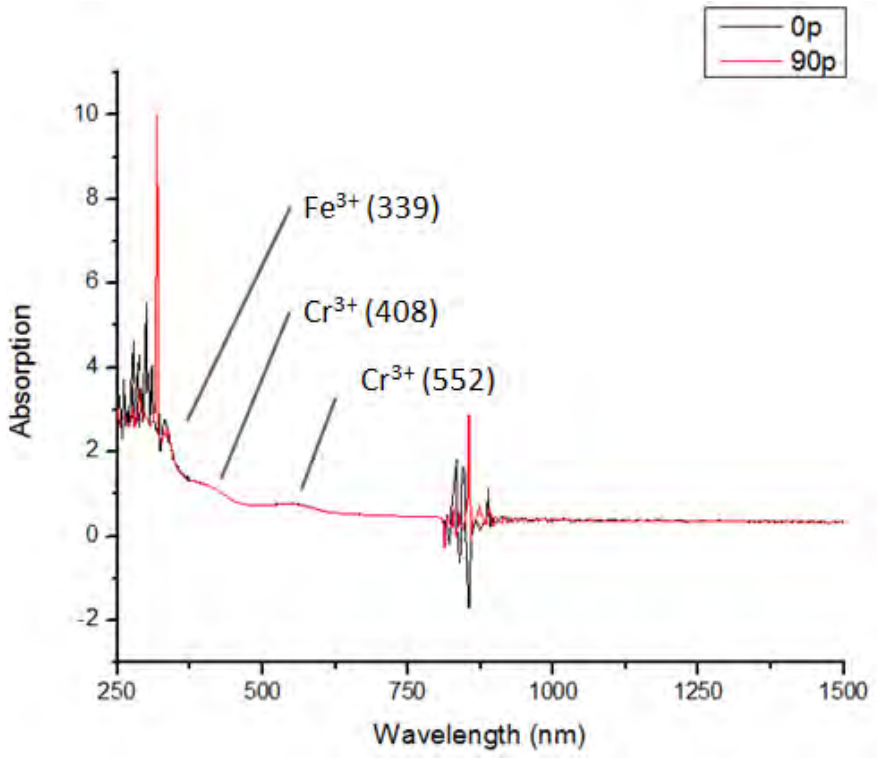

Figure C17 UV-Vis-NIR Result of Ppo12

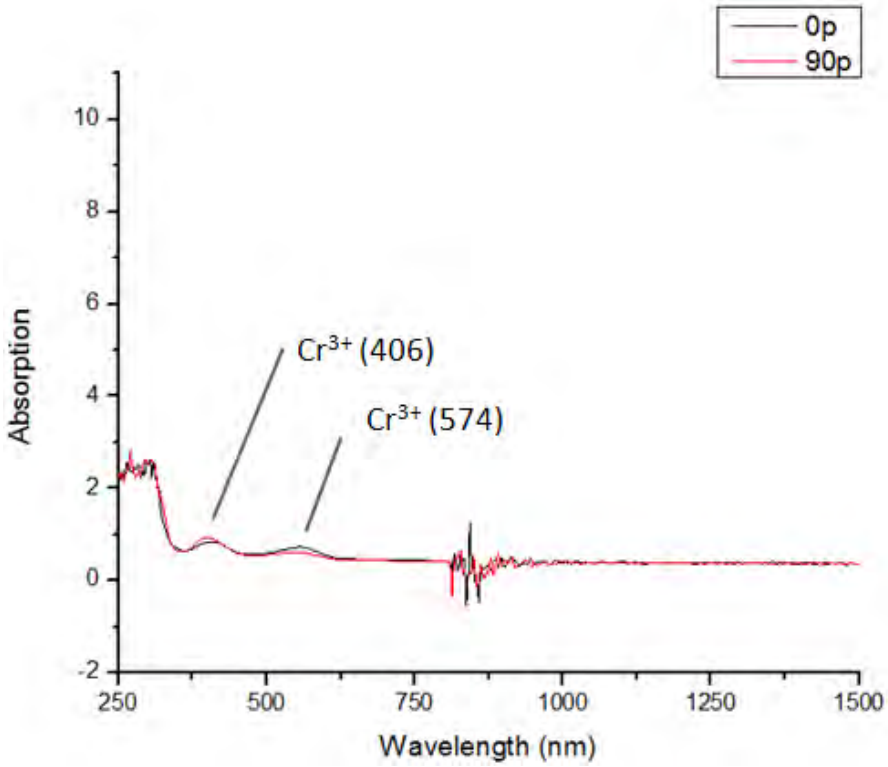

Figure C18 UV-Vis-NIR Result of Ppo13

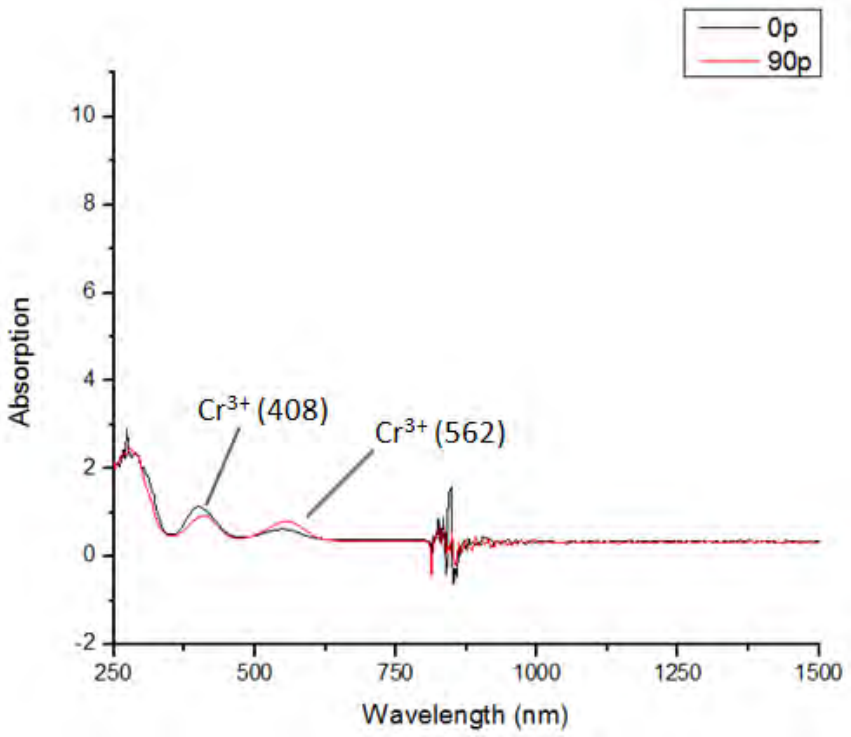

Figure C19 UV-Vis-NIR Result of Pkr1

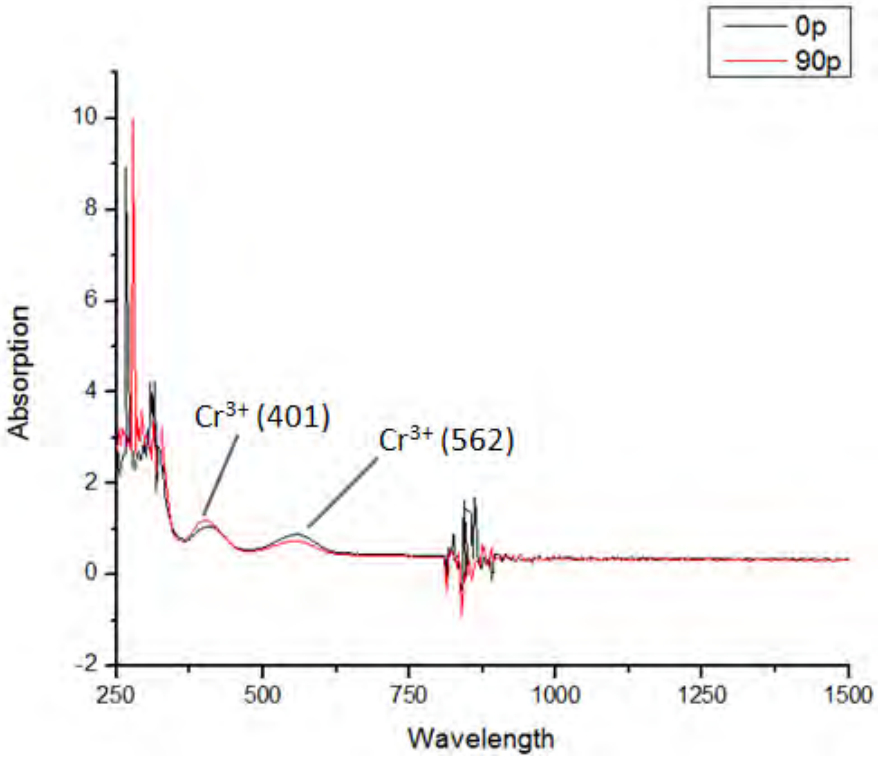

Figure C20 UV-Vis-NIR Result of Pkr2

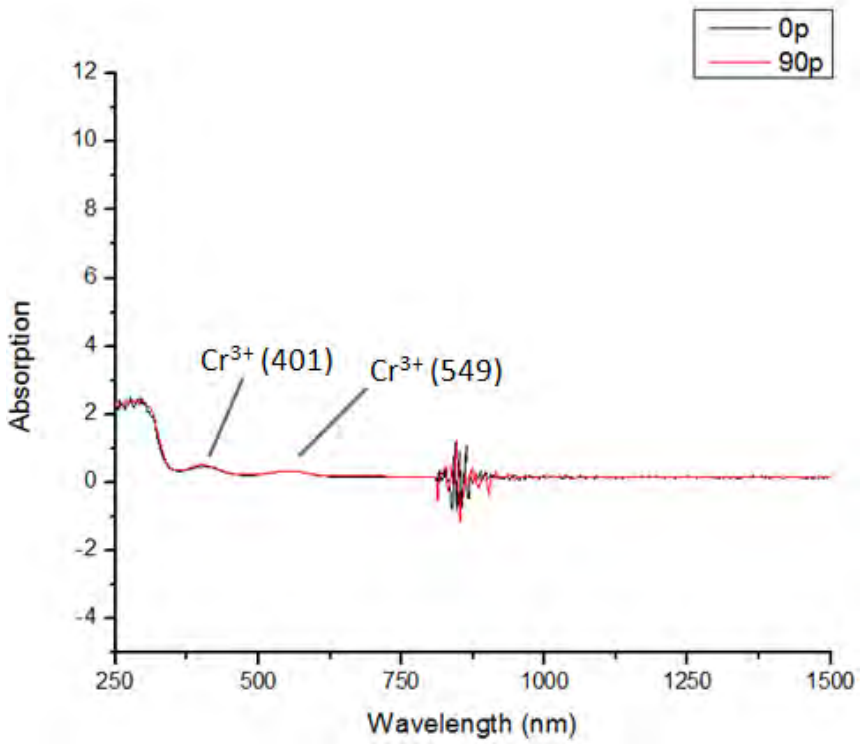

Figure C21 UV-Vis-NIR Result of Pkr3

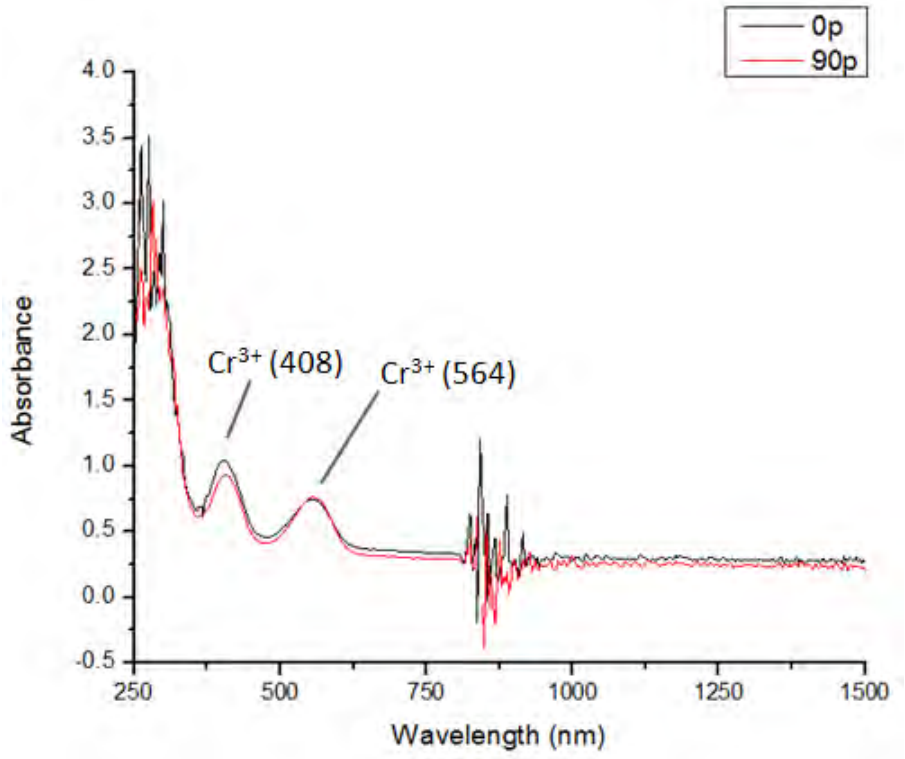

Figure C22 UV-Vis-NIR Result of Pkr4

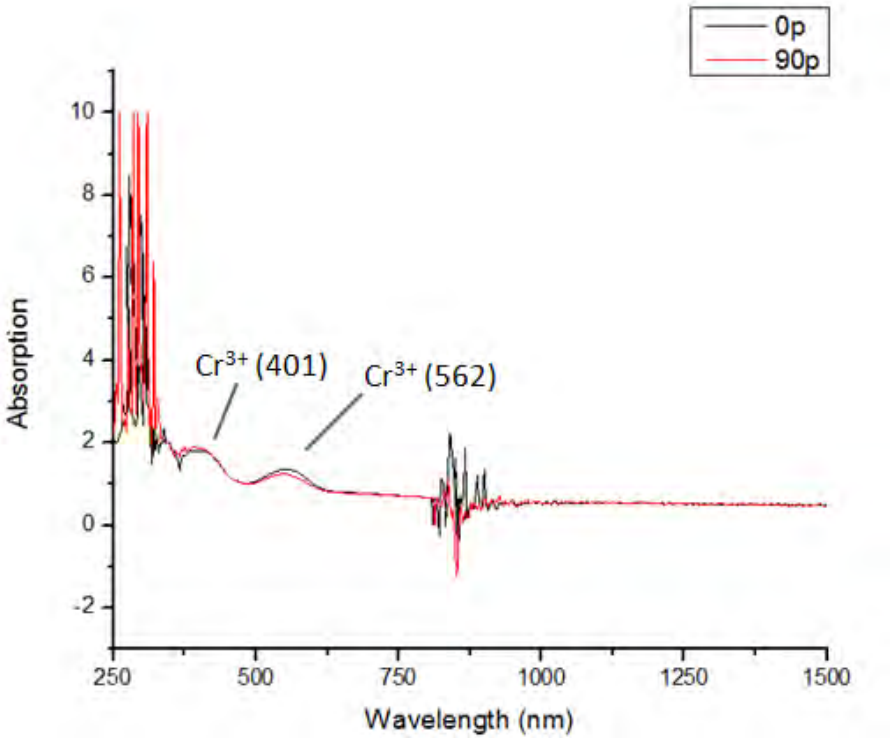

Figure C23 UV-Vis-NIR Result of Pkr5

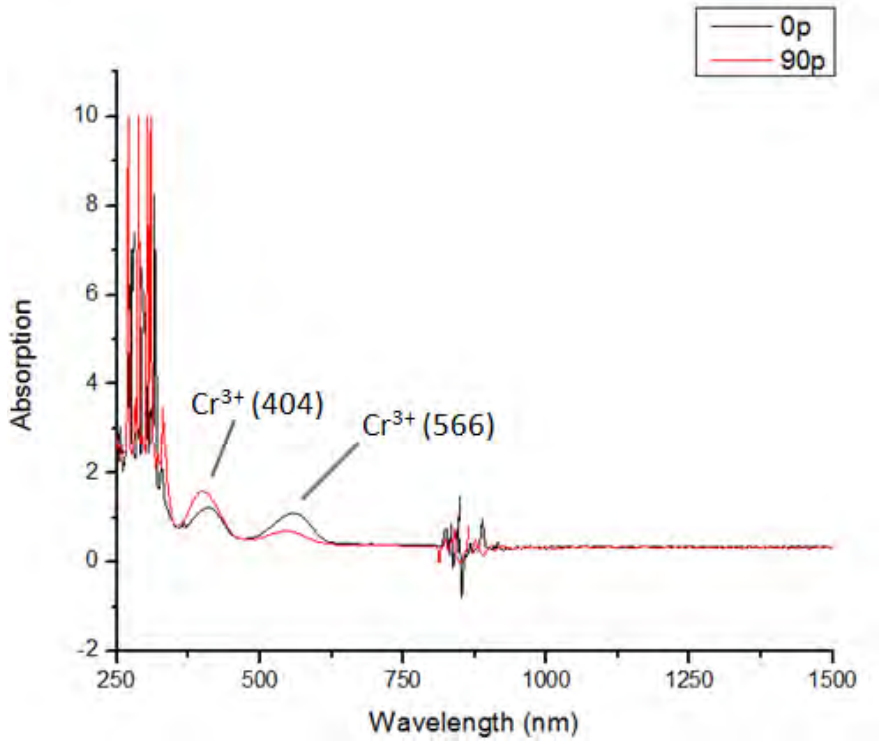

Figure C24 UV-Vis-NIR Result of Pkr6

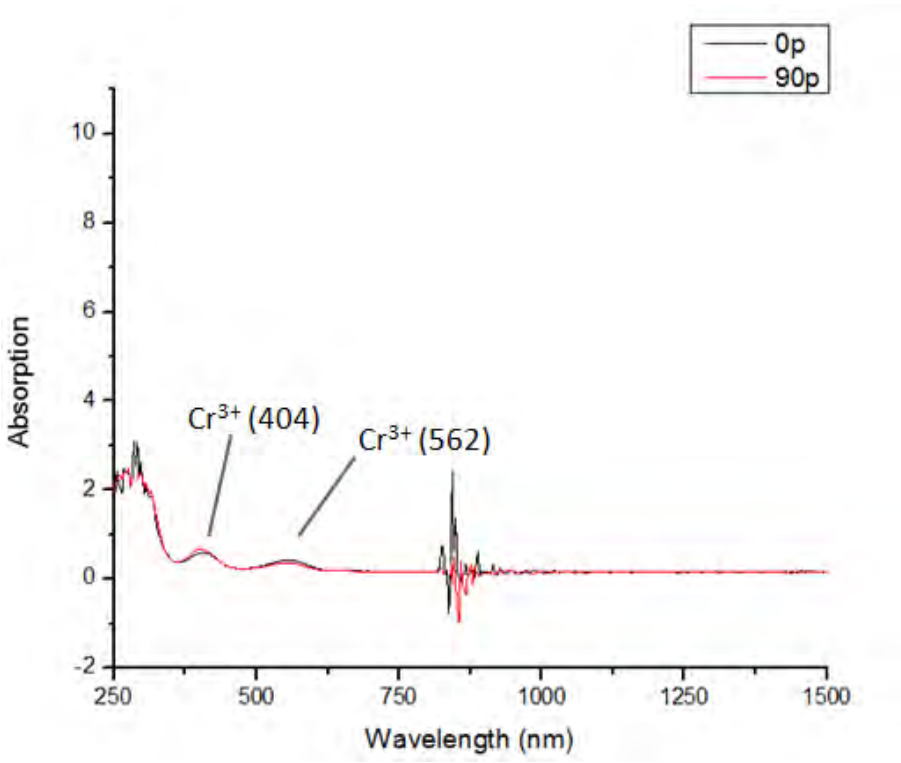

Figure C25 UV-Vis-NIR Result of Pkr7

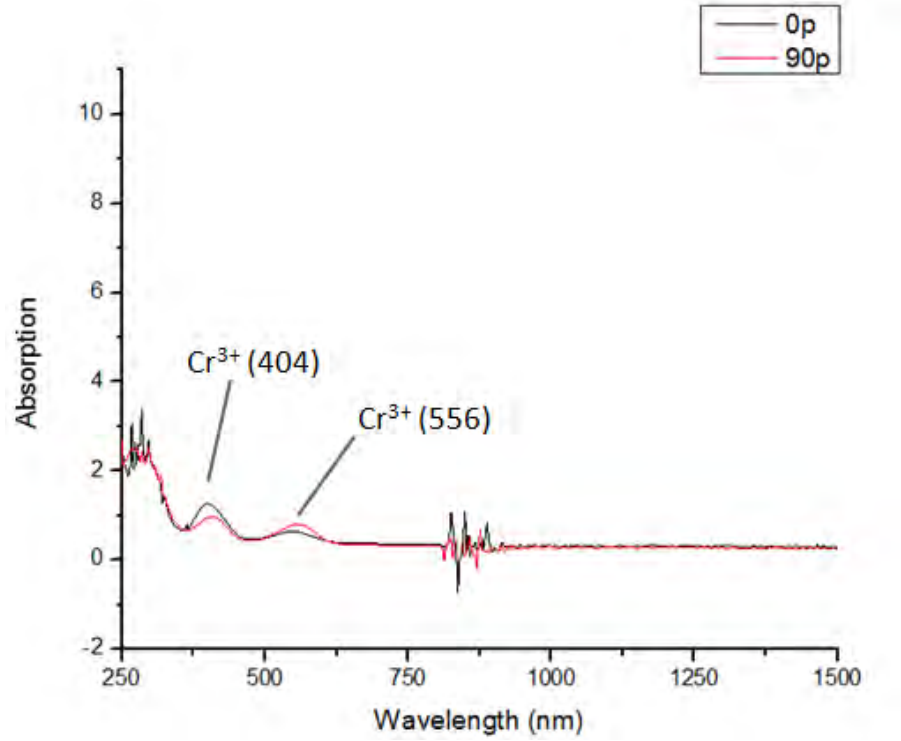

Figure C26 UV-Vis-NIR Result of Pkr8

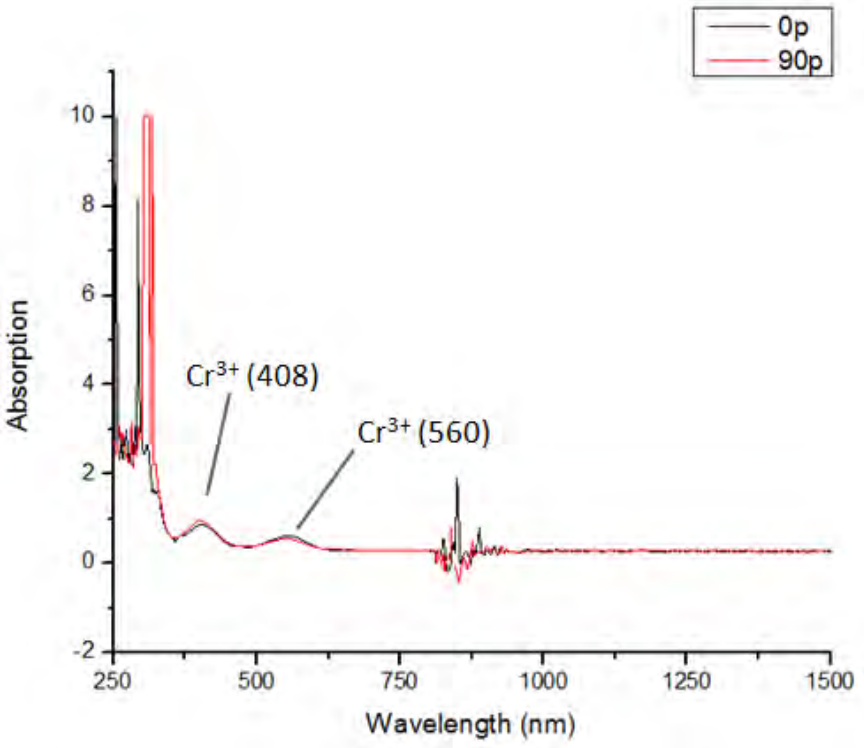

Figure C27 UV-Vis-NIR Result of Pkr9

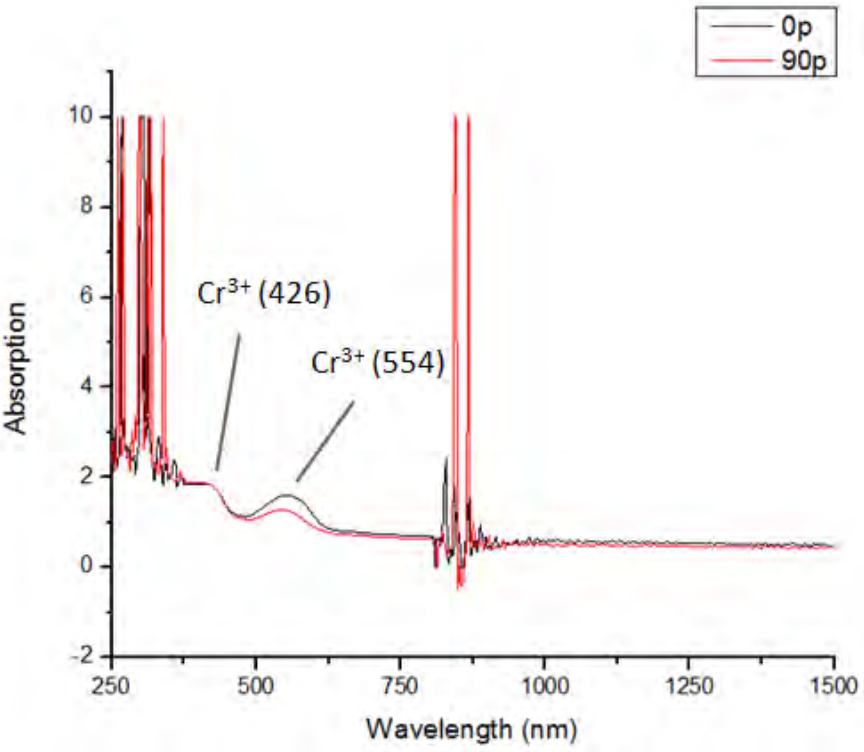

Figure C28 UV-Vis-NIR Result of Pkr10

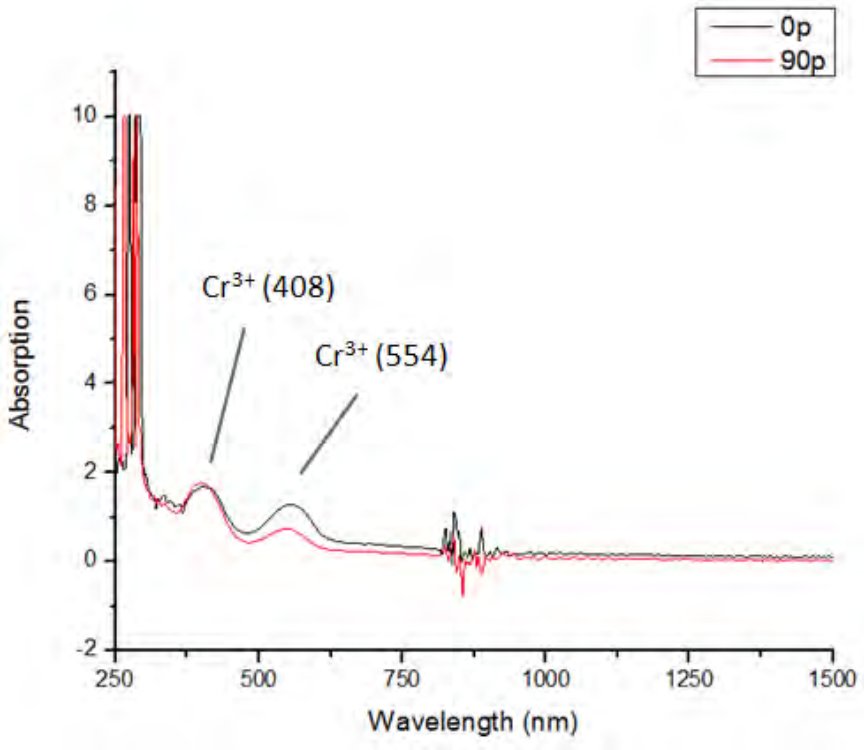

Figure C30 UV-Vis-NIR Result of Pkr11

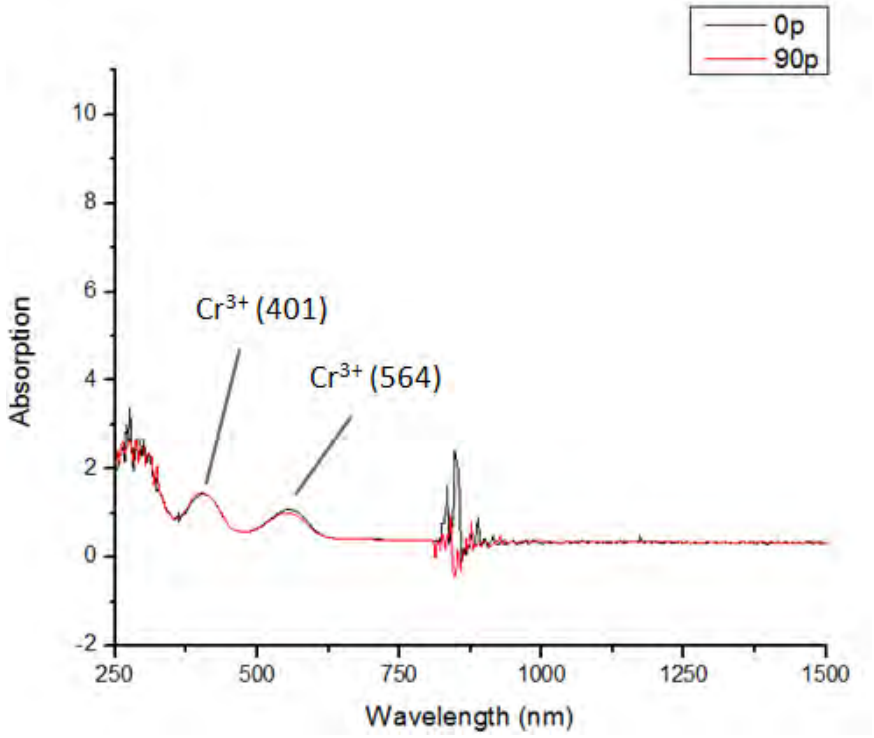

Figure 6.30C UV-Vis-NIR Result of Pkr12

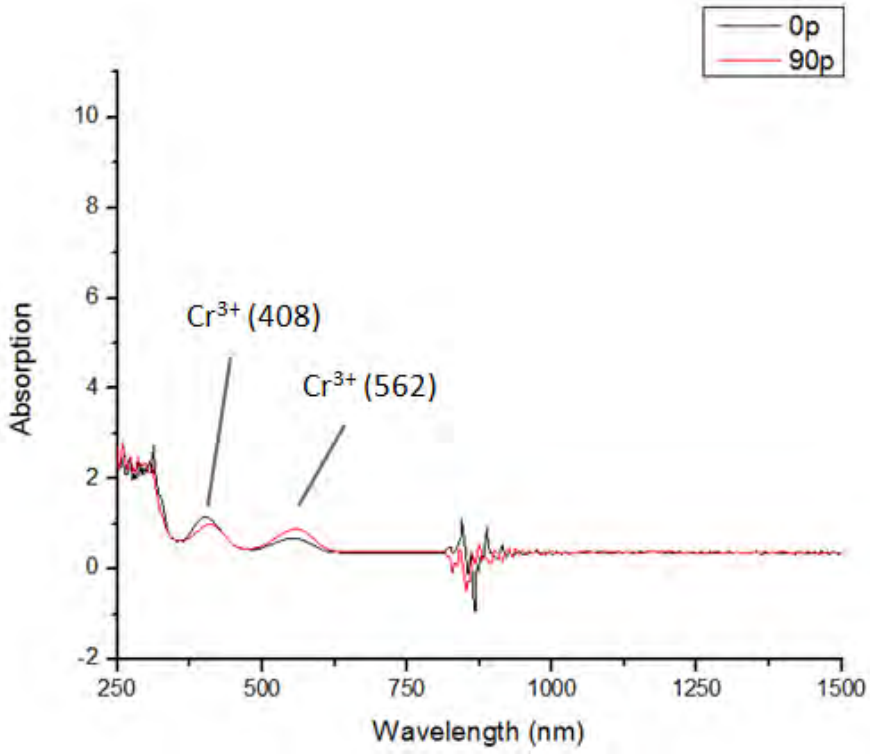

Figure C31 UV-Vis-NIR Result of Pkr13

SECTION D: EDXRF ANALYSIS

Table D1 EDXRF results of B1 to B5

Element	B1	B2	B3	B4	B5
Al_2O_3	99.8669	99.6816	99.6513	99.6742	99.7107
TiO_2	0.08	0.0275	0.0353	0.0342	0.0262
V_2O_5	0.0083	0.0081	0.0065	0.0075	0.0073
Cr_2O_3	0.0074	0.0332	0.053	0.0259	0.0214
Fe_2O_3	0.0268	0.2446	0.243	0.2543	0.2284
Ga_2O_3	0.0107	0.0049	0.011	0.0039	0.0059

Table D2 EDXRF results of Ppo1 to Ppo5

Element	Ppo1	Ppo2	Ppo3	Ppo4	Ppo5
Al_2O_3	99.8692	99.9346	99.6707	99.933	99.8087
TiO_2	0.0823	0.0039	0.0073	0.0071	0.1438
V_2O_5	0.0073	0.0043	0.0051	0.0043	0.0115
Cr_2O_3	0.0178	0.0242	0.0264	0.0298	0.0148
Fe_2O_3	0.0142	0.0203	0.289	0.0152	0.0107
Ga_2O_3	0.0093	0.0127	0.0014	0.0106	0.0105

Table D3 EDXRF results of Ppo6 to Ppo10

Element	Ppo6	Ppo7	Ppo8	Ppo9	Ppo10
Al_2O_3	99.9251	99.8343	99.8871	99.8229	99.8868
TiO_2	0.0103	0.112	0.0386	0.1191	0.0455
V_2O_5	0.0061	0.0087	0.0123	0.0097	0.0077
Cr_2O_3	0.0319	0.0231	0.0285	0.0264	0.0276
Fe_2O_3	0.0176	0.0136	0.0247	0.0167	0.0214
Ga_2O_3	0.009	0.0084	0.0087	0.0052	0.011

Table D4 EDXRF results of Ppo11 to Ppo13

Element	Ppo11	Ppo12	Ppo13
Al_2O_3	99.865	99.8237	99.9032
TiO_2	0.0746	0.0903	0.0204
V_2O_5	0.0095	0.0138	0.0061
Cr_2O_3	0.0184	0.0371	0.0464
Fe_2O_3	0.0229	0.0172	0.0173
Ga_2O_3	0.0096	0.0178	0.0067

Table D5 EDXRF results of Pkr1 to Pkr5

Element	Pkr1	Pkr2	Pkr3	Pkr4	Pkr5
Al_2O_3	99.8087	99.8903	99.8778	99.8711	99.727
TiO_2	0.0215	0.0296	0.0337	0.0136	0.0343
V_2O_5	0.0082	0.0127	0.0064	0.0055	0.006
Cr_2O_3	0.1383	0.0358	0.054	0.0902	0.0927
Fe_2O_3	0.0176	0.0182	0.025	0.0093	0.1277
Ga_2O_3	0.0057	0.0133	0.0032	0.0103	0.0123

Table D6 EDXRF results of Pkr6 to Pkr10

Element	Pkr6	Pkr7	Pkr8	Pkr9	Pkr10
Al_2O_3	99.8023	99.908	99.8556	99.9135	99.7491
TiO_2	0.0398	0.0114	0.0193	0.0108	0.1027
V_2O_5	0.0157	0.0078	0.0301	0.0018	0.007
Cr_2O_3	0.1207	0.0454	0.0563	0.056	0.112
Fe_2O_3	0.0156	0.0107	0.0085	0.0121	0.0176
Ga_2O_3	0.0059	0.0166	0.0302	0.0057	0.0114

Table D7 EDXRF results of Pkr11 to Pkr13

Element	Pkr11	Pkr12	Pkr13
Al_2O_3	99.5596	99.8352	99.884
TiO_2	0.0127	0.0133	0.0117
V_2O_5	0.0064	0.0076	0.0043
Cr_2O_3	0.2738	0.1168	0.0818
Fe_2O_3	0.136	0.0241	0.013
Ga_2O_3	0.0115	0.003	0.0053

SECTION E: EPMA ANALYSIS

Table E1 EPMA Results Summarization

No.	Al2O3	MgO	CaO	MnO	FeO	SiO2	TiO2	Ga2O3	K2O	Cr2O3	V2O3	Total	Comment
1	99.27	0.00	0.01	0.00	0.01	0.00	0.13	0.01	0.00	0.00	0.00	99.42	B1-1
2	99.78	0.00	0.00	0.00	0.01	0.00	0.11	0.00	0.00	0.00	0.01	99.91	B1-2
3	98.39	0.00	0.01	0.05	0.03	0.00	0.12	0.00	0.00	0.02	0.00	98.62	B1-3
4	98.71	0.00	0.00	0.02	0.28	0.00	0.02	0.11	0.00	0.02	0.00	99.17	B2-1
5	99.00	0.00	0.00	0.04	0.27	0.00	0.01	0.06	0.00	0.02	0.00	99.41	B2-2
6	98.36	0.00	0.01	0.00	0.30	0.00	0.00	0.00	0.00	0.04	0.00	98.73	B2-3
7	98.86	0.00	0.00	0.03	0.19	0.00	0.03	0.02	0.01	0.02	0.00	99.16	B3-1
8	98.81	0.00	0.01	0.02	0.25	0.00	0.06	0.00	0.00	0.07	0.00	99.23	B3-2
9	98.59	0.00	0.00	0.00	0.27	0.00	0.03	0.00	0.00	0.00	0.02	98.91	B3-3
10	98.94	0.00	0.00	0.00	0.23	0.00	0.05	0.02	0.00	0.04	0.01	99.30	B4-1
11	98.97	0.00	0.00	0.00	0.22	0.00	0.05	0.11	0.01	0.05	0.00	99.41	B4-2
12	98.59	0.00	0.00	0.03	0.26	0.00	0.05	0.06	0.00	0.02	0.00	99.01	B4-3
13	99.50	0.00	0.01	0.00	0.29	0.00	0.04	0.02	0.00	0.00	0.00	99.86	B5-1
14	98.72	0.00	0.01	0.00	0.28	0.00	0.03	0.00	0.00	0.09	0.00	99.13	B5-2
15	98.87	0.00	0.01	0.02	0.21	0.00	0.05	0.00	0.01	0.03	0.01	99.20	B5-3
16	98.57	0.01	0.00	0.00	0.03	0.02	0.16	0.02	0.00	0.00	0.02	98.83	PO1-1
17	98.45	0.01	0.00	0.00	0.00	0.00	0.09	0.01	0.00	0.00	0.01	98.57	PO1-2
18	98.25	0.00	0.08	0.00	0.02	0.02	0.13	0.05	0.08	0.04	0.00	98.67	PO1-3
19	99.19	0.00	0.00	0.00	0.00	0.00	0.03	0.00	0.00	0.05	0.01	99.28	PO2-1
20	98.38	0.00	0.00	0.00	0.05	0.01	0.07	0.01	0.00	0.00	0.00	98.52	PO2-2
21	98.53	0.00	0.00	0.01	0.02	0.00	0.07	0.05	0.01	0.00	0.01	98.70	PO2-3
22	98.21	0.00	0.00	0.00	0.41	0.00	0.01	0.00	0.00	0.00	0.00	98.64	PO3-1
23	98.14	0.01	0.01	0.00	0.35	0.00	0.02	0.06	0.00	0.02	0.00	98.61	PO3-2
24	99.24	0.00	0.03	0.00	0.35	0.00	0.02	0.00	0.00	0.03	0.01	99.67	PO3-3
25	99.50	0.00	0.02	0.00	0.01	0.02	0.02	0.01	0.00	0.08	0.01	99.66	PO4-1
26	98.53	0.00	0.01	0.01	0.01	0.02	0.01	0.03	0.00	0.00	0.00	98.63	PO4-2
27	98.57	0.00	0.00	0.00	0.05	0.00	0.00	0.08	0.00	0.02	0.02	98.75	PO4-3
28	98.86	0.00	0.03	0.00	0.01	0.02	0.26	0.02	0.00	0.00	0.00	99.19	PO5-1
29	99.50	0.00	0.00	0.03	0.02	0.00	0.26	0.04	0.00	0.00	0.01	99.86	PO5-2
30	99.53	0.03	0.01	0.00	0.02	0.01	0.26	0.02	0.01	0.00	0.01	99.90	PO5-3
31	98.53	0.00	0.00	0.03	0.00	0.00	0.00	0.00	0.01	0.02	0.01	98.60	PO6-1
32	99.03	0.00	0.00	0.00	0.04	0.02	0.02	0.03	0.00	0.00	0.02	99.15	PO6-2
33	98.52	0.00	0.01	0.00	0.00	0.00	0.01	0.02	0.01	0.01	0.00	98.59	PO6-3
34	99.59	0.01	0.00	0.00	0.01	0.01	0.11	0.05	0.00	0.01	0.00	99.80	PO7-1
35	98.95	0.00	0.01	0.00	0.06	0.00	0.07	0.00	0.00	0.01	0.00	99.11	PO7-2

Table E2 EPMA Results Summarization 2

No.	Al2O3	MgO	CaO	MnO	FeO	SiO2	TiO2	Ga2O3	K2O	Cr2O3	V2O3	Total	Comment
36	99.65	0.01	0.00	0.00	0.00	0.00	0.10	0.00	0.00	0.02	0.01	99.78	PO7-3
37	98.28	0.00	0.00	0.03	0.02	0.00	0.02	0.02	0.00	0.02	0.00	98.38	PO8-1
38	98.23	0.00	0.03	0.00	0.00	0.00	0.09	0.04	0.01	0.05	0.00	98.44	PO8-2
39	99.05	0.00	0.00	0.00	0.03	0.02	0.00	0.14	0.00	0.07	0.00	99.30	PO8-3
40	99.07	0.00	0.00	0.00	0.01	0.00	0.14	0.00	0.01	0.02	0.02	99.26	PO9-1
41	99.06	0.00	0.00	0.04	0.00	0.01	0.13	0.03	0.02	0.03	0.00	99.33	PO9-2
42	99.24	0.00	0.01	0.00	0.03	0.02	0.09	0.03	0.01	0.02	0.00	99.45	PO9-3
43	98.59	0.00	0.00	0.01	0.02	0.00	0.08	0.00	0.00	0.10	0.01	98.83	PO10-1
44	98.21	0.00	0.01	0.00	0.00	0.00	0.04	0.00	0.00	0.00	0.00	98.27	PO10-2
45	98.39	0.00	0.00	0.02	0.01	0.00	0.07	0.08	0.00	0.02	0.00	98.59	PO10-3
46	98.68	0.00	0.02	0.03	0.02	0.00	0.13	0.07	0.00	0.00	0.00	98.95	PO11-1
47	98.88	0.00	0.00	0.05	0.01	0.01	0.11	0.03	0.01	0.00	0.00	99.11	PO11-2
48	99.18	0.00	0.00	0.00	0.02	0.00	0.11	0.05	0.01	0.05	0.00	99.42	PO11-3
49	99.95	0.02	0.00	0.00	0.01	0.01	0.17	0.00	0.00	0.03	0.00	100.19	PO12-1
50	98.35	0.00	0.01	0.00	0.03	0.01	0.08	0.00	0.00	0.00	0.03	98.52	PO12-2
51	98.39	0.00	0.02	0.00	0.00	0.01	0.07	0.04	0.02	0.05	0.03	98.62	PO12-3
52	99.04	0.00	0.00	0.00	0.02	0.00	0.00	0.03	0.00	0.08	0.02	99.20	PO13-1
53	99.06	0.01	0.01	0.06	0.01	0.03	0.01	0.00	0.00	0.06	0.00	99.26	PO13-2
54	98.97	0.00	0.02	0.00	0.01	0.03	0.00	0.00	0.01	0.08	0.02	99.13	PO13-3
55	99.35	0.00	0.01	0.00	0.02	0.02	0.00	0.01	0.00	0.30	0.00	99.70	Pr1-1
56	99.34	0.00	0.00	0.00	0.00	0.00	0.02	0.08	0.00	0.19	0.00	99.63	Pr1-2
57	99.03	0.00	0.00	0.00	0.00	0.00	0.01	0.06	0.01	0.13	0.00	99.24	Pr1-3
58	98.46	0.00	0.00	0.00	0.00	0.00	0.03	0.10	0.00	0.06	0.01	98.66	Pr2-1
59	98.53	0.00	0.01	0.00	0.01	0.00	0.05	0.00	0.00	0.05	0.00	98.66	Pr2-2
60	98.74	0.00	0.00	0.00	0.03	0.00	0.01	0.11	0.01	0.02	0.03	98.96	Pr2-3
61	98.34	0.01	0.00	0.03	0.02	0.01	0.01	0.04	0.01	0.04	0.01	98.52	Pr3-1
62	98.54	0.00	0.01	0.00	0.03	0.01	0.02	0.02	0.00	0.02	0.00	98.66	Pr3-2
63	98.41	0.00	0.01	0.00	0.00	0.00	0.03	0.07	0.00	0.04	0.03	98.57	Pr3-3
64	98.19	0.00	0.01	0.03	0.00	0.00	0.04	0.07	0.00	0.13	0.01	98.48	Pr4-1
65	98.63	0.00	0.00	0.00	0.05	0.00	0.00	0.00	0.00	0.06	0.01	98.76	Pr4-2
66	98.39	0.00	0.00	0.00	0.01	0.00	0.03	0.00	0.00	0.08	0.02	98.54	Pr4-3
67	98.96	0.00	0.01	0.04	0.14	0.00	0.04	0.00	0.01	0.08	0.00	99.28	Pr5-1
68	98.06	0.00	0.00	0.00	0.16	0.00	0.04	0.02	0.01	0.11	0.04	98.43	Pr5-2
69	98.44	0.00	0.00	0.00	0.12	0.00	0.00	0.00	0.00	0.12	0.01	98.70	Pr5-3
70	98.84	0.00	0.00	0.00	0.03	0.00	0.07	0.00	0.00	0.11	0.03	99.08	Pr6-1

Table E3 EPMA Results Summarization 3

No.	Al2O3	MgO	CaO	MnO	FeO	SiO2	TiO2	Ga2O3	K2O	Cr2O3	V2O3	Total	Comment
71	98.53	0.00	0.01	0.03	0.01	0.01	0.03	0.00	0.00	0.10	0.03	98.76	Pr6-2
72	99.09	0.00	0.00	0.00	0.01	0.01	0.04	0.06	0.00	0.16	0.02	99.39	Pr6-3
73	99.04	0.01	0.00	0.00	0.00	0.00	0.00	0.02	0.01	0.02	0.02	99.12	Pr7-1
74	98.85	0.00	0.04	0.00	0.03	0.00	0.00	0.01	0.01	0.06	0.01	99.00	Pr7-2
75	98.82	0.00	0.00	0.01	0.00	0.00	0.00	0.01	0.00	0.03	0.00	98.86	Pr7-3
76	98.49	0.00	0.00	0.00	0.01	0.00	0.02	0.07	0.00	0.16	0.02	98.76	Pr8-1
77	98.67	0.00	0.00	0.02	0.02	0.00	0.01	0.09	0.00	0.08	0.04	98.94	Pr8-2
78	98.20	0.00	0.00	0.00	0.01	0.00	0.03	0.07	0.00	0.15	0.01	98.48	Pr8-3
79	98.36	0.00	0.01	0.00	0.00	0.01	0.02	0.00	0.01	0.08	0.00	98.48	Pr9-1
80	98.31	0.00	0.00	0.00	0.03	0.01	0.03	0.00	0.00	0.00	0.00	98.38	Pr9-2
81	98.49	0.00	0.02	0.07	0.00	0.00	0.03	0.03	0.00	0.08	0.03	98.74	Pr9-3
82	98.26	0.01	0.01	0.00	0.04	0.00	0.16	0.02	0.01	0.13	0.02	98.66	Pr10-1
83	98.06	0.00	0.00	0.01	0.01	0.00	0.18	0.02	0.00	0.19	0.00	98.47	Pr10-2
84	98.01	0.00	0.00	0.05	0.02	0.00	0.00	0.00	0.00	0.33	0.02	98.42	Pr10-3
85	98.90	0.00	0.01	0.01	0.19	0.01	0.02	0.00	0.00	0.09	0.01	99.24	Pr11-1
86	98.93	0.00	0.00	0.01	0.17	0.00	0.03	0.02	0.00	0.43	0.01	99.60	Pr11-2
87	98.46	0.00	0.00	0.00	0.17	0.00	0.00	0.00	0.00	0.39	0.03	99.04	Pr11-3
88	98.48	0.01	0.01	0.00	0.00	0.00	0.02	0.00	0.00	0.12	0.02	98.65	Pr12-1
89	98.32	0.00	0.00	0.00	0.02	0.00	0.02	0.04	0.01	0.09	0.00	98.49	Pr12-2
90	98.17	0.00	0.00	0.08	0.00	0.00	0.03	0.03	0.00	0.15	0.01	98.47	Pr12-3
91	98.09	0.00	0.00	0.02	0.00	0.00	0.01	0.02	0.00	0.13	0.01	98.28	Pr13-1
92	98.89	0.00	0.01	0.00	0.01	0.00	0.02	0.05	0.00	0.17	0.01	99.16	Pr13-2
93	98.06	0.00	0.00	0.00	0.00	0.00	0.04	0.00	0.00	0.13	0.00	98.23	Pr13-3

Table E4 EPMA Stoichiometry Results Summarization

Element	B1-1	B1-2	B1-3	B2-1	B2-2	B2-3	B3-1	B3-2	B3-3	B4-1	B4-2	B4-3	B5-1	B5-2	B5-3
SiO2	0.00	0.00	0.00	0.00	0.00	0.00	0.00	0.00	0.00	0.00	0.00	0.00	0.00	0.00	0.00
TiO2	0.13	0.11	0.12	0.02	0.01	0.00	0.03	0.06	0.03	0.05	0.05	0.05	0.04	0.03	0.05
Al2O3	99.27	99.78	98.39	98.71	99.00	98.36	98.86	98.81	98.59	98.94	98.97	98.59	99.50	98.72	98.87
FeO	0.01	0.01	0.03	0.28	0.27	0.30	0.19	0.25	0.27	0.23	0.22	0.26	0.29	0.28	0.21
MnO	0.00	0.00	0.05	0.02	0.04	0.00	0.03	0.02	0.00	0.00	0.00	0.03	0.00	0.00	0.02
MgO	0.00	0.00	0.00	0.00	0.00	0.00	0.00	0.00	0.00	0.00	0.00	0.00	0.00	0.00	0.00
CaO	0.01	0.00	0.01	0.00	0.00	0.01	0.00	0.01	0.00	0.00	0.00	0.00	0.01	0.01	0.01
K2O	0.00	0.00	0.00	0.00	0.00	0.00	0.01	0.00	0.00	0.00	0.01	0.00	0.00	0.00	0.01
Cr2O3	0.00	0.00	0.02	0.02	0.02	0.04	0.02	0.07	0.00	0.04	0.05	0.02	0.00	0.09	0.03
V2O3	0.00	0.01	0.00	0.00	0.00	0.00	0.00	0.00	0.02	0.01	0.00	0.00	0.00	0.00	0.01
Total	2.00	2.00	2.00	2.00	2.00	2.00	2.00	2.00	2.00	2.00	2.00	2.00	2.00	2.00	2.00
Formula	3(O)	3(O)	3(O)	3(O)	3(O)	3(O)	3(O)	3(O)	3(O)	3(O)	3(O)	3(O)	3(O)	3(O)	3(O)
Si	0.000	0.000	0.000	0.000	0.000	0.000	0.000	0.000	0.000	0.000	0.000	0.000	0.000	0.000	0.000
Ti	0.002	0.001	0.002	0.000	0.000	0.000	0.000	0.001	0.000	0.001	0.001	0.001	0.000	0.000	0.001
Al	1.998	1.998	1.997	1.996	1.996	1.996	1.997	1.995	1.997	1.996	1.996	1.996	1.996	1.995	1.996
Fe	0.000	0.000	0.000	0.004	0.004	0.004	0.003	0.004	0.004	0.003	0.003	0.004	0.004	0.004	0.003
Mn	0.000	0.000	0.001	0.000	0.001	0.000	0.000	0.000	0.000	0.000	0.000	0.000	0.000	0.000	0.000
Mg	0.000	0.000	0.000	0.000	0.000	0.000	0.000	0.000	0.000	0.000	0.000	0.000	0.000	0.000	0.000
Ca	0.000	0.000	0.000	0.000	0.000	0.000	0.000	0.000	0.000	0.000	0.000	0.000	0.000	0.000	0.000
K	0.000	0.000	0.000	0.000	0.000	0.000	0.000	0.000	0.000	0.000	0.000	0.000	0.000	0.000	0.000
Cr	0.000	0.000	0.000	0.000	0.000	0.001	0.000	0.001	0.000	0.001	0.001	0.000	0.000	0.001	0.000
V	0.000	0.000	0.000	0.000	0.000	0.000	0.000	0.000	0.000	0.000	0.000	0.000	0.000	0.000	0.000
Total	99.422	99.910	98.619	99.167	99.409	98.726	99.160	99.231	98.913	99.302	99.409	99.011	99.855	99.130	99.202

Table E5 EPMA Stoichiometry Results Summarization 2

Element	Ppo1-1	Ppo1-2	Ppo1-3	Ppo2-1	Ppo2-2	Ppo2-3	Ppo3-1	Ppo3-2	Ppo3-3	Ppo4-1	Ppo4-2	Ppo4-3	Ppo5-1	Ppo5-2	Ppo5-3
SiO2	0.02	0.00	0.02	0.00	0.01	0.00	0.00	0.00	0.00	0.02	0.02	0.00	0.02	0.00	0.01
TiO2	0.16	0.09	0.13	0.03	0.07	0.07	0.01	0.02	0.02	0.02	0.01	0.00	0.26	0.26	0.26
Al2O3	98.57	98.45	98.25	99.19	98.38	98.53	98.21	98.14	99.24	99.50	98.53	98.57	98.86	99.50	99.53
FeO	0.03	0.00	0.02	0.00	0.05	0.02	0.41	0.35	0.35	0.01	0.01	0.05	0.01	0.02	0.02
MnO	0.00	0.00	0.00	0.00	0.00	0.01	0.00	0.00	0.00	0.00	0.01	0.00	0.00	0.03	0.00
MgO	0.01	0.01	0.00	0.00	0.00	0.00	0.00	0.01	0.00	0.00	0.00	0.00	0.00	0.00	0.03
CaO	0.00	0.00	0.08	0.00	0.00	0.00	0.00	0.01	0.03	0.02	0.01	0.00	0.03	0.00	0.01
K2O	0.00	0.00	0.08	0.00	0.00	0.01	0.00	0.00	0.00	0.00	0.00	0.00	0.00	0.00	0.01
Cr2O3	0.00	0.00	0.04	0.05	0.00	0.00	0.00	0.02	0.03	0.08	0.00	0.02	0.00	0.00	0.00
V2O3	0.02	0.01	0.00	0.01	0.00	0.01	0.00	0.00	0.01	0.01	0.00	0.02	0.00	0.01	0.01
Total	2.00	2.00	2.00	2.00	2.00	2.00	2.00	2.00	2.00	2.00	2.00	2.00	2.00	2.00	2.00
Formula	3(O)	3(O)	3(O)	3(O)	3(O)	3(O)	3(O)	3(O)	3(O)	3(O)	3(O)	3(O)	3(O)	3(O)	3(O)
Si	0.000	0.000	0.000	0.000	0.000	0.000	0.000	0.000	0.000	0.000	0.000	0.000	0.000	0.000	0.000
Ti	0.002	0.001	0.002	0.000	0.001	0.001	0.000	0.000	0.000	0.000	0.000	0.000	0.003	0.003	0.003
Al	1.996	1.998	1.995	1.999	1.998	1.998	1.996	1.996	1.996	1.998	1.999	1.999	1.995	1.995	1.994
Fe	0.000	0.000	0.000	0.000	0.001	0.000	0.006	0.005	0.005	0.000	0.000	0.001	0.000	0.000	0.000
Mn	0.000	0.000	0.000	0.000	0.000	0.000	0.000	0.000	0.000	0.000	0.000	0.000	0.000	0.000	0.000
Mg	0.000	0.000	0.000	0.000	0.000	0.000	0.000	0.000	0.000	0.000	0.000	0.000	0.000	0.000	0.001
Ca	0.000	0.000	0.001	0.000	0.000	0.000	0.000	0.000	0.000	0.000	0.000	0.000	0.000	0.000	0.000
K	0.000	0.000	0.002	0.000	0.000	0.000	0.000	0.000	0.000	0.000	0.000	0.000	0.000	0.000	0.000
Cr	0.000	0.000	0.001	0.001	0.000	0.000	0.000	0.000	0.000	0.001	0.000	0.000	0.000	0.000	0.000
V	0.000	0.000	0.000	0.000	0.000	0.000	0.000	0.000	0.000	0.000	0.000	0.000	0.000	0.000	0.000
Total	98.834	98.565	98.667	99.284	98.524	98.698	98.636	98.606	99.665	99.660	98.627	98.745	99.186	99.859	99.898

Table E6 EPMA Stoichiometry Results Summarization 3

Element	Ppo6-1	Ppo6-2	Ppo6-3	Ppo7-1	Ppo7-2	Ppo7-3	Ppo8-1	Ppo8-2	Ppo8-3	Ppo9-1	Ppo9-2	Ppo9-3	Ppo10-1	Ppo10-2	Ppo10-3
SiO2	0.00	0.02	0.00	0.01	0.00	0.00	0.00	0.00	0.02	0.00	0.01	0.02	0.00	0.00	0.00
TiO2	0.00	0.02	0.01	0.11	0.07	0.10	0.02	0.09	0.00	0.14	0.13	0.09	0.08	0.04	0.07
Al2O3	98.53	99.03	98.52	99.59	98.95	99.65	98.28	98.23	99.05	99.07	99.06	99.24	98.59	98.21	98.39
FeO	0.00	0.04	0.00	0.01	0.06	0.00	0.02	0.00	0.03	0.01	0.00	0.03	0.02	0.00	0.01
MnO	0.03	0.00	0.00	0.00	0.00	0.00	0.03	0.00	0.00	0.00	0.04	0.00	0.01	0.00	0.02
MgO	0.00	0.00	0.00	0.01	0.00	0.01	0.00	0.00	0.00	0.00	0.00	0.00	0.00	0.00	0.00
CaO	0.00	0.00	0.01	0.00	0.01	0.00	0.00	0.03	0.00	0.00	0.00	0.01	0.00	0.01	0.00
K2O	0.01	0.00	0.01	0.00	0.00	0.00	0.00	0.01	0.00	0.01	0.02	0.01	0.00	0.00	0.00
Cr2O3	0.02	0.00	0.01	0.01	0.01	0.02	0.02	0.05	0.07	0.02	0.03	0.02	0.10	0.00	0.02
V2O3	0.01	0.02	0.00	0.00	0.00	0.01	0.00	0.00	0.00	0.02	0.00	0.00	0.01	0.00	0.00
Total	2.00	2.00	2.00	2.00	2.00	2.00	2.00	2.00	2.00	2.00	2.00	2.00	2.00	2.00	2.00
Formula	3(O)	3(O)	3(O)	3(O)	3(O)	3(O)	3(O)	3(O)	3(O)	3(O)	3(O)	3(O)	3(O)	3(O)	3(O)
Si	0.000	0.000	0.000	0.000	0.000	0.000	0.000	0.000	0.000	0.000	0.000	0.000	0.000	0.000	0.000
Ti	0.000	0.000	0.000	0.001	0.001	0.001	0.000	0.001	0.000	0.002	0.002	0.001	0.001	0.000	0.001
Al	1.999	1.999	1.999	1.997	1.998	1.998	1.999	1.997	1.998	1.997	1.997	1.997	1.997	1.999	1.998
Fe	0.000	0.001	0.000	0.000	0.001	0.000	0.000	0.000	0.000	0.000	0.000	0.000	0.000	0.000	0.000
Mn	0.000	0.000	0.000	0.000	0.000	0.000	0.000	0.000	0.000	0.000	0.001	0.000	0.000	0.000	0.000
Mg	0.000	0.000	0.000	0.000	0.000	0.000	0.000	0.000	0.000	0.000	0.000	0.000	0.000	0.000	0.000
Ca	0.000	0.000	0.000	0.000	0.000	0.000	0.000	0.000	0.000	0.000	0.000	0.000	0.000	0.000	0.000
K	0.000	0.000	0.000	0.000	0.000	0.000	0.000	0.000	0.000	0.000	0.000	0.000	0.000	0.000	0.000
Cr	0.000	0.000	0.000	0.000	0.000	0.000	0.000	0.001	0.001	0.000	0.000	0.000	0.001	0.000	0.000
V	0.000	0.000	0.000	0.000	0.000	0.000	0.000	0.000	0.000	0.000	0.000	0.000	0.000	0.000	0.000
Total	98.596	99.154	98.593	99.795	99.114	99.783	98.382	98.444	99.301	99.263	99.327	99.450	98.825	98.271	98.590

Table E7 EPMA Stoichiometry Results Summarization 4

Element	Ppo11-1	Ppo11-2	PPo11-3	Ppo12-1	Ppo12-2	Ppo12-3	Ppo13-1	Ppo13-2	Ppo13-3	Pkr1-1	Pkr1-2	Pkr1-3	Pkr2-1	Pkr2-2	Pkr2-3
SiO2	0.00	0.01	0.00	0.01	0.01	0.01	0.00	0.03	0.03	0.02	0.00	0.00	0.00	0.00	0.00
TiO2	0.13	0.11	0.11	0.17	0.08	0.07	0.00	0.01	0.00	0.00	0.02	0.01	0.03	0.05	0.01
Al2O3	98.68	98.88	99.18	99.95	98.35	98.39	99.04	99.06	98.97	99.35	99.34	99.03	98.46	98.53	98.74
FeO	0.02	0.01	0.02	0.01	0.03	0.00	0.02	0.01	0.01	0.02	0.00	0.00	0.00	0.01	0.03
MnO	0.03	0.05	0.00	0.00	0.00	0.00	0.00	0.06	0.00	0.00	0.00	0.00	0.00	0.00	0.00
MgO	0.00	0.00	0.00	0.02	0.00	0.00	0.00	0.01	0.00	0.00	0.00	0.00	0.00	0.00	0.00
CaO	0.02	0.00	0.00	0.00	0.01	0.02	0.00	0.01	0.02	0.01	0.00	0.00	0.00	0.01	0.00
K2O	0.00	0.01	0.01	0.00	0.00	0.02	0.00	0.00	0.01	0.00	0.00	0.01	0.00	0.00	0.01
Cr2O3	0.00	0.00	0.05	0.03	0.00	0.05	0.08	0.06	0.08	0.30	0.19	0.13	0.06	0.05	0.02
V2O3	0.00	0.00	0.00	0.00	0.03	0.03	0.02	0.00	0.02	0.00	0.00	0.00	0.01	0.00	0.03
Total	2.00	2.00	2.00	2.00	2.00	2.00	2.00	2.00	2.00	2.00	2.00	2.00	2.00	2.00	2.00
Formula	3(O)	3(O)	3(O)	3(O)	3(O)	3(O)	3(O)	3(O)	3(O)	3(O)	3(O)	3(O)	3(O)	3(O)	3(O)
Si	0.000	0.000	0.000	0.000	0.000	0.000	0.000	0.000	0.001	0.000	0.000	0.000	0.000	0.000	0.000
Ti	0.002	0.001	0.001	0.002	0.001	0.001	0.000	0.000	0.000	0.000	0.000	0.000	0.000	0.001	0.000
Al	1.997	1.997	1.997	1.996	1.997	1.997	1.998	1.997	1.998	1.995	1.997	1.998	1.998	1.998	1.999
Fe	0.000	0.000	0.000	0.000	0.000	0.000	0.000	0.000	0.000	0.000	0.000	0.000	0.000	0.000	0.000
Mn	0.000	0.001	0.000	0.000	0.000	0.000	0.000	0.001	0.000	0.000	0.000	0.000	0.000	0.000	0.000
Mg	0.000	0.000	0.000	0.000	0.000	0.000	0.000	0.000	0.000	0.000	0.000	0.000	0.000	0.000	0.000
Ca	0.000	0.000	0.000	0.000	0.000	0.000	0.000	0.000	0.000	0.000	0.000	0.000	0.000	0.000	0.000
K	0.000	0.000	0.000	0.000	0.000	0.000	0.000	0.000	0.000	0.000	0.000	0.000	0.000	0.000	0.000
Cr	0.000	0.000	0.001	0.000	0.000	0.001	0.001	0.001	0.001	0.004	0.003	0.002	0.001	0.001	0.000
V	0.000	0.000	0.000	0.000	0.000	0.000	0.000	0.000	0.000	0.000	0.000	0.000	0.000	0.000	0.000
Total	98.946	99.109	99.422	100.187	98.521	98.622	99.204	99.260	99.129	99.697	99.634	99.240	98.664	98.660	98.956

Table E8 EPMA Stoichiometry Results Summarization 5

Element	Pkr3-1	Pkr3-2	Pkr3-3	Pkr4-1	Pkr4-2	Pkr4-3	Pkr5-1	Pkr5-2	Pkr5-3	Pkr6-1	Pkr6-2	Pkr6-3	Pkr7-1	Pkr7-2	Pkr7-3
SiO2	0.01	0.01	0.00	0.00	0.00	0.00	0.00	0.00	0.00	0.00	0.01	0.01	0.00	0.00	0.00
TiO2	0.01	0.02	0.03	0.04	0.00	0.03	0.04	0.04	0.00	0.07	0.03	0.04	0.00	0.00	0.00
Al2O3	98.34	98.54	98.41	98.19	98.63	98.39	98.96	98.06	98.44	98.84	98.53	99.09	99.04	98.85	98.82
FeO	0.02	0.03	0.00	0.00	0.05	0.01	0.14	0.16	0.12	0.03	0.01	0.01	0.00	0.03	0.00
MnO	0.03	0.00	0.00	0.03	0.00	0.00	0.04	0.00	0.00	0.00	0.03	0.00	0.00	0.00	0.01
MgO	0.01	0.00	0.00	0.00	0.00	0.00	0.00	0.00	0.00	0.00	0.00	0.00	0.01	0.00	0.00
CaO	0.00	0.01	0.01	0.01	0.00	0.00	0.01	0.00	0.00	0.00	0.01	0.00	0.00	0.04	0.00
K2O	0.01	0.00	0.00	0.00	0.00	0.00	0.01	0.01	0.00	0.00	0.00	0.00	0.01	0.01	0.00
Cr2O3	0.04	0.02	0.04	0.13	0.06	0.08	0.08	0.11	0.12	0.11	0.10	0.16	0.02	0.06	0.03
V2O3	0.01	0.00	0.03	0.01	0.01	0.02	0.00	0.04	0.01	0.03	0.03	0.02	0.02	0.01	0.00
Total	2.00	2.00	2.00	2.00	2.00	2.00	2.00	2.00	2.00	2.00	2.00	2.00	2.00	2.00	2.00
Formula	3(O)	3(O)	3(O)	3(O)	3(O)	3(O)	3(O)	3(O)	3(O)	3(O)	3(O)	3(O)	3(O)	3(O)	3(O)
Si	0.000	0.000	0.000	0.000	0.000	0.000	0.000	0.000	0.000	0.000	0.000	0.000	0.000	0.000	0.000
Ti	0.000	0.000	0.000	0.001	0.000	0.000	0.001	0.001	0.000	0.001	0.000	0.001	0.000	0.000	0.000
Al	1.998	1.999	1.998	1.997	1.998	1.998	1.996	1.995	1.997	1.996	1.997	1.996	1.999	1.998	2.000
Fe	0.000	0.000	0.000	0.000	0.001	0.000	0.002	0.002	0.002	0.000	0.000	0.000	0.000	0.000	0.000
Mn	0.000	0.000	0.000	0.000	0.000	0.000	0.001	0.000	0.000	0.000	0.000	0.000	0.000	0.000	0.000
Mg	0.000	0.000	0.000	0.000	0.000	0.000	0.000	0.000	0.000	0.000	0.000	0.000	0.000	0.000	0.000
Ca	0.000	0.000	0.000	0.000	0.000	0.000	0.000	0.000	0.000	0.000	0.000	0.000	0.000	0.001	0.000
K	0.000	0.000	0.000	0.000	0.000	0.000	0.000	0.000	0.000	0.000	0.000	0.000	0.000	0.000	0.000
Cr	0.001	0.000	0.000	0.002	0.001	0.001	0.001	0.001	0.002	0.001	0.001	0.002	0.000	0.001	0.000
V	0.000	0.000	0.000	0.000	0.000	0.000	0.000	0.000	0.000	0.000	0.000	0.000	0.000	0.000	0.000
Total	98.516	98.661	98.572	98.481	98.756	98.538	99.281	98.434	98.702	99.083	98.755	99.385	99.124	99.004	98.864

Table E9 EPMA Stoichiometry Results Summarization 6

Element	Pkr8-1	Pkr8-2	Pkr8-3	Pkr9-1	Pkr9-2	Pkr9-3	Pkr10-1	Pkr10-2	Pkr10-3	Pkr11-1	Pkr11-2	Pkr11-3	Pkr12-1	Pkr12-2	Pkr12-3
SiO2	0.00	0.00	0.00	0.01	0.01	0.00	0.00	0.00	0.00	0.01	0.00	0.00	0.00	0.00	0.00
TiO2	0.02	0.01	0.03	0.02	0.03	0.03	0.16	0.18	0.00	0.02	0.03	0.00	0.02	0.02	0.03
Al2O3	98.49	98.67	98.20	98.36	98.31	98.49	98.26	98.06	98.01	98.90	98.93	98.46	98.48	98.32	98.17
FeO	0.01	0.02	0.01	0.00	0.03	0.00	0.04	0.01	0.02	0.19	0.17	0.17	0.00	0.02	0.00
MnO	0.00	0.02	0.00	0.00	0.00	0.07	0.00	0.01	0.05	0.01	0.01	0.00	0.00	0.00	0.08
MgO	0.00	0.00	0.00	0.00	0.00	0.00	0.01	0.00	0.00	0.00	0.00	0.00	0.01	0.00	0.00
CaO	0.00	0.00	0.00	0.01	0.00	0.02	0.01	0.00	0.00	0.01	0.00	0.00	0.01	0.00	0.00
K2O	0.00	0.00	0.00	0.01	0.00	0.00	0.01	0.00	0.00	0.00	0.00	0.00	0.00	0.01	0.00
Cr2O3	0.16	0.08	0.15	0.08	0.00	0.08	0.13	0.19	0.33	0.09	0.43	0.39	0.12	0.09	0.15
V2O3	0.02	0.04	0.01	0.00	0.00	0.03	0.02	0.00	0.02	0.01	0.01	0.03	0.02	0.00	0.01
Total	2.00	2.00	2.00	2.00	2.00	2.00	2.00	2.00	2.00	2.00	2.00	2.00	2.00	2.00	2.00
Formula	3(O)	3(O)	3(O)	3(O)	3(O)	3(O)	3(O)	3(O)	3(O)	3(O)	3(O)	3(O)	3(O)	3(O)	3(O)
Si	0.000	0.000	0.000	0.000	0.000	0.000	0.000	0.000	0.000	0.000	0.000	0.000	0.000	0.000	0.000
Ti	0.000	0.000	0.000	0.000	0.000	0.000	0.002	0.002	0.000	0.000	0.000	0.000	0.000	0.000	0.000
Al	1.997	1.997	1.997	1.998	1.999	1.997	1.994	1.994	1.995	1.996	1.992	1.993	1.998	1.998	1.996
Fe	0.000	0.000	0.000	0.000	0.000	0.000	0.001	0.000	0.000	0.003	0.002	0.002	0.000	0.000	0.000
Mn	0.000	0.000	0.000	0.000	0.000	0.001	0.000	0.000	0.001	0.000	0.000	0.000	0.000	0.000	0.001
Mg	0.000	0.000	0.000	0.000	0.000	0.000	0.000	0.000	0.000	0.000	0.000	0.000	0.000	0.000	0.000
Ca	0.000	0.000	0.000	0.000	0.000	0.000	0.000	0.000	0.000	0.000	0.000	0.000	0.000	0.000	0.000
K	0.000	0.000	0.000	0.000	0.000	0.000	0.000	0.000	0.000	0.000	0.000	0.000	0.000	0.000	0.000
Cr	0.002	0.001	0.002	0.001	0.000	0.001	0.002	0.003	0.004	0.001	0.006	0.005	0.002	0.001	0.002
V	0.000	0.000	0.000	0.000	0.000	0.000	0.000	0.000	0.000	0.000	0.000	0.000	0.000	0.000	0.000
Total	98.763	98.938	98.476	98.481	98.378	98.742	98.662	98.470	98.418	99.243	99.602	99.040	98.645	98.493	98.471

Table E10 EPMA Stoichiometry Results Summarization 7

Element	Pkr13-1	Pkr13-2	Pkr13-3
SiO2	0.00	0.00	0.00
TiO2	0.01	0.02	0.04
Al2O3	98.09	98.89	98.06
FeO	0.00	0.01	0.00
MnO	0.02	0.00	0.00
MgO	0.00	0.00	0.00
CaO	0.00	0.01	0.00
K2O	0.00	0.00	0.00
Cr2O3	0.13	0.17	0.13
V2O3	0.01	0.01	0.00
Total	2.00	2.00	2.00
Formula	3(O)	3(O)	3(O)
Si	0.000	0.000	0.000
Ti	0.000	0.000	0.000
Al	1.998	1.997	1.998
Fe	0.000	0.000	0.000
Mn	0.000	0.000	0.000
Mg	0.000	0.000	0.000
Ca	0.000	0.000	0.000
K	0.000	0.000	0.000
Cr	0.002	0.002	0.002
V	0.000	0.000	0.000
Total	98.277	99.161	98.231

REFERENCES

Pham Van Long, Gaston Giuliani, Virginie Gaenier, Daniel Ohnenstetter. Gemstone in Vietnam. The Australian Gemmologist, Vol 22, Number 4 (2004)

Nguyen Ngoc Khoi, Chakkaphan Sutthirat, Duong Anh Tuan, Nguyen Van Nam, Nguyen Thi Minh Thuyet, Nguy Tuyet Nhung. Ruby and Sapphire from the Tan Huong- Truc Lau Area, YenBai Province, Northern Vietnam. GEMS & GEMOLOGY, Vol 47, No 3 (2011), pp. 185-195

Nam, Tran Ngoc. The geology of vietnam: A brief summary and problems.Geoscience reports of Shizuoka University. 22 (1995), p. 1-9

Robert C. Kammerling, Alice S. keller, Kenneth V. Scarratt, Saverio Repetto. Update on Mining Rubies and Fancy Sapphires in Northern Vietnam. GEMS & GEMMOLOGY, Vol 30 (1994), pp. 109-114

Garnier et al. Marble-hosgted ruby deposits from Central and South East Asia toward a new genetic model. Ore Geology Reviews 34 (2008) pp. 169-191

Ganier et al., Ar-Ar in phlogopites from marble-hosted ruby deposits in northern Vietnam: evidence for Cenozoic ruby formation. Chemical Geology. 188 (2002), p 33-49

A. Laachachi, M. Ferriol, M. Cochex, J.-M. Lopez Cuesta, D. Ruch., A comparison of the role of bohemite (AlOOH) and alumina (Al_2O_3) in the thermal stability and flammability of poly (methyl methacrylate). Polymer Degradation and Stability. Vol 94 (2009) pp.1373-1378

P. Diep., Internal characteristics, chemical compounds and spectroscopy of sapphire as single crystals (2015)

C. Lepvier, H. maluski, Vu Van Tich, A. Leyreloup, Phan Troung Thi, Nguyen Van Voung., The

Early Triassic Indosinian orogeny in Vietnam (Truong Son Belt and Kontum Massif); implications for geodynamic evolution of Indochina. Tectonophysics 393 (2004) pp. 87-118

Long et al., Gem corundum deposit in Vietnam. Gemmological Association and Gem Testing Laboratory of Great Britain. 29 (2004) pp. 129-147

V. Baalen., Titanium mobility in metamorphic systems: a review. Chemical Geology. 110 (1993) 233-249

Nakano et al., Tectonic evolution of high-grade metamorphic terranes in central Vietnam Constraints from large-scale monazite geochronology. Journal of Asian Earth Sciences. 73 (2013) 520-539